EVALUATION OF PERFORMANCE-BASED DEFORMATION LIMITS FOR REINFORCED CONCRETE COLUMNS

A THESIS SUBMITTED TO
THE GRADUATE SCHOOL OF NATURAL AND APPLIED SCIENCES
OF
MIDDLE EAST TECHNICAL UNIVERSITY

BY

ALPEREN ŞENOCAK

IN PARTIAL FULFILLMENT OF THE REQUIREMENTS
FOR
THE DEGREE OF MASTER OF SCIENCE
IN
CIVIL ENGINEERING

SEPTEMBER 2023

Approval of the thesis:

EVALUATION OF PERFORMANCE-BASED DEFORMATION LIMITS FOR REINFORCED CONCRETE COLUMNS

submitted by **ALPEREN ŞENOCAK** in partial fulfillment of the requirements for the degree of **Master of Science** i**n Civil Engineering, Middle East Technical University** by,

Prof. Dr. Halil Kalıpçılar
Dean, Graduate School of **Natural and Applied Sciences** _____

Prof. Dr. Erdem Canbay
Head of the Department, **Civil Engineering** _____

Prof. Dr. Ahmet Yakut
Supervisor, **Civil Engineering, METU** _____

Prof. Dr. Barış Binici
Co-Supervisor, **Civil Engineering, METU** _____

Examining Committee Members:

Prof. Dr. Kağan Tuncay
Civil Engineering, METU _____

Prof. Dr. Ahmet Yakut
Civil Engineering, METU _____

Prof. Dr. Barış Binici
Civil Engineering, METU _____

Prof. Dr. Murat Altuğ Erberik
Civil Engineering, METU _____

Prof. Dr. İlker Kazaz
Civil Engineering, Erzurum Technical University _____

Date: 11.09.2023

I hereby declare that all information in this document has been obtained and presented in accordance with academic rules and ethical conduct. I also declare that, as required by these rules and conduct, I have fully cited and referenced all material and results that are not original to this work.

Name Last name: Alperen Şenocak

Signature:

ABSTRACT

EVALUATION OF PERFORMANCE-BASED DEFORMATION LIMITS FOR REINFORCED CONCRETE COLUMNS

Şenocak, Alperen
Master of Science, Civil Engineering
Supervisor: Prof. Dr. Ahmet Yakut
Co-Supervisor: Prof. Dr. Barış Binici

September 2023, 122 pages

Reinforced concrete columns, as fundamental load-bearing elements in structures, play a crucial role in overall stability and safety of the buildings. A precise assessment of their performance, especially concerning deformation capacities, becomes essential in mitigating potential risks posed by seismic events. Performance-based design principles consider both the strength and displacement capacities of columns. The study of performance-based displacement limits for reinforced concrete columns necessitates a comprehensive understanding of factors impacting column deformation behavior. Current seismic codes contain deformation limits for each performance state. To assess the precision of these limits, 186 experimental column specimens extracted from the PEER database are used. After verifying the accuracy of OpenSees software by using 37 experimental column specimens from the PEER database and one portal frame experiment that was conducted at METU, 3072 columns are generated. Performance limits of the seismic guidelines are compared with experimental and analytical results. The effect of various parameters on the plastic rotation capacity and the capability of each seismic guideline to capture this effect are examined. It is found that the predictive safety of the seismic guidelines -TBEC (2018), ASCE/SEI 41-17, Eurocode 8-3- is affected

from the axial load ratio and transverse reinforcement ratio. Safety of the guidelines is examined for each performance limit.

Keywords: RC Column, Rotation Capacity, Performance Limits, Assessment

ÖZ

BETONARME KOLONLARIN PERFORMANSA DAYALI DEFORMASYON LİMİTLERİNİN İNCELENMESİ

Şenocak, Alperen
Master of Science, Civil Engineering
Supervisor: Prof. Dr. Ahmet Yakut
Co-Supervisor: Prof. Dr. Barış Binici

Eylül 2023, 122 sayfa

Yapılardaki temel yük taşıyıcı elemanlar olan betonarme kolonlar, binaların genel stabilitesi ve güvenliğinde çok önemli bir rol oynamaktadır. Özellikle deformasyon kapasitelerine ilişkin performanslarının kesin bir değerlendirmesi, sismik olayların oluşturduğu potansiyel risklerin azaltılmasında hayati önem taşımaktadır. Performansa dayalı tasarım ilkeleri kolonların hem mukavemetini hem de yer değiştirme kapasitelerini dikkate alır. Betonarme kolonlar için performansa dayalı deplasman sınırlarının incelenmesi, kolon deformasyon davranışını etkileyen faktörlerin kapsamlı bir şekilde anlaşılmasını gerektirir. Mevcut yönetmelikler, her performans durumu için deformasyon sınırlarını belirtir. Bu sınırların kesinliğini değerlendirmek için PEER veri tabanından alınan 186 kolon deneyi kullanılmıştır. OpenSees yazılımının doğruluğu PEER veri tabanından alınan 37 adet deneysel kolon sonucu ve ODTÜ'de gerçekleştirilen bir adet çerçeve deneyi kullanılarak doğrulandıktan sonra 3072 adet kolon oluşturulmuştur. Bu kolonların ve deney veri tabanındaki kolonların performans sınırları yönetmelik sonuçları ile karşılaştırılmıştır. Çeşitli parametrelerin plastik dönme kapasitesi üzerindeki etkisi ve her bir yönetmeliğin bu etkiyi yakalama kabiliyeti incelenmiştir. TBDY (2018), ASCE/SEI 41-17, Eurocode 8-3 yönetmeliklerinin belirlediği performans

sınırlarının güvenliğinin eksenel yük oranından ve enine donatı oranından etkilendiği görülmüştür. Yönetmeliklerin her performans limiti için güvenliği incelenmiştir.

Anahtar Kelimeler: Betonarme Kolon, Rotasyon Kapasitesi, Performans Limitleri, Değerlendirme

To my Family

ACKNOWLEDGMENTS

This study was conducted under the supervision of Prof. Dr. Ahmet Yakut. I would like to express my sincere gratitude for his support, guidance, patience, and always making time for my questions. I would also like to extend my thanks to my co-supervisor, Prof. Dr. Barış Binici, for his contributions and help whenever I needed it.

I would like to thank the committee members, Prof. Dr. Kağan Tuncay, Prof. Dr. Murat Altuğ Erberik and Prof. Dr. İlker Kazaz for their time and contributions on this thesis

I want to express my gratitude to Prof. Dr. İlker Kazaz and Dr. Koray Kadaş for their support and valuable feedback on the study.

I would like to thank my colleagues, Volkan Emren and Furkan Gökmen for their friendship and support.

I would like to thank Halil İbrahim İşler and Ayşenur Andaç for being my friends for more than half of my life. I feel very lucky to have known them.

I want to thank Dr. Nefize Shaban and Dr. Mehdi H. Afshar, two of the most kind-hearted people I have met, for their kind friendship and support. The conversations we had during our coffee breaks were usually the highlight of my day.

Last but not least, I want to thank my family, Deniz Dilek, and Emre Şensoy for their lifelong support and friendship, and, of course, my parents for their endless support throughout my educational journey. This thesis would not have been possible without them.

TABLE OF CONTENTS

LIST OF TABLES

TABLES

LIST OF FIGURES

FIGURES

LIST OF ABBREVIATIONS

ASCE/SEI: American Society of Civil Engineers / Structural Engineering Institute

CP: Collapse Prevention

DL: Damage Limitation

IO: Immediate Occupancy

LS: Life Safety

METU: Middle East Technical University

NC: Near Collapse

OpenSees: The Open System for Earthquake Engineering Simulation

PEER: Pacific Earthquake Engineering Center

RC: Reinforced Concrete

SD: Significant Damage

TBEC: Turkish Building Earthquake Code

LIST OF SYMBOLS

$\triangle_p$: Plastic displacement

$\triangle_y$: Yield displacement

$\emptyset_u$: Ultimate curvature

$\emptyset_y$: Yield curvature

E_c : Elastic modulus of concrete

E_s : Elastic modulus of steel

ε_c : Concrete strain

ε_s : Steel strain

θ_p : Plastic rotation

θ_u : Ultimate rotation

θ_y : Yield rotation

A_g : Gross cross-sectional area of the column

a_i : The distance between the axes of the longitudinal reinforcements supported by a stirrup or a tie.

A_{sh} : Cross-sectional area of transverse reinforcement in the considered direction.

b_k : The core dimension in the perpendicular direction

b_w : Width of the section

d : effective depth

d_b : Diameter of the tension reinforcement

f_c : Concrete compressive strength

f_{cc} : Confined concrete strength

f_{ctm} : Tensile strength of the concrete

f_{yl} : Yielding strength of longitudinal reinforcement

f_{yw} : Yielding strength of transverse reinforcement

h : section height

k_e : Confinement effectiveness coefficient

L : Column length

L_p : Plastic hinge length

L_s : Shear span

s : The spacing of transverse reinforcement in the considered direction.

V_e : Design shear force

V_{Col} : Shear capacity of the column according to ASCE/SEI 41-17

ρ_l : Longitudinal reinforcement ratio

ρ_t : Transverse reinforcement ratio

τ_e : Bond stress in the pre-yield range of rebar along development length

ω , ω' : Mechanical reinforcement ratio of the tension and compression reinforcement, respectively

CHAPTER 1

INTRODUCTION

1.1 General

The evaluation of performance-based displacement limits for reinforced concrete columns is a key focus of modern structural engineering work. As the built environment continues to evolve, the significance of ensuring structural integrity and resilience becomes more obvious. This has caused a shift from traditional design approaches to more sophisticated methodologies that account for the dynamic behavior of structures under varying loads, particularly seismic forces.

Reinforced concrete columns, as primary load-bearing components within structures, play a critical role in the overall stability and safety of buildings. The accurate evaluation of their performance, especially concerning their deformation capacities, is crucial in safeguarding against the potential hazards of seismic events. Performance-based design principles consider not only the strength but also the displacement capacities of columns. This approach aligns with the understanding that under seismic forces, a structure's ability to absorb and dissipate energy through controlled deformations can significantly mitigate potential damage.

The study of performance-based displacement limits for reinforced concrete columns involves a comprehensive understanding of the interaction between load-bearing capacities, material properties, and the overall structural response. It requires a deep understanding of the factors influencing the deformation behavior of columns, such as concrete strength, reinforcement detailing, column dimensions, and the arrangement of lateral ties. By identifying and analyzing these factors, engineers can

establish more accurate displacement limits that guide the design, assessment, and retrofitting of columns to ensure their optimal performance during seismic events.

Advancements in technology, computational tools, and analytical techniques have opened up new paths for investigating the complex behavior of reinforced concrete columns. Through numerical simulations, experimental studies, and real-world observations, researchers are able to refine the understanding of column performance under various loading conditions. The insights gained from such efforts contribute to the development of guidelines and recommendations for setting displacement limits that find a balance between structural safety, operational functionality, and economic considerations.

1.2 Literature Survey

Özcan and Binici (2023) assessed the plastic rotation capacities of RC columns by using a database containing 196 RC column specimens. Among these, 138 were subjected to biaxial loading and the remaining 58 columns were subjected to uniaxial loading. Majority of the columns had a rectangular cross-section, with only 18 of them having a circular cross-section. After converting the experimental curves of lateral load versus lateral deflection into bilinear representations, the values for yield rotation and plastic rotation were obtained. The results of the experimental dataset were compared with the seismic guidelines ASCE/SEI 41-17, Eurocode 8-3, and TBEC (2018). Based on the findings of this study, the following conclusions can be drawn:

- Predictive safety of ASCE/SEI 41-17 decreased as the confinement ratio increased. In contrast, for Eurocode 8-3 rotation predictions, an opposite trend was observed where predictive safety improved as the confinement ratio increased.
- Among the considered standards, TBEC (2018) exhibited the strictest criteria and the highest level of variability.

- The confinement ratio and axial load ratio were recognized as the primary factors that influence the lateral displacement response of the column.

Erduran and Yakut (2004) examined a wide range of parameters that impact the deformation of RC columns. They carried out this study by using the finite element software ANSYS v6.1. After confirming the accurate representation of the actual behavior in the finite element model, the study proceeded to analyze the impact of various parameters on the deformation capacity of reinforced concrete columns. This was achieved by conducting multiple analyses, changing a single parameter in each case. The main findings derived from this research can be summarized as follows:

- The axial load ratio and transverse reinforcement ratio were identified as the most significant parameters affecting the ultimate ductility of the columns.
- The slenderness ratio and the yield strength of the longitudinal reinforcement were identified as the most significant parameters affecting the yield drift ratio.
- The concrete strength and longitudinal reinforcement ratio significantly impact the load carrying capacity, but they do not significantly affect the deformation characteristics of the reinforced concrete columns.

Acun and Sucuoglu (2010) conducted an experimental study employing twelve full-scale column specimens designed for pure flexural failure. Two standard column designs were used in the tests. The first type represents substandard columns and the second type represents columns conforming to the material and special seismic detailing standards of modern concrete design codes. The axial load ratio remained constant in all specimens except for one. The imposed displacement histories were the experiment's primary variable. The study leads to the following conclusions:

- The deformation-based performance limits suggested for nonconforming columns by Eurocode 8 (2005) were observed to be more tolerant in comparison to ASCE/SEI 41 (2007). However, both codes were considerably cautious in establishing rotation limits for ensuring life safety (significant

damage) and collapse prevention (near collapse) based on the outcomes of the tests.

- When comparing ASCE/SEI 41 (2007) and Eurocode 8 (2005), Eurocode 8 provides more accurate estimations for the performance limits than those offered by ASCE/SEI 41.
- The target drift demands are significantly influenced by the imposed displacement histories; however, the capacity curves are not significantly affected.

Yakut and Solmaz (2012) examined the seismic behavior of reinforced concrete columns analytically using the finite element analysis software OpenSees. Displacement limits based on performance levels were compared with the limits derived from various seismic provisions. They concluded that for the majority of columns, TEC (2007), FEMA 356 (2000), Eurocode 8 (2003), and ASCE/SEI 41 Update (2009) tend to underestimate seismic performance. They also concluded that Eurocode 8 (2003) and ASCE/SEI 41 Update (2009) offer performance limits that are closer compared to TEC (2007) and FEMA 356 (2000).

Vintzileou and Stathatos (2007) analyzed experimental test findings for more than 450 reinforced concrete columns in order to check the efficiency of Eurocode 8 and Greek Code for the Design of RC Structures (EKOS). They have considered various parameters to evaluate the behavior, including factors such as the arrangement of hoops within the cross-section, the effective confinement ratio, and the spacing of hoops relative to the diameter of the longitudinal bars. The primary findings derived from this study are as follows:

- The provisions of current European Codes for Earthquake Resistant Design regarding RC columns are consistent in the sense that columns that observe the code provisions exhibit a cyclic behavior which conforms to the expected one.
- The main factor influencing the cyclic behavior of columns is the arrangement of hoops within the section.

- The constraints set by the codes, such as axial force limits, normalized spacing of hoops relative to longitudinal bar diameter, and minimum effective confinement ratio, are effective. These parameters significantly impact the behavior of columns.

Ozdemir et al. (2017) analyzed a total of 69 experimental columns, selected from the PEER Structural Performance Database, using the finite element analysis program ANSYS. Their primary focus was to assess the accuracy of the current damage limits given in the seismic guidelines. Based on the findings of this study, the following conclusions can be drawn:

- In general, plastic rotation proves to be a more reliable and predictable factor compared to concrete's ultimate strain.
- For ASCE/SEI 41-13, the calculated results are generally on the safe side when it comes to plastic rotation limits, except for columns with high axial loads or made from high-strength concrete.
- 73% of the RC column specimens fall into the unsafe category with respect to the chord rotation angle when considering Eurocode 8 limit states.

Panagiotakos and Fardis (2001) used a database including more than 1000 tests, mainly cyclic, conducted on specimens that represent various types of reinforced concrete (RC) members such as beams, columns, and walls. The objective was to develop equations that capture the deformations of RC members at the stages of yielding or ultimate failure. The study's findings lead to the following conclusions:

- The deformability of a member greatly depends on the ductility of the steel used. When using brittle cold-worked steel, the member's ability to deform is reduced by almost half.
- The effects of bond-slip contribute to an increase in deformability by an average of about 40%, especially under cyclic loading.

- The deformation capacity reduces in an almost linear manner with axial load, dropping to around 50% of its value at zero-load when reaching the balance load.

Lam et al. (2003) conducted an experimental study involving nine square-shaped column specimens. These specimens possessed characteristics such as low-lateral confinement, a shear span varying from low to moderate, and high axial loads. The transverse reinforcement detailing included both 90° and 135° hooks. They have found that:

- Specimens with low shear span exhibited brittle shear failures, while those with moderate shear span and a lateral confinement ratio of 0.003 showed flexural failures.
- The level of lateral confinement significantly impacted the ultimate drift, with an increase from 0.001 to 0.003 potentially doubling the ultimate drift capacity.
- The usage of 90° hooks, instead of 135°, in transverse reinforcement detailing led to a 40% reduction in ultimate drift capacity

Elwood and Moehle (2005), conducted a study where they used a database consisting of 50 shear-critical columns. Their aim was to derive an empirical equation for drift capacity. The newly developed model for drift capacity highlights the key factors that have the most significant impact on shear-critical column drift capacity, specifically, transverse reinforcement ratio, shear stress demand, and the axial load ratio. Ghannoum and Matamoros (2014) used a database containing 490 pseudo-static tests conducted on reinforced concrete columns. Their objective was to establish relationships for nonlinear modeling parameters that define the lateral force-deformation behavior of these columns during seismic activity. They determined that the significant parameters for both rectangular and circular columns include the axial load ratio, the transverse reinforcement ratio, and the ratio V_y/V_o.

1.3 Objective and Scope

Understanding how RC columns respond to events like earthquakes is quite complex. Seismic guidelines set limits on how much they can deform based on various parameters. While experimental test results are very important, they do not always show how one factor affects column behavior by itself. This is why both experimental tests and computer-based analyses are needed in order to accurately figure out the performance-based deformation limits of RC columns.

The main objectives of this study are as follows:

- Collecting an experimental database to investigate the performance-based deformation limits of RC columns.
- Comparing the limits obtained from experimental results with seismic guidelines and assessing their accuracy in estimating the performance limits of RC columns.
- Utilizing the OpenSees software, calibrated with the experimental database, to conduct analytical investigations into the performance limits of RC columns.
- Investigating the effects of important parameters such as axial load ratio, transverse reinforcement ratio, concrete compressive strength, and yielding strength of the longitudinal steel on the capacity curves and rotation capacities of RC columns.
- Assessing whether the existing guidelines accurately account for the influence of these parameters on the performance limits.
- Comparing the limits found from the analytical results with the current seismic guidelines and examining their safeties.
- Examining how the axial load ratio and transverse reinforcement ratio impact the predictive safety of performance limits given in seismic guidelines.

Chapter 2 focuses on collecting the experimental database and investigating it. Pacific Earthquake Engineering Research Center's (PEER) Structural Performance Database is used for selecting the experimental column specimens. The experimental results are analyzed to find the limits for Immediate Occupancy, Life Safety, and Collapse Prevention. These limits are then compared with the limits set by the guidelines, Turkish Building Earthquake Code (2018), ASCE/SEI 41-17 (2017), and Eurocode 8-3 (2010).

In Chapter 3, OpenSees software is used to create 3072 unique columns by considering a combination of various different parameters. The accuracy of OpenSees model is verified by using 37 experimental column specimens from the PEER database and the result of portal frame experiment that was conducted at METU Structural Mechanics Laboratory. Effect of each parameter on the capacity curve and rotational capacity is examined. The performance limits obtained from the analytical studies are compared with the seismic guidelines. Effect of axial load ratio and transverse reinforcement ratio on the predictive safety of performance limits given in the seismic guidelines is examined.

In Chapter 4, the summary of the findings is presented with the conclusion.

CHAPTER 2

EVALUATION OF THE RC COLUMNS FROM THE EXPERIMENTAL DATABASE

2.1 Introduction

The Pacific Earthquake Engineering Research (PEER) Center's Structural Performance Database was created to offer academics the necessary data to investigate seismic performance of RC columns. As of January 2004, the database includes 253 tests of rectangular RC columns and 163 tests of spiral RC columns. For each test, the database offers essential information, including force-displacement histories, material properties for concrete and steel, test geometry, reinforcing details, loading, maximum shear force, yield displacement, and ultimate displacement.

Among the 253 rectangular RC columns, the ones with concrete compressive strength larger than 70 MPa and section width and depth less than 200 mm are eliminated and the rest, 186 rectangular RC columns, are chosen for evaluation. Geometric and material properties of each column can be found in Appendix A. In Figure 2.1 the histograms of the key column properties are presented. The y-axis represents the number of specimens, and the x-axis represents properties such as axial load ratio, transverse reinforcement ratio (ρ_t), longitudinal reinforcement ratio (ρ_l), yielding strength of longitudinal reinforcement (f_{yl}), yielding strength of transverse reinforcement (f_{yw}), slenderness ratio (L/d), concrete compressive strength (f_c), effective depth (d).

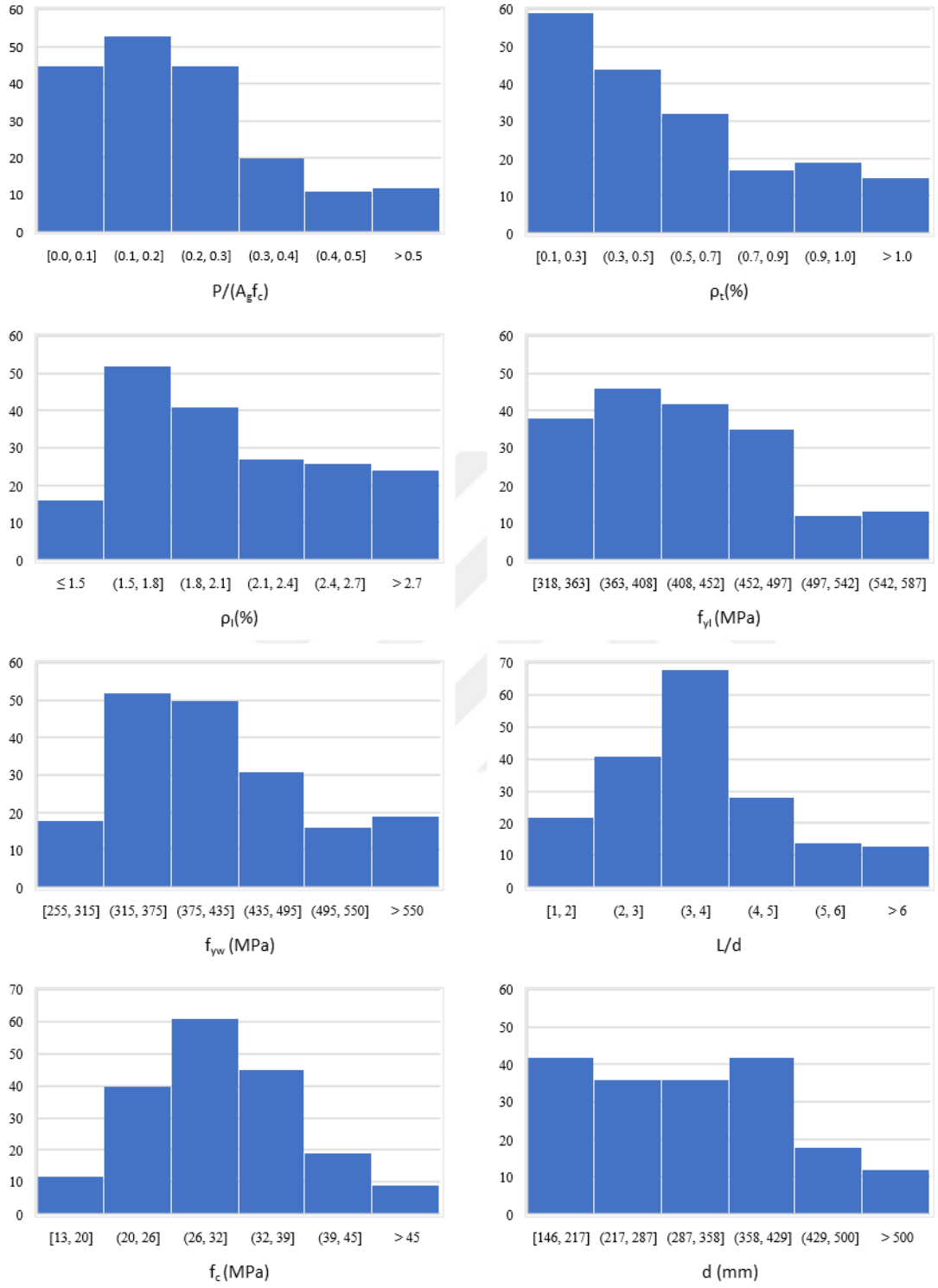

Figure 2.1 Distribution of the Material and Geometric Properties of the 186 Experimental Tests

2.2 Estimated Performance Limits of the Selected Columns

The PEER database provides the yield and ultimate displacements of each test. While calculating the rotation capacities from the given displacements, lumped plasticity idealization is used as shown in Figure 2.2. Plastic hinge length (L_p) is taken as half of the section height. The yield and plastic rotations are calculated using Equations 2.1-2.5

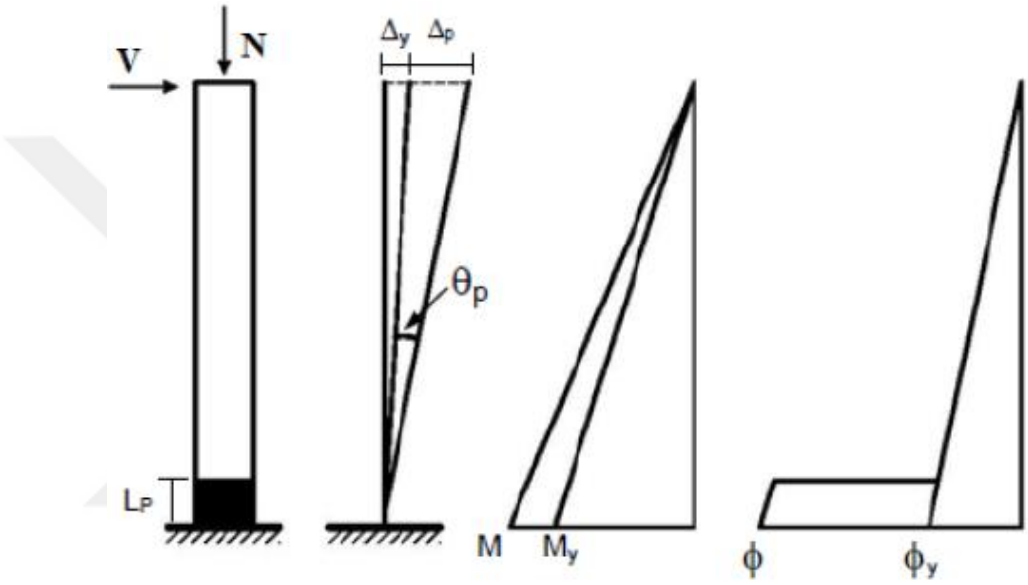

Figure 2.2 Lumped plasticity idealization of a cantilever (Ozmen et. al. (2007).

For yield rotation:

$$\triangle_y = \frac{\emptyset_y L^2}{3} \quad \text{Eq 2.1}$$

$$\theta_y = \frac{\emptyset_y L}{2} \quad \text{Eq 2.2}$$

For plastic rotation:

$$\triangle_p = \left(\emptyset_u - \emptyset_y\right) L_p \left(L - \frac{L_p}{2}\right) \quad \text{Eq 2.3}$$

$$\theta_p = \left(\emptyset_u - \emptyset_y\right) L_p \quad \text{Eq 2.4}$$

$$\theta_u = \theta_y + \theta_p \quad \text{Eq 2.5}$$

Where;

$\triangle_y$, $\triangle_p$: Yield displacement and plastic displacement, respectively

$\emptyset_y$, $\emptyset_u$: Yield and ultimate curvature, respectively

L, L_p: Column length and plastic hinge length, respectively

θ_y , θ_p , θ_u: Yield rotation, plastic rotation, and ultimate rotation, respectively

2.3 Application of Seismic Assessment Guidelines to the Selected Columns

2.3.1 General

For this study, three seismic assessment guidelines are examined. These are Turkish Building Earthquake Code (TBEC (2018)), ASCE/SEI 41-17 (2017), and Eurocode 8 Part 3 (2010).

The Turkish Building Earthquake Code (TBEC (2018)) is a comprehensive set of regulations and standards produced by the Turkish government to guarantee that buildings and structures in Turkey are built in a way that minimizes the danger caused by earthquakes. Given Turkey's location in a seismically active region where earthquakes are a major natural hazard, this code is crucial in improving the seismic resilience of the structures. The code considers the possible effects of various levels of seismic activity and sets guidelines for building type structures, including residential buildings, commercial complexes, and infrastructure.

ASCE/SEI 41-17 refers to the American Society of Civil Engineers/Structural Engineering Institute standard titled "Seismic Evaluation and Retrofit of Existing Buildings." It is a widely recognized guideline that provides procedures and criteria for the seismic assessment and retrofitting of existing structures to improve their earthquake resistance. The main objective of ASCE/SEI 41-17 is to establish procedures for assessing the seismic vulnerability of older structures, especially those designed before modern seismic design codes. It defines various

methodologies for assessing the structural integrity and seismic resistance of existing buildings, as well as retrofitting techniques to improve their performance during earthquakes.

Eurocode 8 Part 3 is a specific part of the European standard EN 1998 that deals with the design of earthquake-resistant structures. It focuses on the assessment and retrofitting of existing structures to improve their seismic performance and provides guidelines for evaluating the seismic vulnerability of existing structures and determining the necessary retrofitting measures to improve their earthquake resistance.

2.3.2 Application of TBEC (2018)

In TBEC (2018), three damage states and their corresponding limits are defined for ductile members at the cross-section level. These states are Limited Damage (LD), Controlled Damage (CD), and Collapse Prevention (CP). Limited Damage represents a restricted amount of behavior beyond the elastic range, Controlled Damage refers to behavior beyond elastic range where section strength can still be safely sustained, and Collapse Prevention signifies advanced behavior beyond elastic range at the section (Figure 2.3).

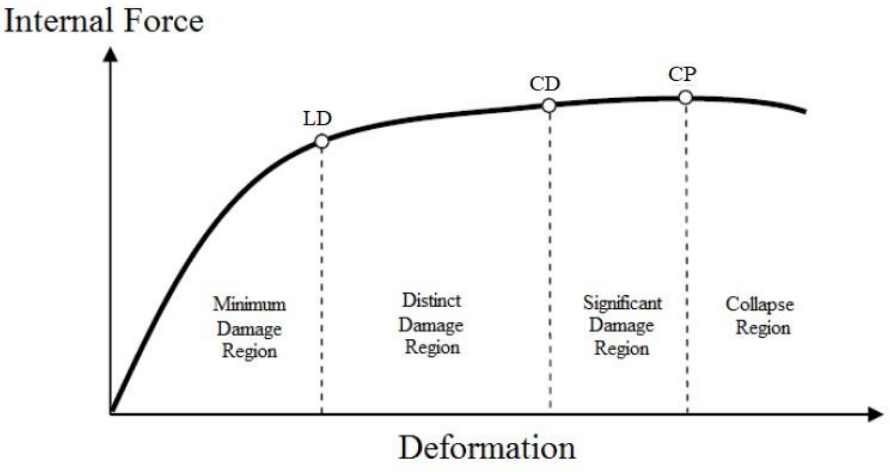

Figure 2.3 Damage Levels According to TBEC (2018)

For rectangular RC columns, concrete strain limit at CP is given as:

$$\varepsilon_c^{(CP)} = 0.0035 + 0.04\sqrt{\omega_{we}} \leq 0.018 \quad \text{Eq. 2.6}$$

In this equation, ω_{we} represents the mechanical reinforcement ratio of the effective transverse reinforcement and can be calculated as given in Equation 2.7.

$$\omega_{we} = \alpha_{se}\rho_{sh,min}\frac{f_{yw}}{f_c} \quad \text{Eq. 2.7}$$

Here, f_{yw} is the yield strength of the transverse reinforcement, α_{se} represents the confinement effectiveness coefficient, $\rho_{sh,min}$ represents the minimum volumetric transverse reinforcement ratio in the two horizontal directions for a rectangular section, and they can be found as follows:

$$\alpha_{se} = (1 - \frac{\sum a_i^2}{6b_o h_o})(1 - \frac{s}{2b_o})(1 - \frac{s}{2h_o}) \quad \text{Eq. 2.8}$$

$$\rho_{sh} = \frac{A_{sh}}{b_k s} \quad \text{Eq. 2.9}$$

Where;

A_{sh}: The cross-sectional area of transverse reinforcement in the considered direction.

b_k: The core dimension in the perpendicular direction (distance between the outermost transverse reinforcement axes).

s: The spacing of transverse reinforcement in the considered direction.

b_o and h_o: The dimensions of the confined concrete measured from the axes of the spiral reinforcement.

a_i: The distance between the axes of the longitudinal reinforcements supported by a stirrup or a tie.

For rectangular RC columns, steel strain limit at CP is given as:

$$\varepsilon_s^{(CP)} = 0.4\varepsilon_{su} \quad \text{Eq. 2.10}$$

Here, ε_{su} is the ultimate strain of steel.

The plastic rotation limit at CP is given as:

$$\theta_p^{(CP)} = \frac{2}{3}\left[\left(\emptyset_u - \emptyset_y\right)L_p\left(1 - 0.5\frac{L_p}{L_s}\right) + 4.5\emptyset_u d_b\right] \quad \text{Eq. 2.11}$$

Here ϕ_y is the yield curvature, where the tension reinforcement has yielded. ϕ_u is the ultimate curvature, where the reinforcement fails or concrete crushes, whichever happens first. L_p is the plastic hinge length, and it is taken as half of the section dimension in the direction of interest and L_s is the shear span. d_b is the diameter of the tension reinforcement.

For rectangular RC columns, limits for steel strain, concrete strain and plastic rotation at CD are given as:

$$\varepsilon_c^{(CD)} = 0.75\varepsilon_c^{(CP)}\ ;\ \varepsilon_s^{(CD)} = 0.75\varepsilon_s^{(CP)}\ ;\ \theta_p^{(CD)} = 0.75\theta_p^{(CP)} \quad \text{Eq. 2.12}$$

For rectangular RC columns, limits for steel strain, concrete strain and plastic rotation at LD are given as:

$$\varepsilon_c^{(LD)} = 0.0025\ ;\ \varepsilon_s^{(LD)} = 0.0075\ ;\ \theta_p^{(LD)} = 0 \quad \text{Eq. 2.13}$$

The yield rotation can be calculated as follows:

$$\theta_y = \frac{\phi_y L_s}{3} + 0.0015\eta\left(1 + 1.5\frac{h}{L_s}\right) + \frac{\emptyset_y d_b f_y}{8\sqrt{f_c}} \quad \text{Eq. 2.14}$$

For beams and columns, η is taken as 1, for shear walls, η is taken as 0.5. h is the section height. The parameter d_b is the diameter of the reinforcing steel bars. f_c and f_y represent the compressive strength of concrete and the yield strength of the reinforcing steel, respectively.

To find the yield curvature and the ultimate curvature, section analysis must be done. In Chapter 5 of TBEC (2018), material models for steel and concrete are given to use in the section analysis. The material model for confined and unconfined concrete is given in Figure 2.4.

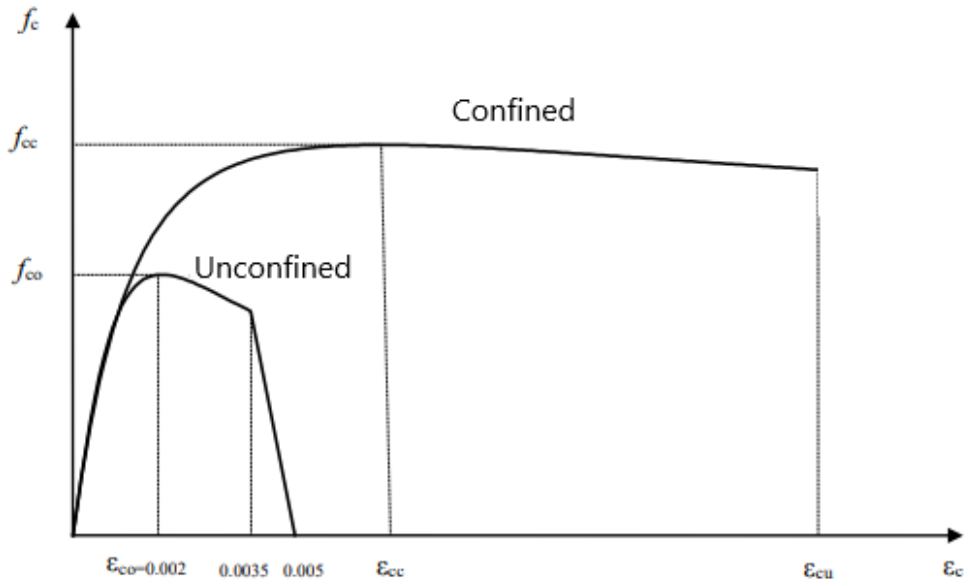

Figure 2.4 Material model for confined and unconfined concrete according to TBEC (2018)

The relationship between the confined concrete strength f_{cc} and the unconfined concrete strength f_{co} is provided as follows:

$$f_{cc} = \lambda_c f_{co} \;\; ; \;\; \lambda_c = 2.254\sqrt{1 + 7.94\frac{f_e}{f_{co}}} - 2\frac{f_c}{f_{co}} - 1.254 \qquad \text{Eq. 2.15}$$

For rectangular cross sections f_e is:

$$f_{ex} = k_e \rho_x f_{yw} \;\; ; \;\; f_{ey} = k_e \rho_y f_{yw} \;\; ; \;\; f_e = (f_{ex} + f_{ey})/2 \qquad \text{Eq. 2.16}$$

In Equation 2.16 k_e is the confinement effectiveness coefficient and it can be calculated as:

$$k_e = \left(1 - \frac{\sum a_i^2}{6 b_o h_o}\right)\left(1 - \frac{s}{2b_o}\right)\left(1 - \frac{s}{2h_o}\right)\left(1 - \frac{A_s}{b_o h_o}\right)^{-1} \qquad \text{Eq. 2.17}$$

Where a_i is the distance between the axes of longitudinal reinforcements, b_o and h_o denote the dimensions of the core concrete that are encased by the stirrups' axes, s is the stirrup spacing, and A_s is the area of longitudinal reinforcement.

The compressive concrete stress f_c is given by:

$$f_c = \frac{f_{cc}\, x\, r}{r-1+x^r} \qquad \text{Eq. 2.18}$$

In Equation 2.18, x and r can be found as:

$$x = \frac{\varepsilon_c}{\varepsilon_{cc}} \;;\; \varepsilon_{cc} = \varepsilon_{co}[1 + 5(\lambda_c - 1)] \;;\; \varepsilon_{co} \cong 0.002 \qquad \text{Eq. 2.19}$$

$$r = \frac{E_c}{E_c - E_{sec}} \;;\; E_c \cong 5000\sqrt{f_{co}}\,[MPa] \;;\; E_{sec} = \frac{f_{cc}}{\varepsilon_{cc}} \qquad \text{Eq. 2.20}$$

The material model for steel is given in Figure 2.5.

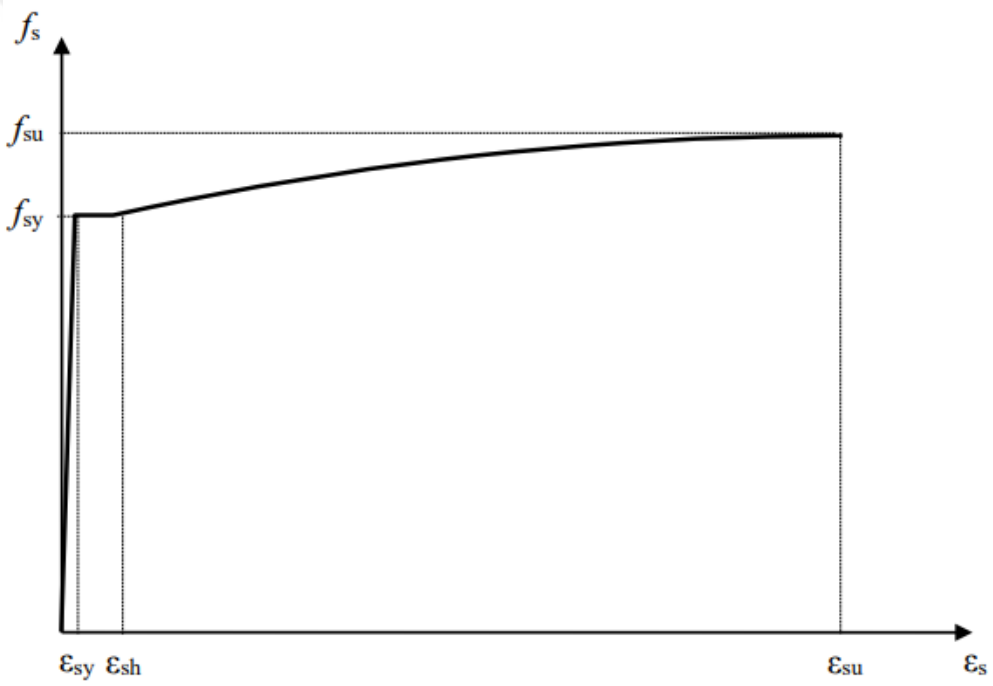

Figure 2.5 Material model for steel according to TBEC (2018)

In the PEER database, strain at hardening and ultimate strain for steel is not given. In TBEC (2018) ε_{sh} and ε_{su} are given for S420 and S220 steel. For S220, ε_{sh} = 0.011 and ε_{su} = 0.12; and for S420, ε_{sh} = 0.008 and ε_{su} = 0.08. In the section analysis, if the yield strength of longitudinal steel is larger than 320 MPa, the strain values for S420

steel are used, and if the yield strength is smaller than 320 MPa, the strain values for S220 steel are used.

According to Chapter 15 of TBEC (2018), the upper limits of deformation must be multiplied with a reduction coefficient depending on the shear force ratio, $V_e / (b_w d f_{ctm})$, that the section is exposed to. Here, V_e is the design shear force, b_w is the width of the section, d is the effective depth, and f_{ctm} is the tensile strength of the concrete. If the shear force ratio is less than 0.65, the upper limits obtained from the previous equations are applicable. If the shear force ratio is greater than 1.30, the calculated deformation limits will be reduced by multiplying them by 0.50. Linear interpolation will be used for intermediate values.

While evaluating the experimental tests, three limits are defined. Immediate Occupancy is taken as the beginning of the plastic deformation ($\theta^{(LD)} = \theta_y$), Life Safety is defined as the chord rotation where 75 percent of plastic rotation capacity is reached ($\theta^{(CD)} = \theta_y + 0.75\theta_p$), and Collapse Prevention is taken as the ultimate rotation capacity ($\theta^{(CP)} = \theta_y + \theta_p$).

Performance limits of each column is determined according to TBEC (2018) and can be found in Appendix A. The comparison of performance limits calculated by TBEC (2018) and observed by experimental results can be seen in Figure 2.6. Detailed comments about the graphs will be provided in the next chapter.

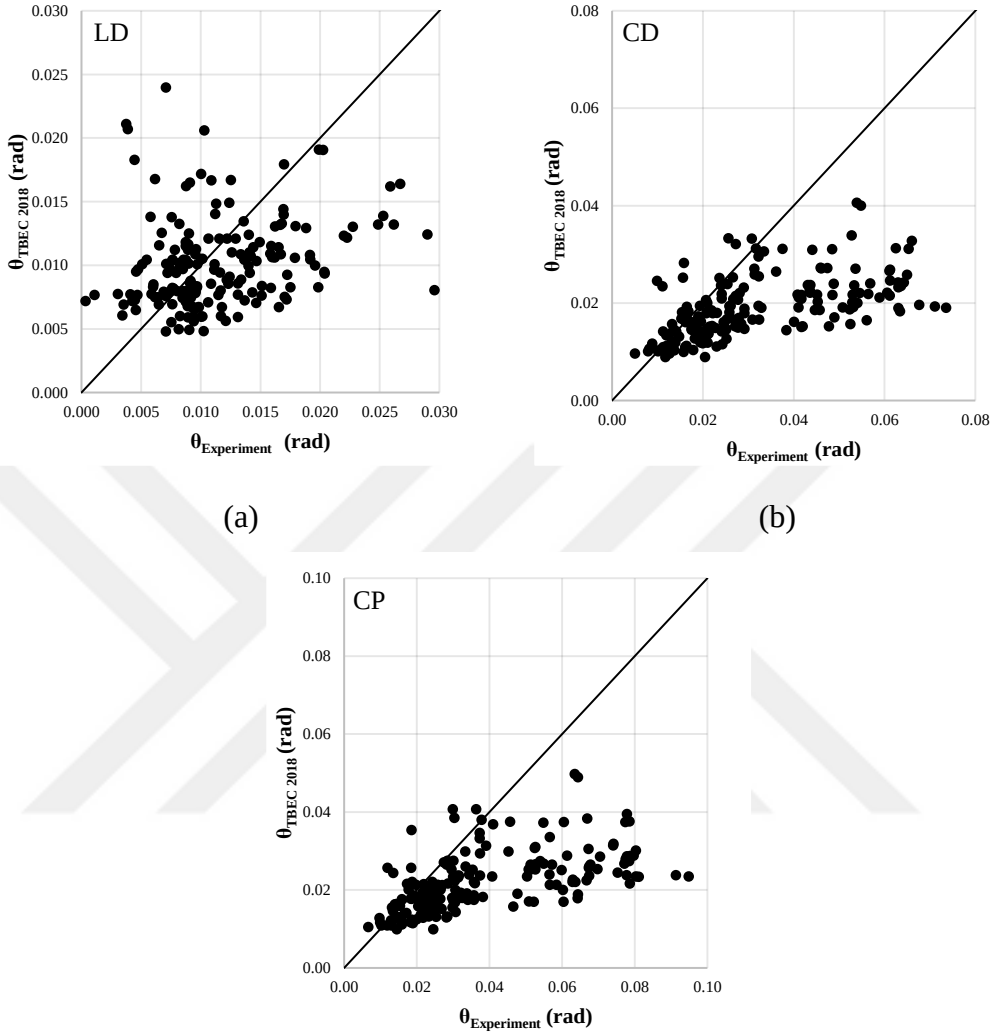

Figure 2.6 Comparison of experimental and TBEC results for (a) Limited Damage; (b) Controlled Damage; (c) Collapse Prevention.

2.3.3 Application of ASCE/SEI 41-17 (2017)

ASCE/SEI 41-17 provides three performance levels, Immediate Occupancy (IO), Life Safety (LS), and Collapse Prevention (CP). In Immediate Occupancy, structures

are expected to remain functional during and after an earthquake with no structural damage that affects the building's integrity. Structures designed to meet the Life Safety performance level are intended to prevent collapse and avoid life-threatening injuries during an earthquake. Limited structural and non-structural damage may occur, but the structure should retain enough strength to prevent significant structural failure. Buildings designed to meet the Collapse Prevention performance level aim to prevent total or partial collapse during an earthquake. Although significant damage may occur, the structural integrity should be preserved. The plastic rotation limits for these performance levels can be found in Table 2.1.

Table 2.1. Rotation limits for rectangular RC columns (ASCE/SEI)

Modeling Parameters	**Acceptance Criteria**		
	Plastic Rotation Angle (radians)		
	Performance Level		
Plastic Rotation Angles, *a* and *b* (radians) **Residual Strength Ratio, *c***	**IO**	**LS**	**CP**
Columns not controlled by inadequate development or splicing along the clear height[a] $a = \left(0.042 - 0.043\frac{N_{UD}}{A_g f'_{cE}} + 0.63\rho_t - 0.023\frac{V_{yE}}{V_{ColOE}}\right) \geq 0.0$ $For\ \frac{N_{UD}}{A_g f'_{cE}} \leq 0.5 \begin{cases} b = \frac{0.5}{5 + \frac{N_{UD}}{0.8 A_g f'_{cE}} \frac{1}{\rho_t} \frac{f'_{cE}}{f_{ytE}}} - 0.01 \geq a^a \end{cases}$ $c = 0.24 - 0.4\frac{N_{UD}}{A_g f'_{cE}} \geq 0.0$	0.15 *a* ≤ 0.005	0.5 b^b	0.7 b^b

[a] The parameter b should be gradually decreased linearly for $\frac{N_{UD}}{A_g f_{cE}}$ values greater than 0.5, starting from its value at $\frac{N_{UD}}{A_g f_{cE}} = 0.5$ and reaching zero at $\frac{N_{UD}}{A_g f_{cE}} = 0.7$. However, b must not be less than the value of a.

[b] $\frac{N_{UD}}{A_g f_{cE}}$ must not be taken as smaller than 0.1.

Where N_{UD} is the axial force on the column, A_g is the gross area of the column, f_{cE} is the concrete compressive strength, ρ_t is the transverse reinforcement ratio, V_{yE} is the effective yield strength of the building, V_{ColOE} is the shear capacity of the column and can be calculated as follows;

$$V_{Col} = \alpha_{Col} \frac{A_{sh} f_{yw} d}{s} + \left(\frac{0.5\sqrt{f_c}}{L/d} \sqrt{1 + \frac{N}{0.5 A_g \sqrt{f_c}}} \right) 0.8 A_g \quad \text{Eq. 2.21}$$

Here, s is stirrup spacing, A_{sh} is the total area of transverse reinforcement, f_{yw} is the yield strength of the transverse reinforcement, d is the effective depth and α_{col} is equal to 1 if s/d is less than 0.75, 0 if s/d is greater than 1, and varies linearly in between.

In Table 2.1 the value of ρ_t must not exceed 0.0175 in all scenarios, and it should also not exceed 0.0075 when the ties are not adequately anchored within the core. The equations provided in the table are not applicable to columns where ρt is less than 0.0005. The value of V_{yE}/V_{ColOE} should not be taken smaller than 0.2.

Yield rotation can be found as follows:

$$\theta_y = \frac{M_y L}{3(EI)_{eff}} \quad \text{Eq 2.22}$$

$$\frac{EI_{eff}}{EI_g} = \begin{cases} 0.3, & n \leq 0.1 \\ n + 0.2, & 0.1 < n < 0.5 \\ 0.7, & n \geq 0.5 \end{cases} \quad \text{Eq 2.23}$$

Where n is the axial load ratio.

While evaluating the experimental tests, three limits are defined. Immediate Occupancy is taken as 15 percent of the plastic deformation ($\theta^{(IO)} = \theta_y + 0.15\theta_p$), Life Safety is defined as the chord rotation where 75 percent of plastic rotation capacity is reached ($\theta^{(LS)} = \theta_y + 0.75\theta_p$), and Collapse Prevention is taken as the ultimate rotation capacity ($\theta^{(CP)} = \theta_y + \theta_p$).

The comparison of safety limits calculated by ASCE/SEI and observed by experimental results can be seen in Figure 2.7. Performance limits of each column is determined according to ASCE/SEI can be found in Appendix A. Detailed comments about the graphs will be provided in the next chapter.

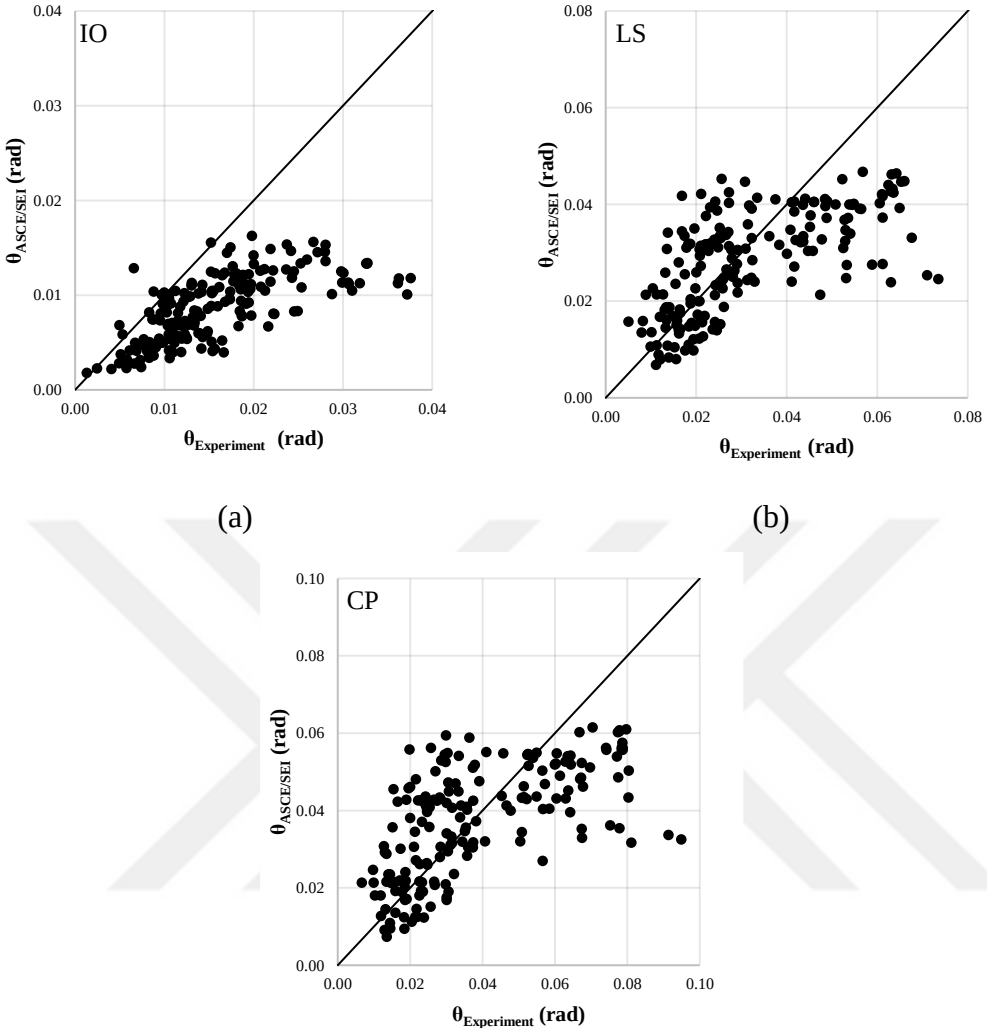

(a) (b)

(c)

Figure 2.7 Comparison of experimental and ASCE/SEI results for (a) Immediate Occupancy; (b) Life Safety; (c) Collapse Prevention.

2.3.4 Application of Eurocode 8 – Part-3 (2010)

Eurocode 8 - Part 3 (EN 1998-3) is titled "Design of structures for earthquake resistance - Assessment and retrofitting of buildings". This part of Eurocode 8 provides guidelines for the seismic assessment and retrofitting of existing buildings to improve their earthquake resistance. It covers procedures and methods for

evaluating the seismic performance of buildings, identifying deficiencies, and comparing their capacity to withstand seismic forces with the expected demand during an earthquake. EN 1998-3 also offers guidance on selecting appropriate retrofitting measures, such as adding shear walls, increasing stiffness, or improving connections between structural elements, to enhance the building's seismic performance and reduce risks. Three damage states are defined for the assessment of existing structures. These states are Near Collapse (NC), Significant Damage (SD), and Damage Limitation (DL).

Limit State of Near Collapse (NC):

The total chord rotation ($\theta_p + \theta_y$) of concrete members subjected to cyclic loading at the ultimate state, θ_u, can be determined using the following formula:

$$\theta_u = \frac{1}{\gamma_{el}} 0.016(0.3^{\nu}) \left[\frac{\max(0.01;\omega')}{\max(0.01;\omega)} f_c\right]^{0.225} \left(\min\left(9;\frac{L_s}{h}\right)\right)^{0.35} 25^{\left(\alpha\rho_{sx}\frac{f_{yw}}{f_c}\right)} \quad \text{Eq. 2.24}$$

Here, γ_{el} is equal to 1.5 for primary seismic elements and to 1.0 for secondary seismic elements, h is the depth of cross-section, L_s is the shear span, ν is equal to $N / (bhf_c)$, ω and ω' are the mechanical reinforcement ratio of the tension and compression reinforcement respectively, f_c is the concrete compressive strength, f_{yw} is the stirrup yield strength, ρ_{sx} is transverse reinforcement ratio, α is the confinement effectiveness factor.

Limit State of Significant Damage (SD):

The chord rotation capacity corresponding to significant damage θ_{SD} is equal to 75 percent of the ultimate chord rotation θ_u.

$$\theta_{SD} = 0.75\ \theta_u \quad \text{Eq. 2.25}$$

Limit State of Damage Limitation (DL):

The capacity considered for DL is defined as the chord rotation at yielding θ_y, calculated as follows:

$$\theta_y = \phi_y \frac{L_s + a_v z}{3} + 0.0014\left(1 + 1.5\frac{h}{L_s}\right) + \frac{\emptyset_y d_b f_y}{8\sqrt{f_c}} \qquad \text{Eq. 2.26}$$

While evaluating the experimental tests, three limits are defined. Damage Limitation is taken as the beginning of the plastic deformation ($\theta^{(DL)} = \theta_y$), Significant Damage is defined as the chord rotation where 75 percent of ultimate rotation capacity is reached ($\theta^{(SD)} = 0.75\theta_y + 0.75\theta_p$), and Near Collapse is taken as the ultimate rotation capacity ($\theta^{(NC)} = \theta_y + \theta_p$).

The comparison of safety limits calculated by Eurocode 8-3 and observed by experimental results can be seen in Figure 2.8. Performance limits of each column is determined according to Eurocode 8 can be found in Appendix A. Detailed comments about the graphs will be provided in the next chapter.

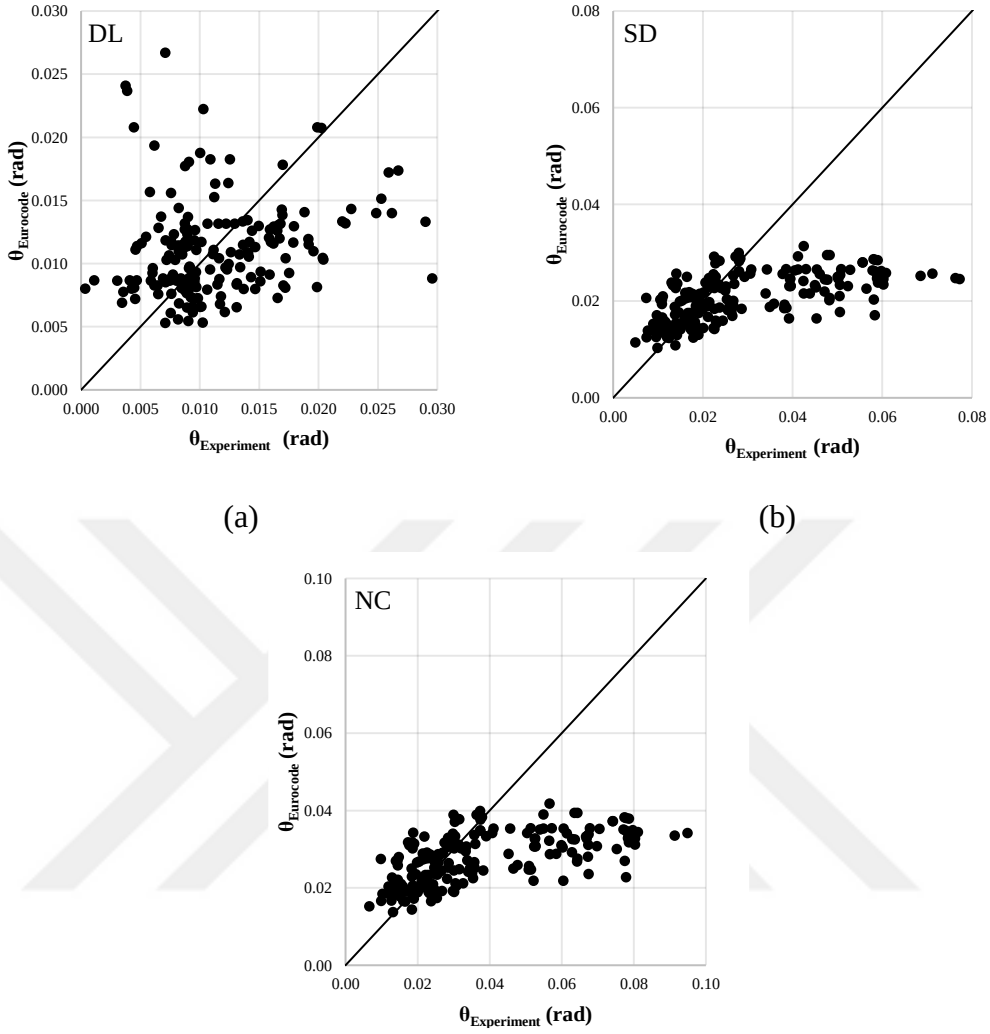

(a) (b)

(c)

Figure 2.8 Comparison of experimental and Eurocode 8 results for (a) Damage Limitation; (b) Significant Damage; (c) Near Collapse.

CHAPTER 3

OPENSEES MODELING AND PARAMETRIC STUDY

3.1 General

Reinforced concrete columns play a crucial role in providing vertical load-bearing capacity and maintaining structural stability. However, their performance during seismic events becomes a critical concern, requiring a comprehensive understanding of their behavior under varying conditions. This chapter explores the detailed analysis of seismic behavior of RC columns, examining how various important parameters impact their performance. Several parameters influence seismic performance of RC columns and determine how they respond to seismic forces. As a result, it becomes crucial to accurately represent the influence of these parameters in a dependable model.

An effective tool in earthquake engineering simulation is the Open System for Earthquake Engineering Simulation (OpenSees), an advanced computer program created by the Pacific Earthquake Engineering Research Center. Using the PEER database, a dataset containing 37 columns is selected for analysis. By employing analytical tests in OpenSees, the main aim is to find the most reliable and precise model for understanding how these columns react to seismic forces. A core strategy to achieve this goal involves conducting pushover analyses, which produce capacity curves offering a deep understanding of how the columns handle progressively higher loads.

3.2 Structural Elements

Structural elements in OpenSees refer to the components that are used to model different parts of a structure, such as beams, columns, braces, and walls. These elements allow engineers to represent the behavior of real-world structural members within the numerical simulation environment of OpenSees. OpenSees provides various types of structural elements that can be used to model different behaviors and interactions. These elements are essential for creating accurate representations of the complex behavior of structures under various loading conditions.

The “forceBeamColumn” element in OpenSees is a non-linear structural element designed to model the behavior of beam-column members. The “forceBeamColumn” element considers both axial and flexural deformations, allowing it to capture the complex interactions that occur in real-world structural members. This element allows the user to define both distributed plasticity and concentrated plasticity. For this study, concentrated plasticity at the end of the element is defined by using the “HingeRadau” command. Plastic hinge length is taken as half of the section height.

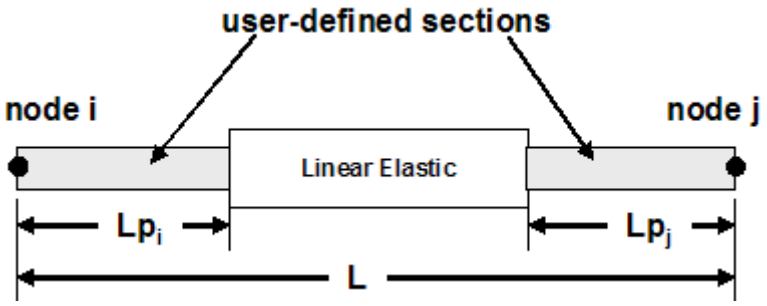

Figure 3.1 "forceBeamColumn" element with concentrated plasticity

Fiber section is used for the analysis. Fiber analysis plays a key role in accurately representing the behavior of different sections within the structural elements. A fiber corresponds to a small section of a structure's cross-sectional area. This approach lets the user to define various material properties and characteristics for each fiber. By

considering the combination of these fibers, the model can accurately predict how the structural element as a whole will respond to different conditions and loads. Essentially, it's a way to break down a complex section into smaller parts, which together provide a detailed picture of the structure's behavior. For confined and unconfined concrete, “patch” command is used to divide the section into rectangular fibers; and for steel, “layer” command is used to create a number of fibers along a line.

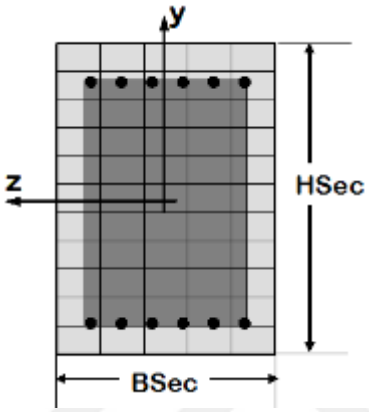

Figure 3.2 Fiber section in OpenSees

3.3 Material Models

3.3.1 Material Model for Concrete

For both confined and unconfined concrete, “Concrete01” is used which is a uniaxial Kent-Scott-Park concrete material with zero tensile strength. Stress-strain relationship for “Concrete01” is shown in Figure 3.3. Also “MinMax” material object is used which lets the user to define a threshold value so that if the material strain passes the defined “Max” value, the material is assumed to have failed.

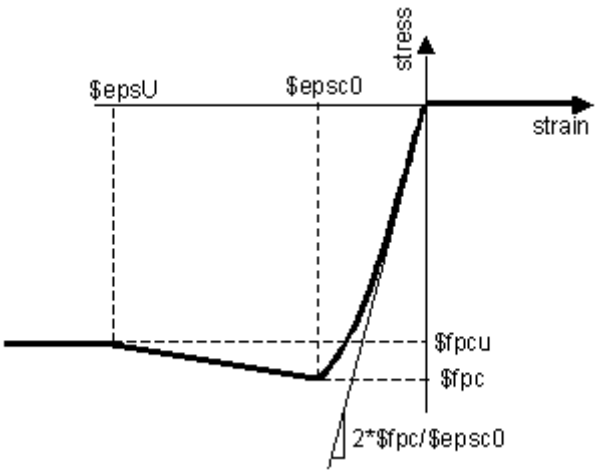

Figure 3.3 Stress-strain relationship for "Concrete01"

The input parameters for this model are concrete compressive strength (f_c), concrete strain at maximum strength (ε_{co}), concrete crushing strength (f_{cu}), concrete strain at crushing strength (ε_{cu}). For confined concrete, these parameters are calculated using Equation 2.15, Equation 2.19, Equation 2.18, Equation 2.6, respectively.

3.3.2 Material Model for Steel

For steel, “Steel01” is used which is a uniaxial bilinear material object. Stress-strain relationship for “Steel01” is shown in Figure 3.4. Again, “MinMax” material object is defined at ultimate strain of steel which is taken as ε_{su} = 0.12 for S220, ε_{su} = 0.08 for S420.

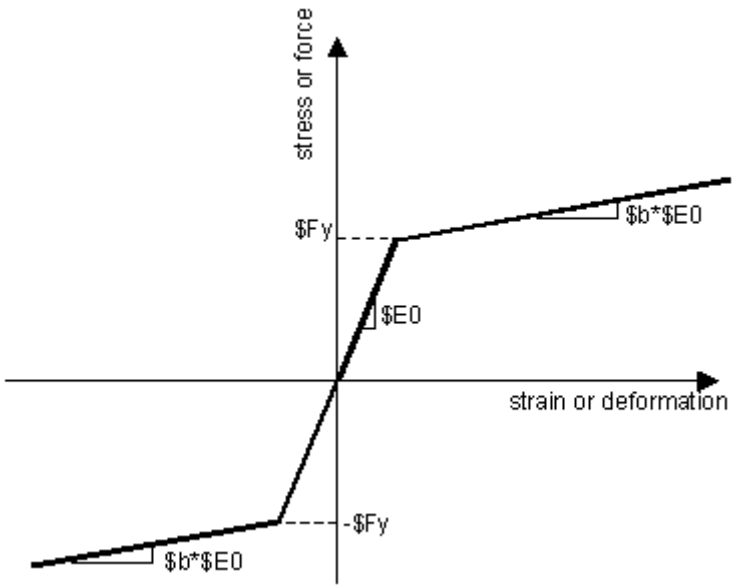

Figure 3.4 Stress-strain relationship for "Steel01"

3.4 Modeling of Bond Slip

Bond slip is a crucial phenomenon that plays a significant role in the behavior of RC columns. In RC columns, the interaction between the concrete and the reinforcing steel bars is critical for ensuring the structural integrity and load-carrying capacity of the column. Bond slip refers to the relative movement between the concrete and the steel reinforcement as the column is subjected to axial loads, bending moments, or lateral forces.

The concept of bond slip comes from the fact that the bond between the concrete and the steel reinforcement is not perfect. As the column experiences various forces, the steel bars embedded in the concrete may elongate or shorten due to the applied loads. However, the concrete surrounding the bars resists this movement, leading to a differential displacement between the steel and the concrete. This difference in displacement between the two materials is referred to as bond slip (Figure 3.5).

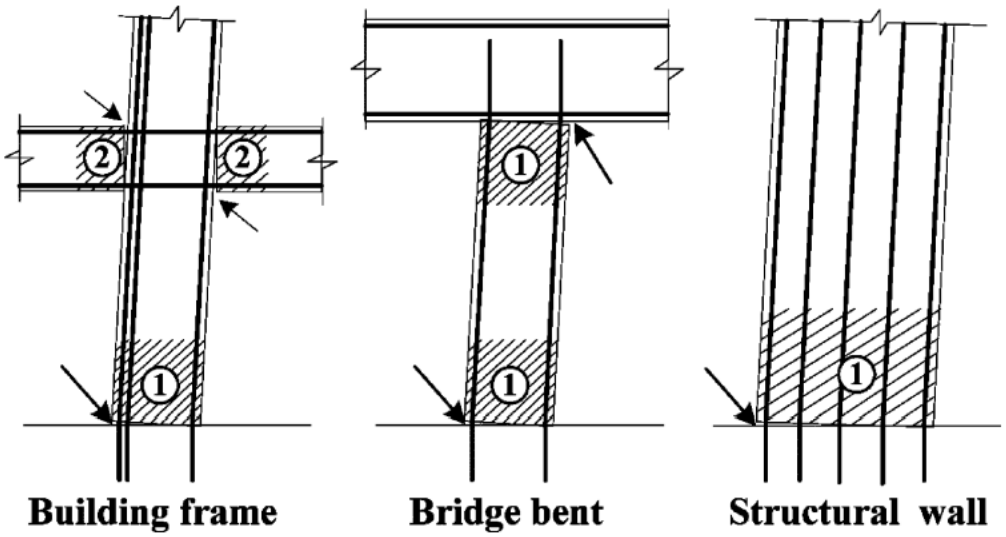

Figure 3.5 Reinforcement slip at building frame, bridge bent, and structural wall

Neglecting the consideration of reinforcement slip in nonlinear analyses of concrete structures will lead to a notable underestimation of deflection while overestimating stiffness and the capacity for energy dissipation through hysteresis. Consequently, it is important to effectively account for the influence of reinforcement slip in the numerical model to ensure accurate results (Wang et al. 2019).

In this study, a bond slip model developed by Wang et al. has been used. In the model, an empirical formula has been derived by using various experimental results. The model defines a reduction coefficient, α, to be applied to the elastic modulus of steel in the tensile stage (Figure 3.6).

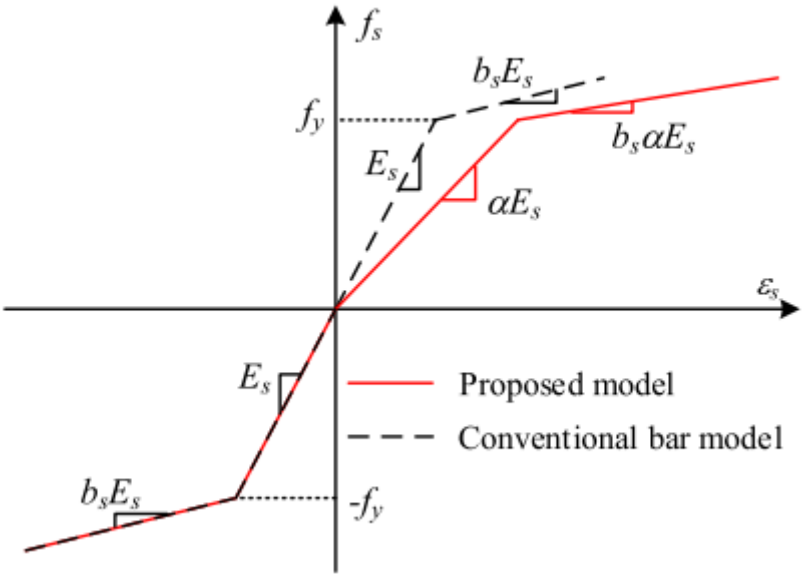

Figure 3.6 Proposed and conventional bar model (Wang et al. 2019)

Here, α is defined as:

$$\alpha = \frac{4\tau_e l_p}{f_y d} \quad \text{Eq. 3.1}$$

$$\tau_e = \sqrt{f_c} \;\; ; \;\; l_p = 0.25h \quad \text{Eq. 3.2}$$

Where, τ_e is the bond stress in the pre-yield range of rebar along development length, l_p is the plastic hinge length.

Figure 3.7 shows the difference between including the bond slip effect into the model and ignoring it. The stiffness and energy dissipation capacity are significantly overestimated when the bond slip effect is ignored.

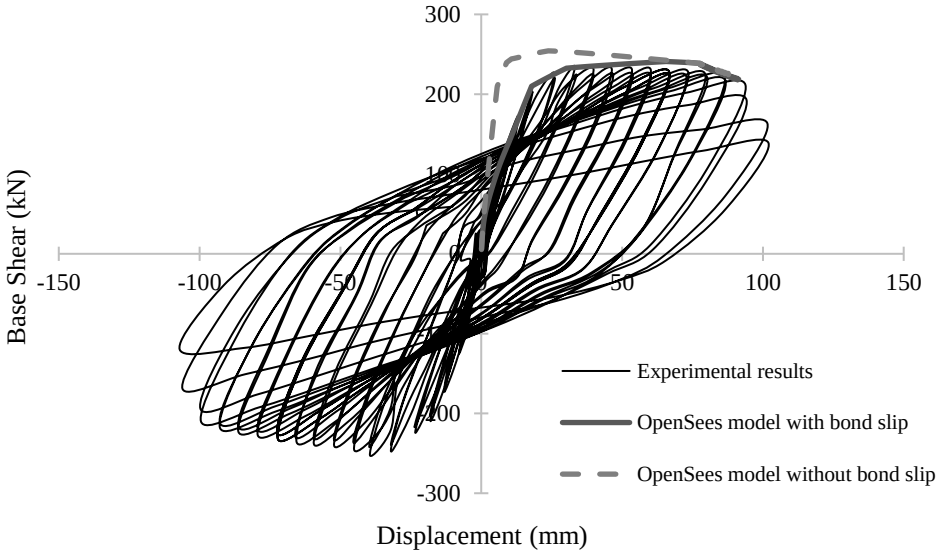

Figure 3.7 Bond slip effect (Mo and Wang C3-1, 2000)

3.5 Estimation of Yield Displacement and Ultimate Displacement

The yield displacement and ultimate displacement are found by making bilinear idealization of the force-displacement curve, according to ASCE/SEI (Figure 3.8). The ultimate displacement is taken as the displacement value where the shear force drops to 80 percent of the maximum shear force. If a 20 percent drop is not observed, then the last point on the pushover curve is considered as the ultimate point. After finding the ultimate displacement, an iterative method is used to find the yield point, which can be summarized as:

1- A point is chosen in the actual force-displacement curve and it is set as ($0.6V_{y\_trial}$, $0.6\Delta_{y\_trial}$).
2- The three points (0,0), (V_{y_trial} , Δ_{y_trial}), and (V_u , Δ_u) are connected and the area of the bilinear idealized shape is calculated.
3- The error between the area of the actual force-displacement curve and idealized one is calculated.

4- If the error is higher than the previous step, go to the next point in the actual force-displacement curve and repeat from step 1. If the error is smaller than the previous step and if $V_{y\_trial} < V_{max}$, set $V_y = V_{y\_trial}$; $\Delta_y = \Delta_{y\_trial}$ and go to the next point and repeat from step 1.

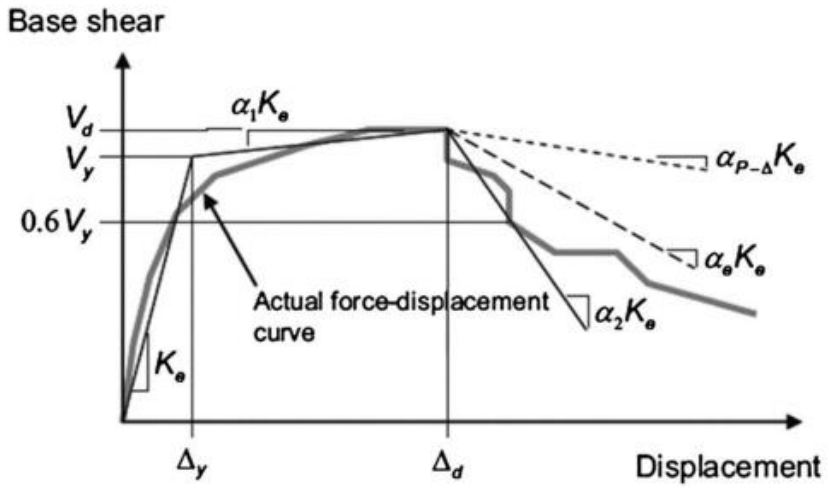

Figure 3.8 Bilinear idealization of the force-displacement curve (ASCE/SEI 41-17)

3.6 Verification of the Model

3.6.1 Selected Columns

37 columns (all cantilever) are selected to perform pushover analysis in OpenSees. Detailed material and geometric information for each model can be found in Appendix A. OpenSees analysis results for maximum base shear, yield displacement, and ultimate displacement are given in Table 3.1.

Table 3.1 OpenSees pushover analysis results

		Experimental Results			OpenSees Results		
Author	**Column Name**	**V_{max} (kN)**	**Δ_y (mm)**	**Δ_u (mm)**	**V_{max} (kN)**	**Δ_y (mm)**	**Δ_u (mm)**
Mo and Wang	C1-1	250.0	15.0	85.7	239.3	18.0	95.4
Mo and Wang	C1-2	267.6	14.8	96.6	249.5	16.3	96.0
Mo and Wang	C1-3	305.3	14.9	81.8	258.1	15.8	77.1
Mo and Wang	C2-1	248.0	16.7	97.1	239.7	17.8	95.6
Mo and Wang	C2-2	285.6	15.6	95.9	249.9	16.0	95.5
Mo and Wang	C2-3	309.8	13.5	72.7	258.8	15.5	76.2
Mo and Wang	C3-1	252.4	17.9	94.2	241.0	17.2	91.4
Mo and Wang	C3-2	282.5	17.9	94.9	250.2	15.8	95.1
Mo and Wang	C3-3	302.7	15.4	84.6	258.7	15.3	83.7
Tanaka and Park	No5	385.6	13.6	76.6	392.1	9.8	81.5
Tanaka and Park	No6	409.2	12.0	112.2	392.1	10.3	100.5
Tanaka and Park	No7	616.7	9.7	82.1	535.7	7.7	75.5
Tanaka and Park	No8	618.6	8.4	85.3	523.2	6.8	74.9
Park and Paulay	No9	395.1	10.7	105.1	389.6	14.8	107.0
Saatcioglu and Ozcebe	U1	276.1	19.7	66.0	275.6	8.3	63.2
Saatcioglu and Ozcebe	U4	325.9	13.1	92.9	321.6	11.0	73.9
Saatcioglu and Ozcebe	U6	342.8	13.6	89.0	323.1	10.2	81.8
Saatcioglu and Ozcebe	U7	341.8	13.6	87.8	324.2	9.8	80.3
Ohno and Nishioka	L1	121.0	9.5	82.1	111.5	9.3	81.3
Ohno and Nishioka	L2	108.7	9.1	98.0	111.5	9.3	81.3
Kono et al.	D1N30	201.0	3.4	18.6	183.7	3.8	20.6
Kono et al.	D1N60	188.1	2.6	12.5	183.7	2.8	13.6
Kono et al.	L1N60	1338.7	3.8	27.0	1370.3	4.8	28.7
Kono et al.	L1N6B	1201.3	3.7	23.2	1129.8	6.2	28.5
Takemura and Kawashima	Test5	159.5	7.4	90.1	159.0	4.8	81.8
Azizinamini et al.	NC-2	466.8	10.7	67.1	444.7	9.8	64.0
Azizinamini et al.	NC-4	489.3	9.3	39.0	466.3	6.2	39.6
Gill et al.	No.1	696.1	7.1	33.9	652.0	7.0	41.8
Gill et al.	No.3	670.4	4.9	21.1	668.5	6.2	28.4
Soesianawati et al.	No.1	199.6	10.4	78.2	199.6	8.7	73.3
Soesianawati et al.	No.2	279.2	9.2	50.3	268.2	7.2	49.4
Soesianawati et al.	No.3	277.0	8.8	44.6	260.4	6.5	39.6
Soesianawati et al.	No.4	264.5	9.6	34.6	237.7	6.2	31.5
Esaki	H-2-1_3	122.3	2.4	7.9	125.1	3.3	13.1

Table 3.2 (cont'd) OpenSees pushover analysis results

		Experimental Results			OpenSees Results		
Author	**Column Name**	**V_{max} (kN)**	**Δ_y (mm)**	**Δ_u (mm)**	**V_{max} (kN)**	**Δ_y (mm)**	**Δ_u (mm)**
Esaki	H-2-1_5	109.2	2.3	10.1	108.8	2.7	16.8
Esaki	HT-2-1_3	119.1	2.4	9.8	112.0	3.0	17.2
Esaki	HT-2-1_5	109.4	2.4	9.9	106.8	3.2	22.8

Comparison of experimental and OpenSees results for the maximum base shear (V_{max}), yield displacement (Δ_y), and ultimate displacement (Δ_u) is given in Figure 3.9. It can be observed that the OpenSees results, particularly for ultimate displacement (Δ_u) and maximum shear force (V_{max}) values, closely align with the experimental findings. Since the yield displacement values are small, percentage errors are larger.

The comparison of experimental and OpenSees force-displacement graphs for all 37 columns can be found in Appendix B.

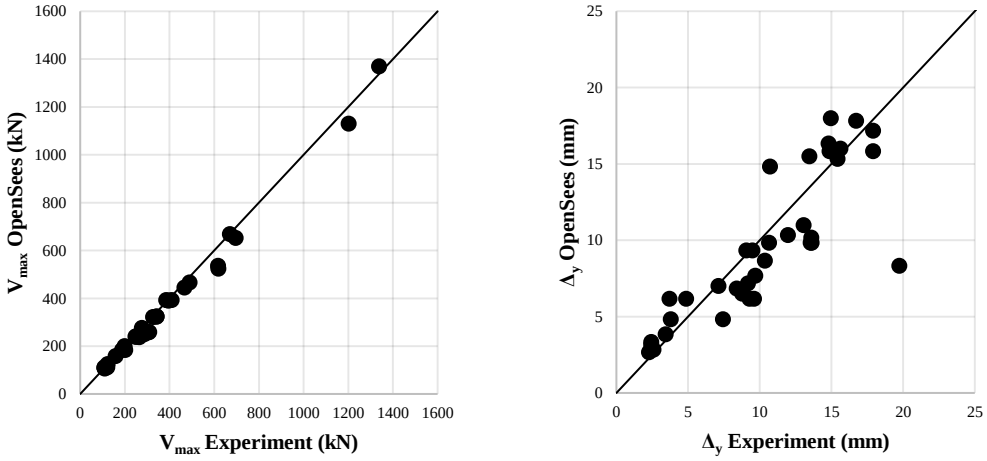

(a) (b)

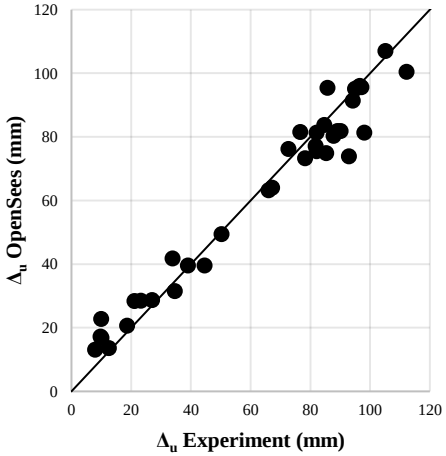

(c)

Figure 3.9 Comparison of experimental results and OpenSees results for (a) maximum base shear, (b) yield displacement, (c) ultimate displacement

3.6.2 Portal Frame

For the verification of the OpenSees model, a portal frame experiment that was conducted at METU Structural Mechanics Laboratory will also be used. In this experiment, a portal frame was constructed consisting of a T-shaped beam and two columns with square cross-sections. The dimensions of the portal frame are given in Figure 3.10.

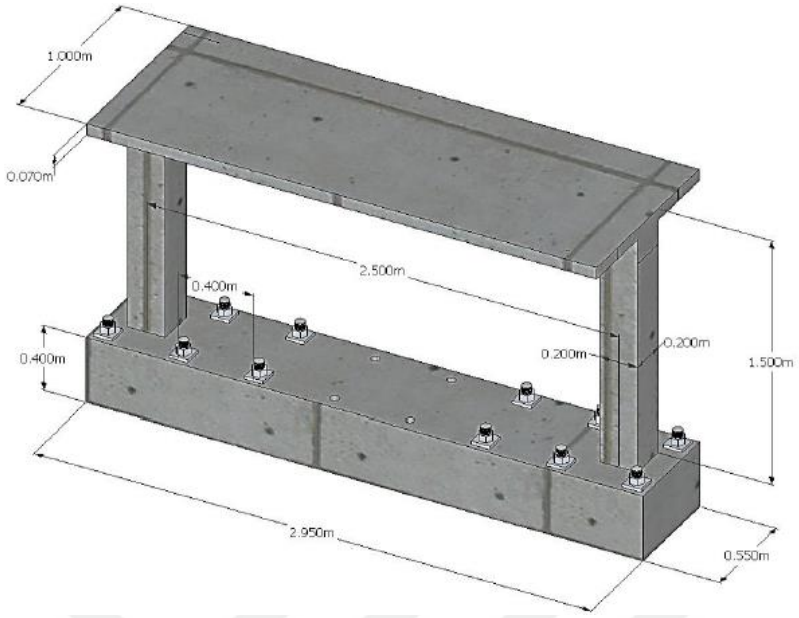

Figure 3.10 Dimensions of the portal frame

The material properties for the portal frame are provided in Table 3.2 and the reinforcement details are presented in Figure 3.11. The picture of the frame with the experimental set-up is shown in Figure 3.12.

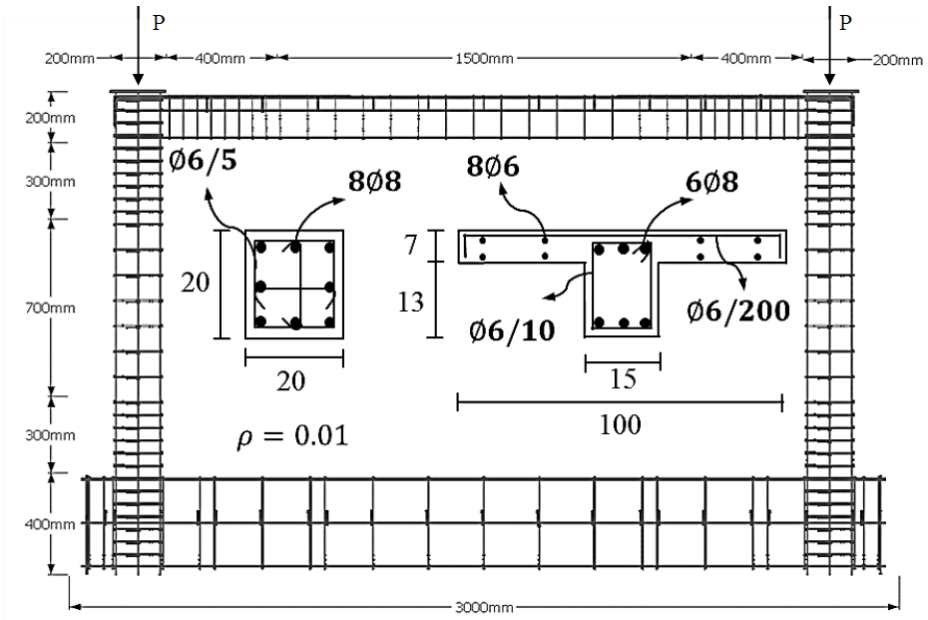

Figure 3.11 Reinforcement details of the portal frame

Figure 3.12 Portal frame

Table 3.3 Material properties of the portal frame

Concrete	Longitudinal Steel			Transverse Reinforcement		
f_{ck} (MPa)	**f_{yk} (MPa)**	**f_{su} (MPa)**	**ε_{su}**	**f_{yk} (MPa)**	**f_{su} (MPa)**	**ε_{su}**
25	405	558	0.24	330	466	0.4

The experiment was conducted on the frame system by applying lateral and axial loads. The lateral load was applied using a displacement-controlled hydraulic actuator, considering different drift ratios. As for the axial load, a distributed load on the beam and point loads to the columns were applied. The point loads on the columns were applied using force-controlled hydraulic cylinders. The distributed load had a magnitude of 10 kN/m, equivalent to 2675 kg. The applied axial load on the columns was determined as 17.5% of the column capacity, which corresponds to 180 kN.

In the OpenSees model, the beam is modelled by using “elasticBeamColumn”. The slab was omitted in the model, as including it would not have significant impact on the pushover behavior of the structural system. Again, a displacement step of 0.1 mm

is used. The comparison for experimental results and OpenSees results is given in Figure 3.13. The similarity of the OpenSees results and experimental results proves that OpenSees model accurately represents the structural system. Hence, it is confirmed that the ability of OpenSees in performing pushover analyses is dependable for evaluating the RC columns included in this study's scope.

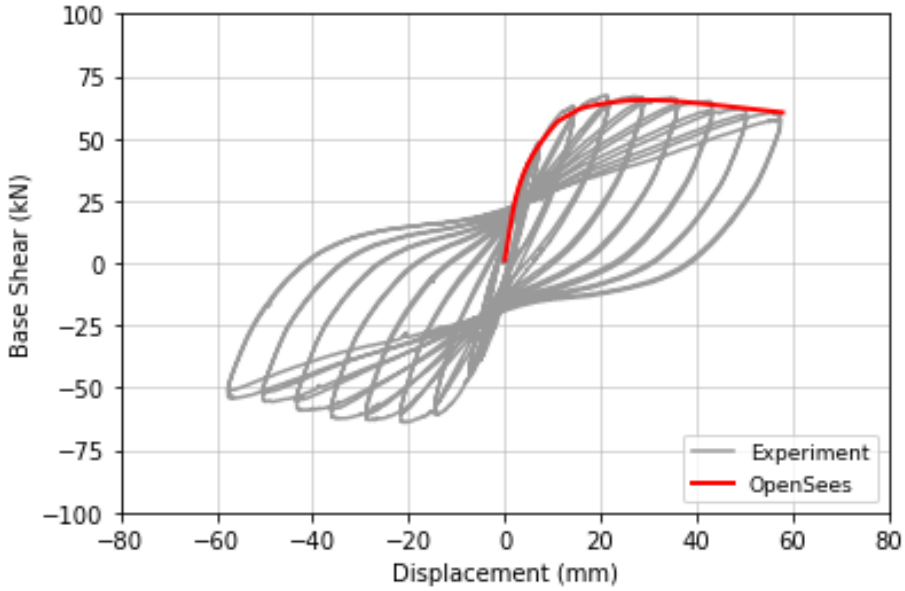

Figure 3.13 Comparison of experimental results and OpenSees results for portal frame

3.7 Column Specimens

The columns selected from PEER database are not enough to properly observe the effect of each parameter to the rotation capacity. To overcome the limitations arising from the selected database, additional columns are modeled using OpenSees. The additional columns have the following geometric and material properties:

- 4 different cross sections which are 300 mm x 300 mm, 400 mm x 400 mm, 500 mm x 500 mm, and 300 mm x 500 mm.
- 2 different heights which are 1.5 meters and 3 meters.
- 4 different axial load ratios (N/N_o) which are 0.1, 0.25, 0.4, and 0.5.

- 4 different concrete compressive strength (f_{ck}) which are 10 MPa, 15 MPa, 20 MPa, and 30 MPa.
- 2 different yield strength of steel for longitudinal reinforcement (f_{yk}), 220 MPa and 420 MPa.
- 2 different yield strength of steel for transverse reinforcement (f_{ywk}), 220 MPa and 420 MPa.
- 2 different longitudinal reinforcement ratios (ρ_l), 0.01 and 0.02.
- 3 different transverse reinforcement ratios (ρ_s), 0.001, 0.006, and 0.01.

Considering all possible combinations of the aforementioned properties results in a total of 3072 different columns. The properties are summarized in Table 3.4.

Table 3.4 Properties of the modeled columns

Cross-section (mm)	**L (m)**	**N/N_o**	**f_{ck} (MPa)**	**f_{yk} (MPa)**	**f_{ywk} (MPa)**	**ρ_l**	**ρ_s**
300x300	1.5	0.1	10	220	220	0.01	0.001
400x400	3	0.25	15	420	420	0.02	0.006
500x500		0.4	20				0.01
300x500		0.5	30				

Clear cover is taken as 25 mm for all columns. For all columns, there is 1 longitudinal steel in each corner and in the middle of each side (Figure 3.14).

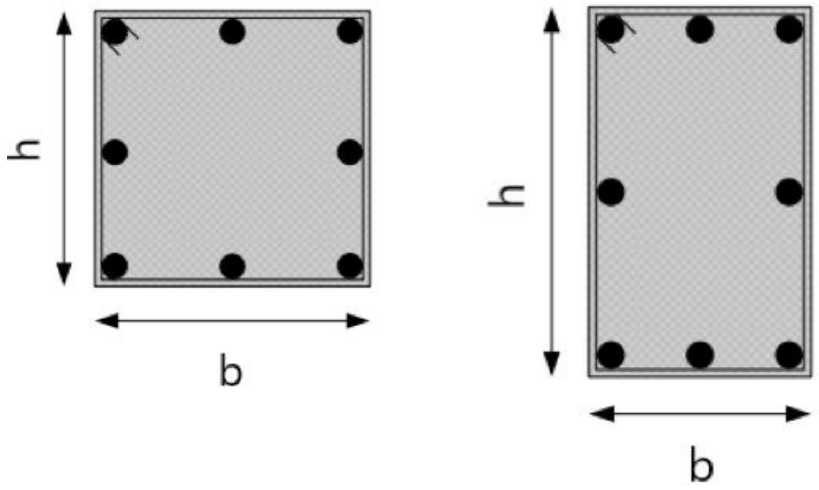

Figure 3.14 Reinforcement details of the modeled columns

3.8 Application of Seismic Assessment Guidelines to the Modeled Columns

In this part, the rotations found using OpenSees will be compared with the seismic guidelines. The yield and ultimate displacement values found using OpenSees, will be used to find the rotation by using Equations 2.1 – 2.5.

3.8.1 Application of TBEC (2018)

The comparison of TBEC (2018) performance limits with experimental results and OpenSees results are given in Figure 3.15. The figure shows that, for TBEC performance limits, the experimental and OpenSees results are consistent with each other.

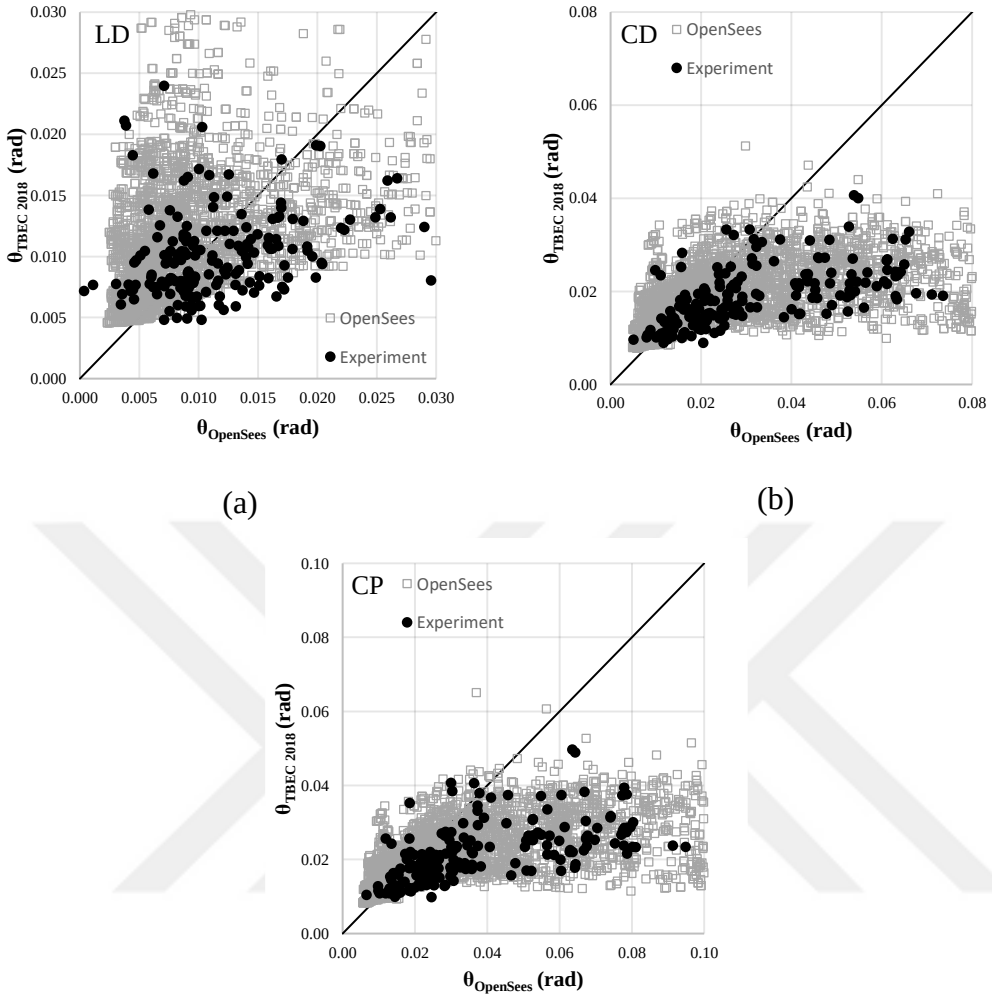

Figure 3.15 Comparison of experimental and OpenSees results with TBEC 2018 results for (a) Limited Damage; (b) Controlled Damage; (c) Collapse Prevention.

The experimentally obtained and OpenSees performance limits are normalized with respect to the guideline predictions ($\theta_{Experiment\ \&\ OpenSees}$ / $\theta_{guideline}$). The average and standard deviation of each performance limit is given in Table 3.5. For the average, values lower than unity indicate overpredictions of the guidelines.

Table 3.5 Average and standard deviation for $\frac{\theta_{Experiment\ \&\ Opensees}}{\theta_{TBEC}}$

	Experimental Results			**OpenSees Results**		
	LD	**CD**	**CP**	**LD**	**CD**	**CP**
$\boldsymbol{\mu}$	1.22	1.71	1.79	0.88	1.48	1.59
$\boldsymbol{\sigma}$	0.57	0.77	0.83	0.412	0.995	1.12

It can be seen that there is a significant difference between the average values for LD between OpenSees results and experimental results. The experimental database contains lower values of axial load ratios, the average of the axial load ratios of the column specimens is 0.21. On the other hand, half of the columns in the dataset created for OpenSees analysis have 0.4 and 0.5 axial load ratio level. It is observed that the predictive safety of LD performance level found by TBEC (2018) decreases as the axial load ratio on the column increases. The columns in the experimental dataset is divided into three with respect to their axial load ratios: columns with axial ratio smaller than 0.2, columns with axial ratio between 0.2 and 0.35, and columns with axial ratio greater than 0.35. For these three range of axial load ratios, the $\theta_{experiment}$ / θ_{TBEC} ratios are found 1.5, 1.05, and 0.61, respectively. Same trend is observed for OpenSees results. For axial load ratios 0.1, 0.25, 0.4, and 0.5; the $\theta_{OpenSees}$ / θ_{TBEC} ratios are found 1.18, 0.89, 0.69, and 0.56, respectively. Figure 3.16 shows the relationship between the axial load ratio and the predictive safety of TBEC (2018) for LD.

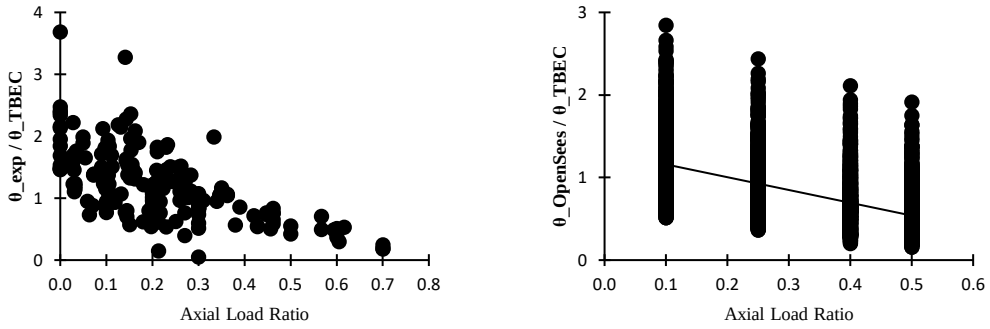

(a) (b)

Figure 3.16 Effect of axial load ratio on the predictive safety of LD performance limit calculated from TBEC and (a) Experimental results, (b) OpenSees results

It is observed that, for low axial load ratio values, CD and CP performance limits becomes too conservative. As the axial load ratio increases, the predictive safety decreases but does not become too unconservative. When CP performance level is considered, for columns with axial load ratio 0.1 and 0.25 the $\theta_{OpenSees} / \theta_{TBEC}$ ratio is 2.15, and for columns with axial load ratio 0.4 and 0.5 $\theta_{OpenSees} / \theta_{TBEC}$ ratio is 1.02

3.8.2 Application of ASCE/SEI 41-17 (2017)

The comparison of ASCE/SEI (2017) performance limits with experimental results and OpenSees results are given in Figure 3.17.

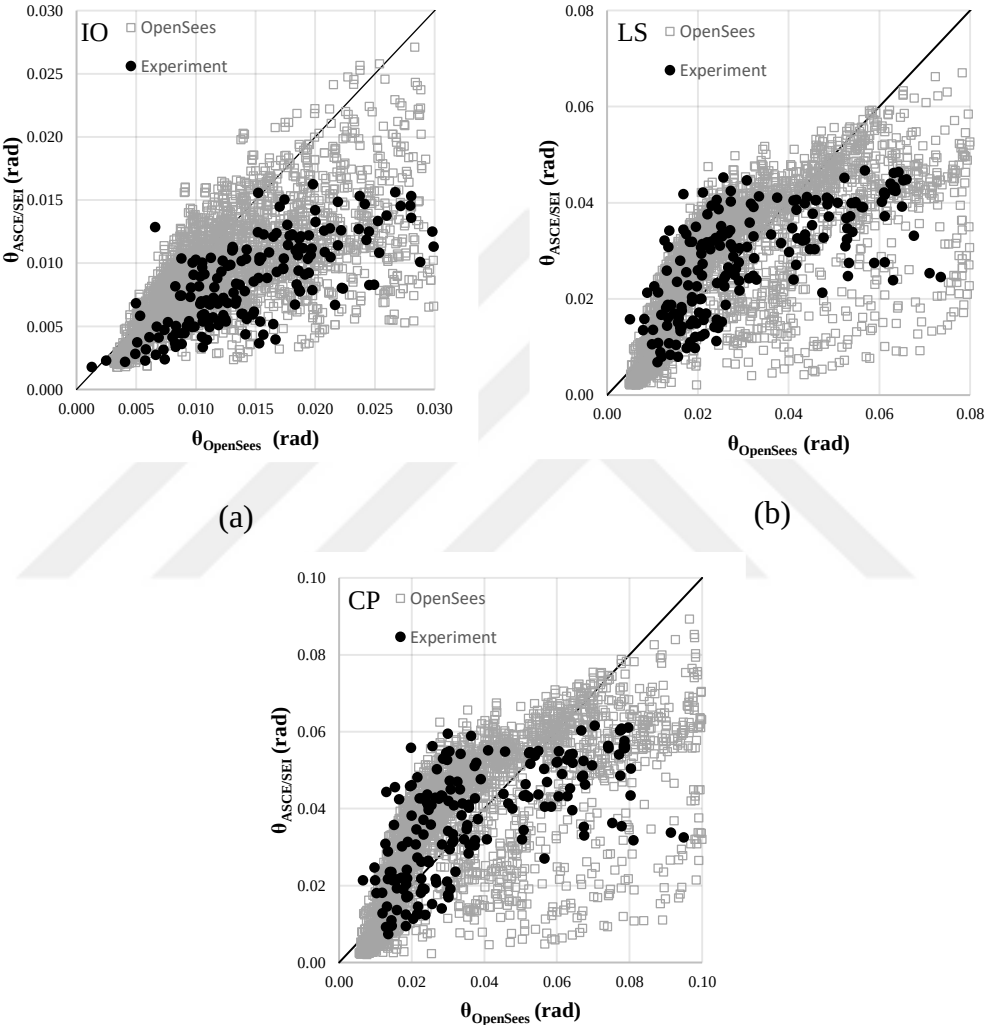

Figure 3.17 Comparison of experimental and OpenSees results with ASCE/SEI results for (a) Immediate Occupancy; (b) Life Safety; (c) Collapse Prevention

The experimentally obtained performance limits are normalized with respect to the guideline predictions. The average and standard deviation of each performance limit is given in Table 3.6.

Table 3.6 Average and standard deviation for $\frac{\theta_{Experiment\ \&\ Opensees}}{\theta_{ASCE}}$

	Experimental Results			**OpenSees Results**		
	IO	**LS**	**CP**	**IO**	**LS**	**CP**
$\boldsymbol{\mu}$	1.89	1.17	1.09	1.43	1.20	1.19
$\boldsymbol{\sigma}$	0.65	0.48	0.48	0.62	0.86	0.97

ASCE/SEI gives more conservative results compared to TBEC for IO, and as can be seen from Figure 3.17 (a), it is less scattered. For LS and CP, ASCE/SEI is less conservative compared to TBEC. For LS and CP, it is observed that as the transverse reinforcement increases, predictive safety decreases (Figure 3.18) and ASCE/SEI gives unsafe predictions.

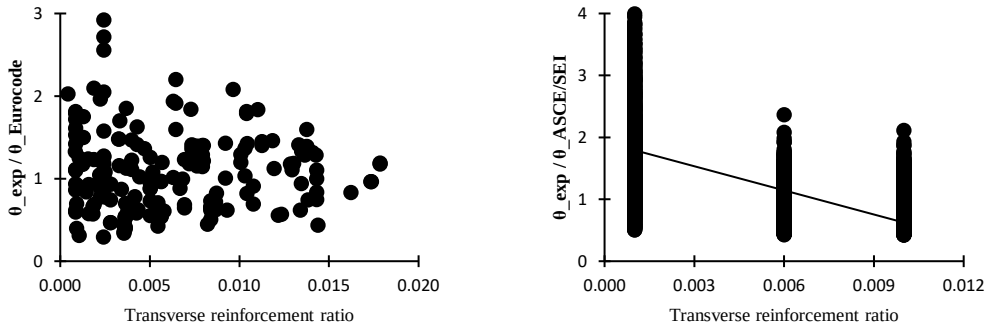

(a) (b)

Figure 3.18 Effect of transverse reinforcement ratio on the predictive safety of CP performance limit calculated from ASCE/SEI and (a) Experimental results, (b) OpenSees results

3.8.3 Application of Eurocode 8 – Part-3 (2010)

The comparison of Eurocode 8 – Part-3 (2010) performance limits with experimental results and OpenSees results are given in Figure 3.19.

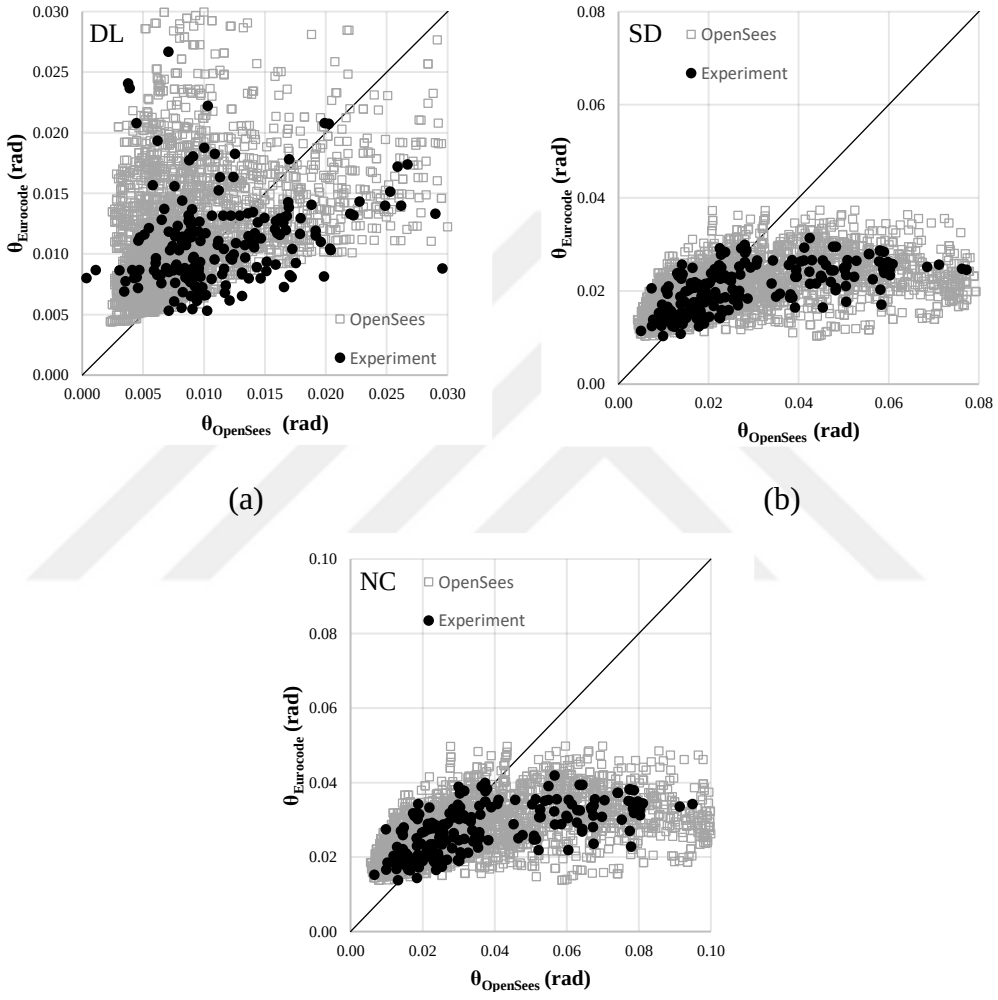

Figure 3.19 Comparison of experimental and OpenSees results with Eurocode 8 results for (a) Damage Limitation; (b) Significant Damage; (c) Near Collapse.

The experimentally obtained performance limits are normalized with respect to the guideline predictions. The average and standard deviation of each performance limit is given in Table 3.7.

Table 3.7 Average and standard deviation for $\frac{\theta_{Experiment\ \&\ Opensees}}{\theta_{Eurocode}}$

	Experimental Results			**OpenSees Results**		
	DL	**SD**	**NC**	**DL**	**SD**	**NC**
$\boldsymbol{\mu}$	1.12	1.38	1.38	0.80	1.28	1.28
$\boldsymbol{\sigma}$	0.524	0.664	0.664	0.388	0.843	0.843

Similar to TBEC, predictive safety of Eurocode for DL decreases as the axial load ratio increase. Figure 3.20 shows the relationship between the axial load ratio and the predictive safety of Eurocode for DL. Eurocode gives mostly unsafe results for DL, especially for high axial load ratios.

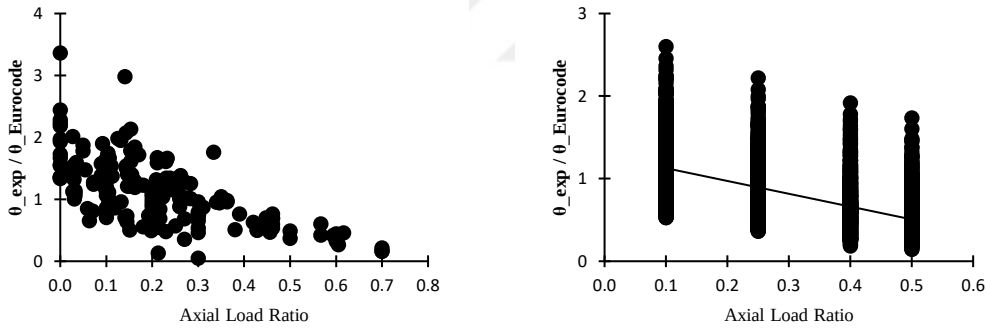

(a) (b)

Figure 3.20 Effect of axial load ratio on the predictive safety of DL performance limit calculated from Eurocode and (a) Experimental results, (b) OpenSees results

It is observed that the predictive safety for SD and NC decreases as the axial load ratio increases. It is also observed that the predictive safety for SD and NC is affected by the transverse reinforcement ratio. Opposite to ASCE/SEI, as the transverse reinforcement ratio increases, the predictive safety of Eurocode tends to increase.

Figure 3.21 shows the relationship between the transverse reinforcement ratio and the predictive safety of Eurocode for NC.

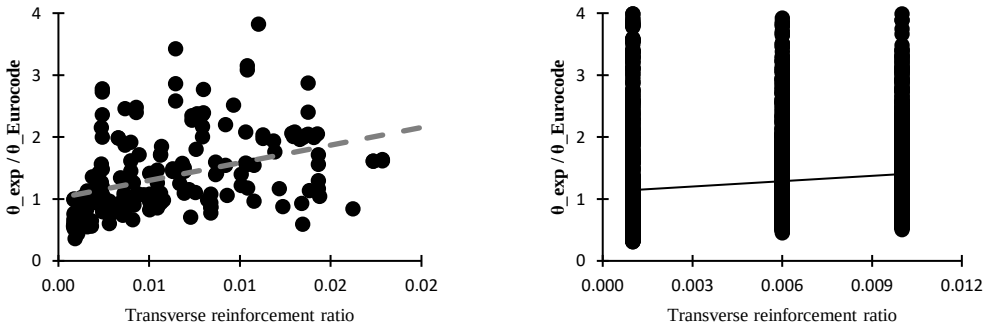

(a) (b)

Figure 3.21 Effect of transverse reinforcement ratio on the predictive safety of NC performance limit calculated from Eurocode and (a) Experimental results, (b) OpenSees results

3.9 Effect of Each Parameter on Plastic Rotation Capacity

The influence of concrete compressive strength, yielding strength of longitudinal reinforcement, yielding strength of transverse reinforcement, axial load ratio, and transverse reinforcement ratio will be separately analyzed with respect to how they affect the capacity curve and plastic rotation capacities of the columns. The influence of these parameters to plastic rotation values calculated from seismic guidelines will also be analyzed. The plastic rotation formulas given for collapse prevention performance level in the seismic guidelines are given below.

TBEC (2018)

$$\theta_p = \frac{2}{3}\left[(\emptyset_u - \emptyset_y)L_p\left(1 - 0.5\frac{L_p}{L_s}\right) + 4.5\emptyset_u d_b\right] \quad \text{Eq. 3.3}$$

ASCE/SEI (2017)

$$\theta_p = 0.042 - 0.043\max(0.1, n) + 0.63\rho_s - 0.023\max(0.2, \frac{V_y}{V_{col}}) \quad \text{Eq. 3.4}$$

Eurocode 8 Part-3

$$\theta_p = \frac{1}{\gamma_{el}} 0.0145(0.25^{\nu}) \left[\frac{\max(0.01;\omega')}{\max(0.01;\omega)}\right]^{0.3} (f_c)^{0.2} \left(\min\left(9;\frac{L_s}{h}\right)\right)^{0.35} 25^{\left(\alpha\rho_{sx}\frac{f_{yw}}{f_c}\right)} \quad \text{Eq. 3.5}$$

3.9.1 Concrete Compressive Strength

To observe the effect of concrete compressive strength on the capacity curve, four columns were selected, all having identical properties except for the concrete compressive strength. The properties of the columns are summarized in Table 3.8. The effect of concrete compressive strength on the capacity curve is shown in Figure 3.22. The results show that the lateral load capacities of the columns increase significantly with higher concrete strength (Figure 3.23). It can be also observed that as the concrete strength increases, the deformation capacity of the columns decreases.

The impact of concrete compressive strength on plastic rotation capacities is shown in Figure 3.24. The figure illustrates a decrease in plastic rotation capacity with increasing concrete strength (Figure 3.24 (a)). This trend is captured by TBEC (2018) and ASCE/SEI (2017) standards (Figure 3.24 (b) and (c)). However, Eurocode contradicts this pattern by suggesting that the plastic rotation capacity slightly increases as concrete compressive strength increases (Figure 3.24 (d)).

Table 3.8 Properties of the selected columns

Cross-section (mm)	**L (m)**	**N/N_o**	**f_{ck} (MPa)**	**f_{yk} (MPa)**	**f_{ywk} (MPa)**	**ρ_l**	**ρ_s**
400x400	1.5	0.25	10	220	220	0.01	0.01
400x400	1.5	0.25	15	220	220	0.01	0.01
400x400	1.5	0.25	20	220	220	0.01	0.01
400x400	1.5	0.25	30	220	220	0.01	0.01

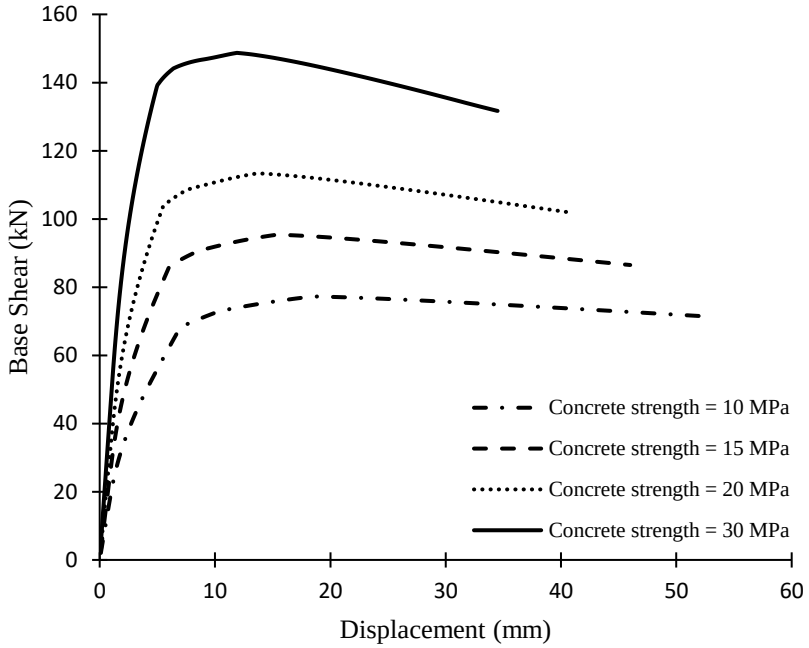

Figure 3.22 Effect of concrete compressive strength on the capacity curve

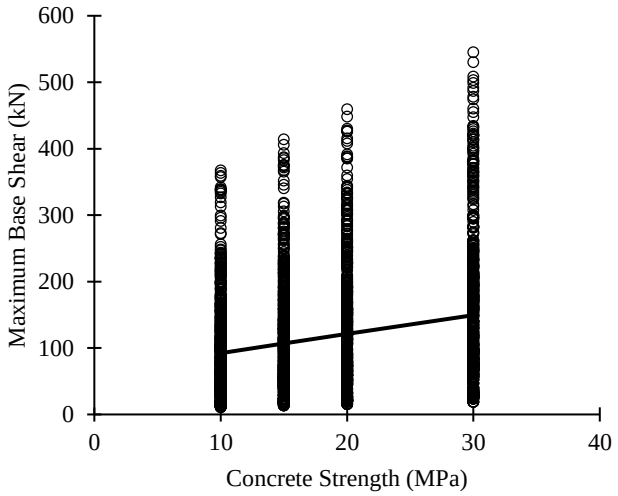

Figure 3.23 Effect of concrete compressive strength on maximum base shear

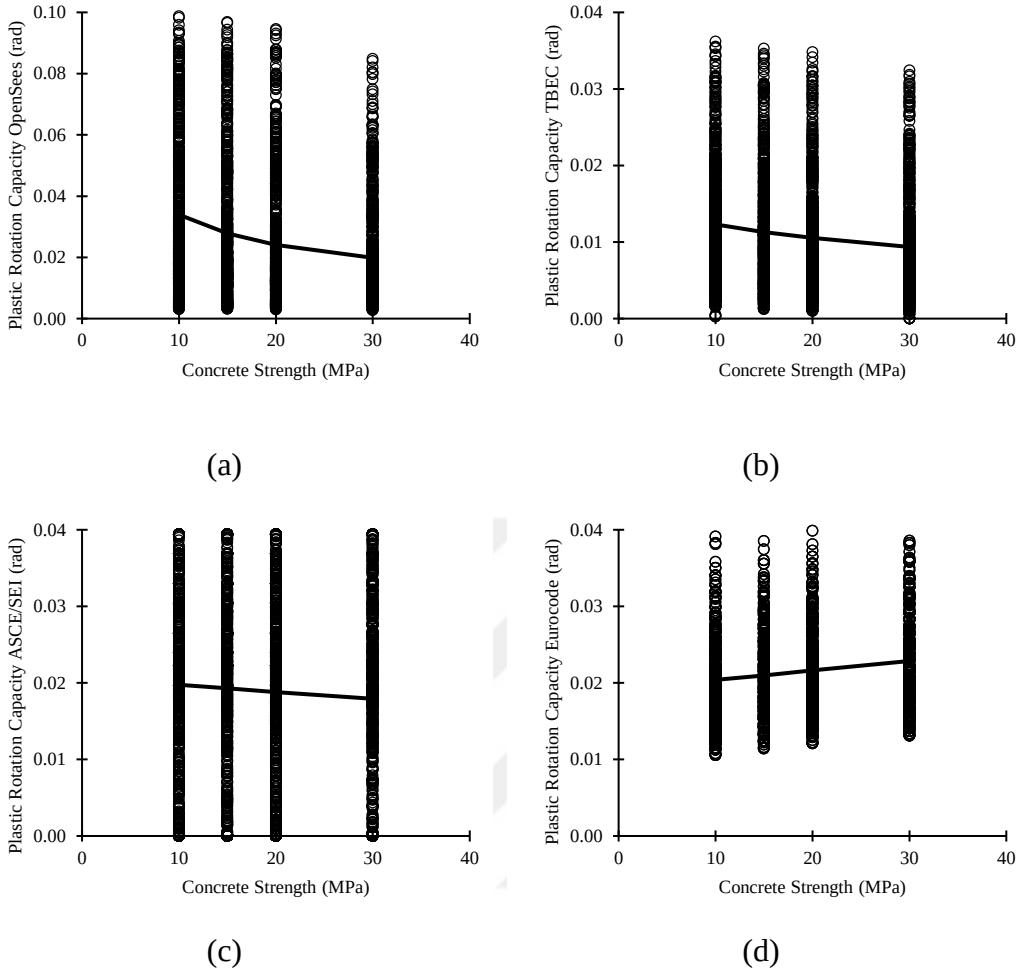

Figure 3.24 Effect of concrete compressive strength on plastic rotation capacities

3.9.2 Yielding Strength of Longitudinal Reinforcement

To observe the effect of yield strength of longitudinal steel on the capacity curve, two columns were selected, both having identical properties except for the yield strength of longitudinal steel. The properties of the columns are summarized in Table 3.9. The effect of yield strength of longitudinal steel on the capacity curve is shown in Figure 3.25. The results show that the lateral load capacities of the columns increase with higher yield strength of longitudinal steel (Figure 3.26).

The impact of yield strength of longitudinal steel on plastic rotation capacities is shown in Figure 3.27. The figure illustrates an increase in plastic rotation capacity with increasing yielding strength of longitudinal reinforcement (Figure 3.27 (a)). Plastic rotation capacity remains the same with increase in the longitudinal yield strength according to Eurocode (Figure 3.27 (d)), which is expected since the formula (Eq. 3.5) does not contain any parameter related to f_{yl}. Plastic rotation capacities slightly decrease with the increase in the yield strength of longitudinal steel according to ASCE/SEI (2017) (Figure 3.27 (c)) but significantly decreases (19% reduction) according to TBEC (2018) (Figure 3.27 (b)), which is expected since the only parameters related to f_{yl} in Equation 3.3 are the curvatures found from section analysis and the ductility, $(\emptyset_u - \emptyset_y)$, tends to decrease with the increase in f_{yl}.

Table 3.9 Properties of the selected columns

Cross-section (mm)	**L (m)**	**N/N$_o$**	**f_{ck} (MPa)**	**f_{yk} (MPa)**	**f_{ywk} (MPa)**	**ρ_l**	**ρ_s**
300x300	1.5	0.1	15	220	220	0.01	0.006
300x300	1.5	0.1	15	420	220	0.01	0.006

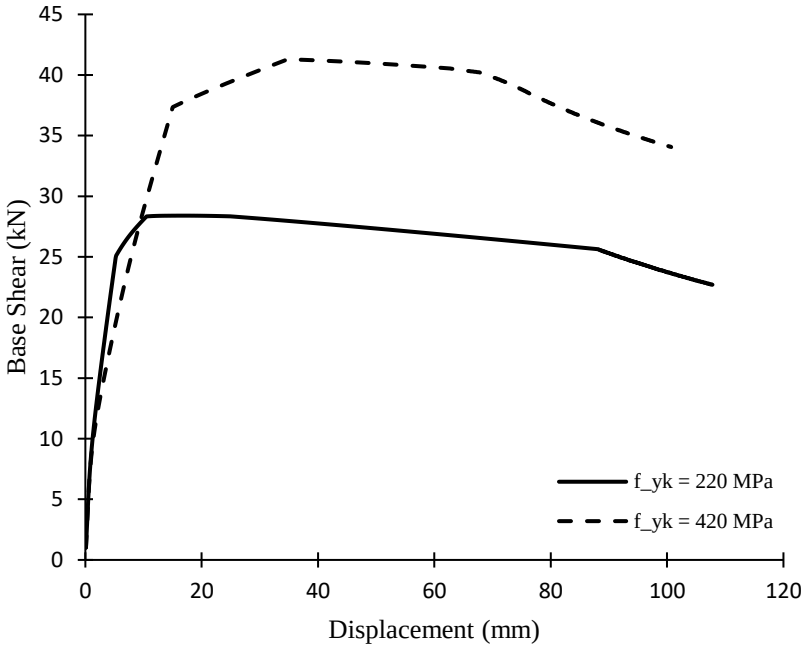

Figure 3.25 Effect of yield strength of longitudinal steel on the capacity curve

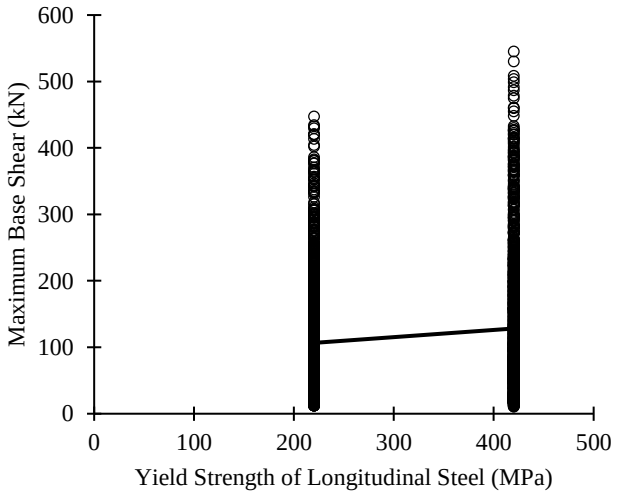

Figure 3.26 Effect of yield strength of longitudinal steel on maximum base shear

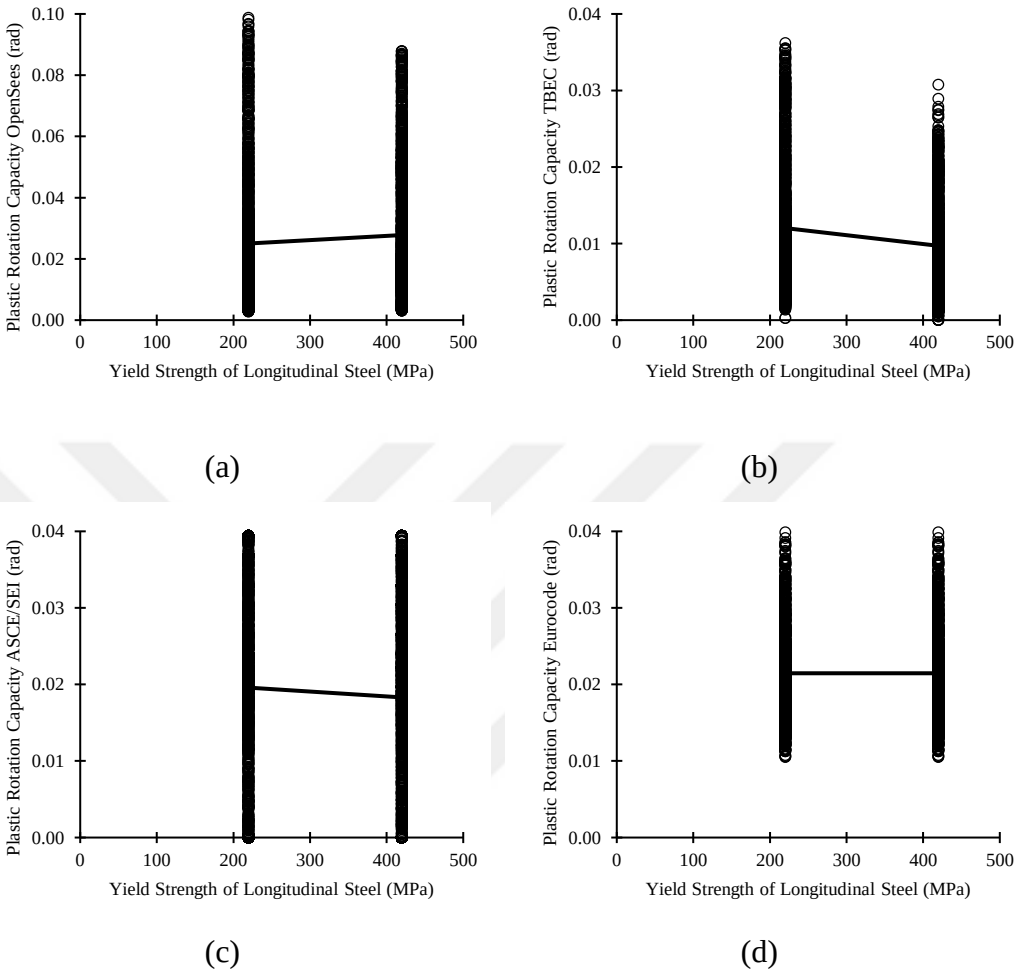

Figure 3.27 Effect of yield strength of longitudinal steel on plastic rotation capacities

3.9.3 Yielding Strength of Transverse Reinforcement

To observe the effect of yielding strength of transverse reinforcement on the capacity curve, two columns were selected, both having identical properties except for the yielding strength of transverse steel. The properties of the columns are summarized in Table 3.10. The effect of yield strength of transverse reinforcement on the capacity curve is shown in Figure 3.28. The results show that the lateral load capacities of the columns slightly increase with higher yield strength of transverse steel (Figure 3.29).

The impact of yield strength of transverse steel on plastic rotation capacities is shown in Figure 3.30. The figure illustrates an increase in plastic rotation capacity with increasing yielding strength of transverse steel (Figure 3.30 (a)). This pattern is consistent across all three guidelines (Figure 3.30 (b), (c), and (d)).

Table 3.10 Properties of the selected columns

Cross-section (mm)	**L (m)**	**N/N_o**	**f_{ck} (MPa)**	**f_{yk} (MPa)**	**f_{ywk} (MPa)**	**ρ_l**	**ρ_s**
400x400	3	0.25	20	420	220	0.01	0.006
400x400	3	0.25	20	420	420	0.01	0.006

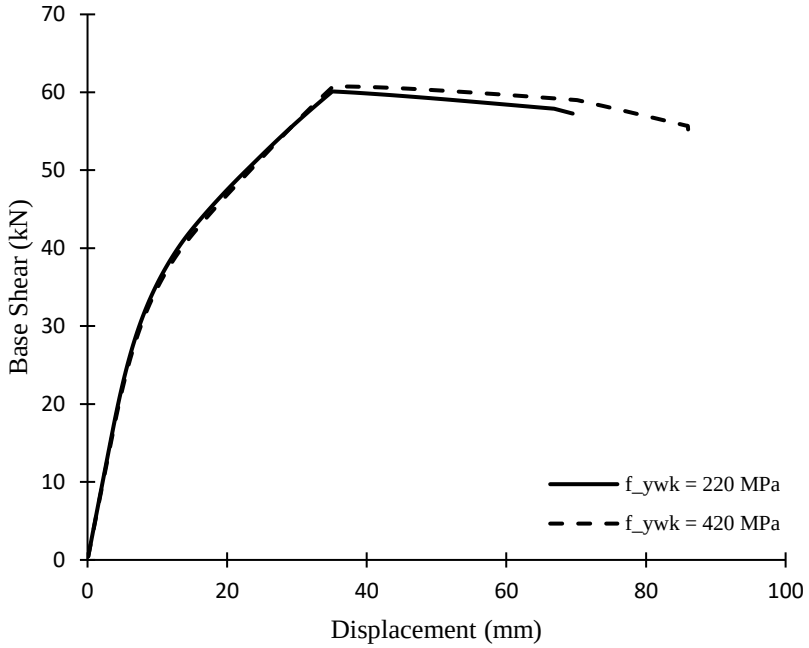

Figure 3.28 Effect of yield strength of transverse steel on the capacity curve

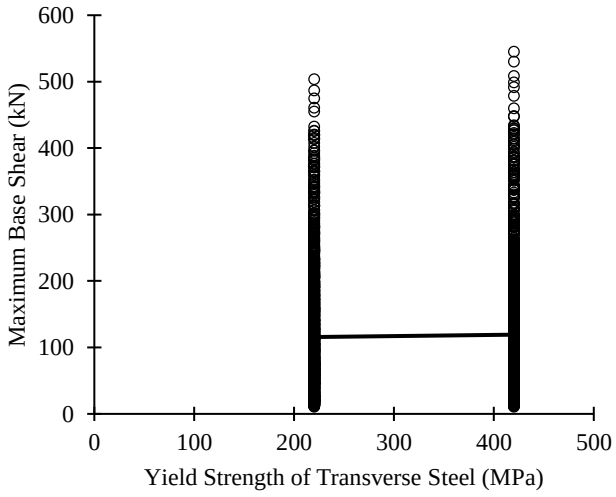

Figure 3.29 Effect of yield strength of transverse steel on maximum base shear

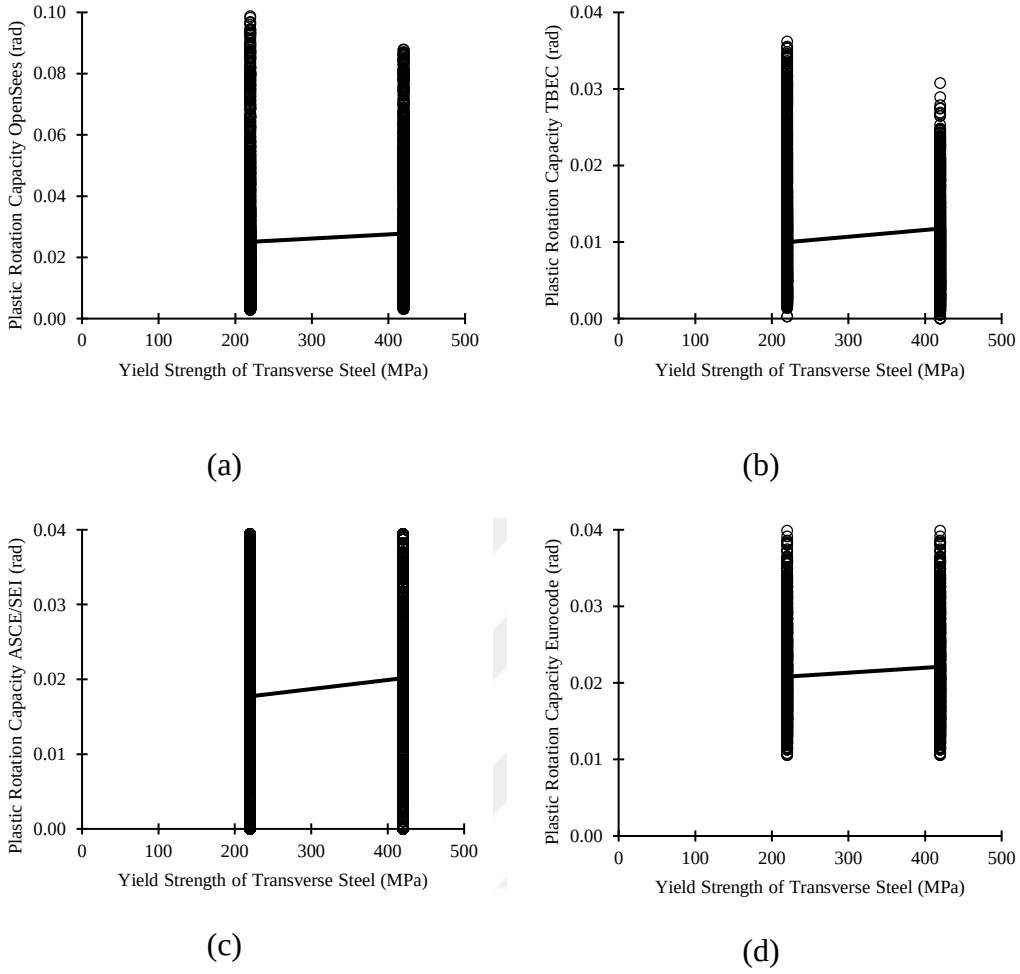

Figure 3.30 Effect of yield strength of transverse steel on plastic rotation capacities

3.9.4 Axial Load Ratio

To observe the effect of axial load ratio on the capacity curve, four columns were selected, all having identical properties except for the axial load ratio. The properties of the columns are summarized in Table 3.11. The effect of axial load ratio on the capacity curve is shown in Figure 3.31. The results indicate that the lateral load capacities of the columns increase (Figure 3.32) with higher axial load ratios (slight decrease from $N/N_o = 0.4$ to $N/N_o = 0.5$).

The impact of axial load ratio on plastic rotation capacities is shown in Figure 3.33. It can be seen that plastic rotation capacity decreases significantly with the increase in axial load ratio (Figure 3.33 (a)). This pattern is consistent across all three guidelines (Figure 3.33 (b), (c), and (d)).

Table 3.11 Properties of the selected columns

Cross-section (mm)	**L (m)**	**N/N_o**	**f_{ck} (MPa)**	**f_{yk} (MPa)**	**f_{ywk} (MPa)**	**ρ_l**	**ρ_s**
400x400	1.5	0.1	20	420	220	0.01	0.006
400x400	1.5	0.25	20	420	420	0.01	0.006
400x400	1.5	0.4	20	420	220	0.01	0.006
400x400	1.5	0.5	20	420	420	0.01	0.006

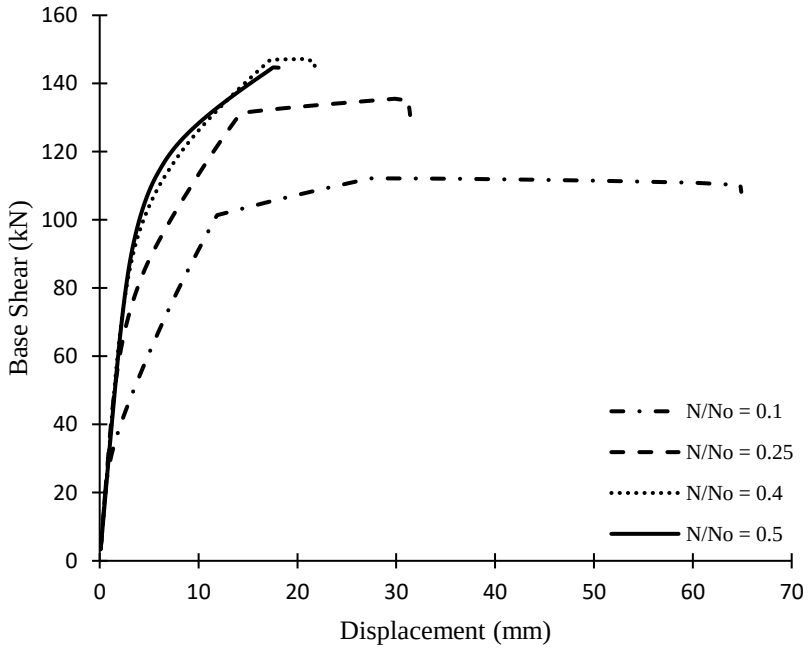

Figure 3.31 Effect of axial load ratio on the capacity curve

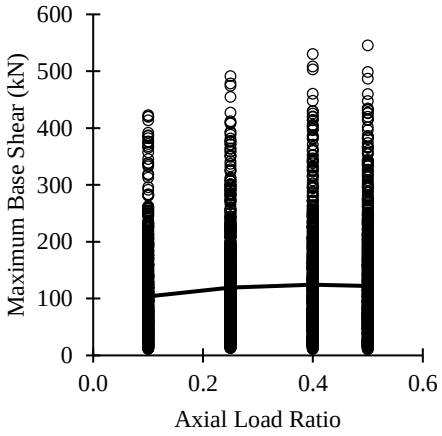

Figure 3.32 Effect of axial load ratio on maximum base shear

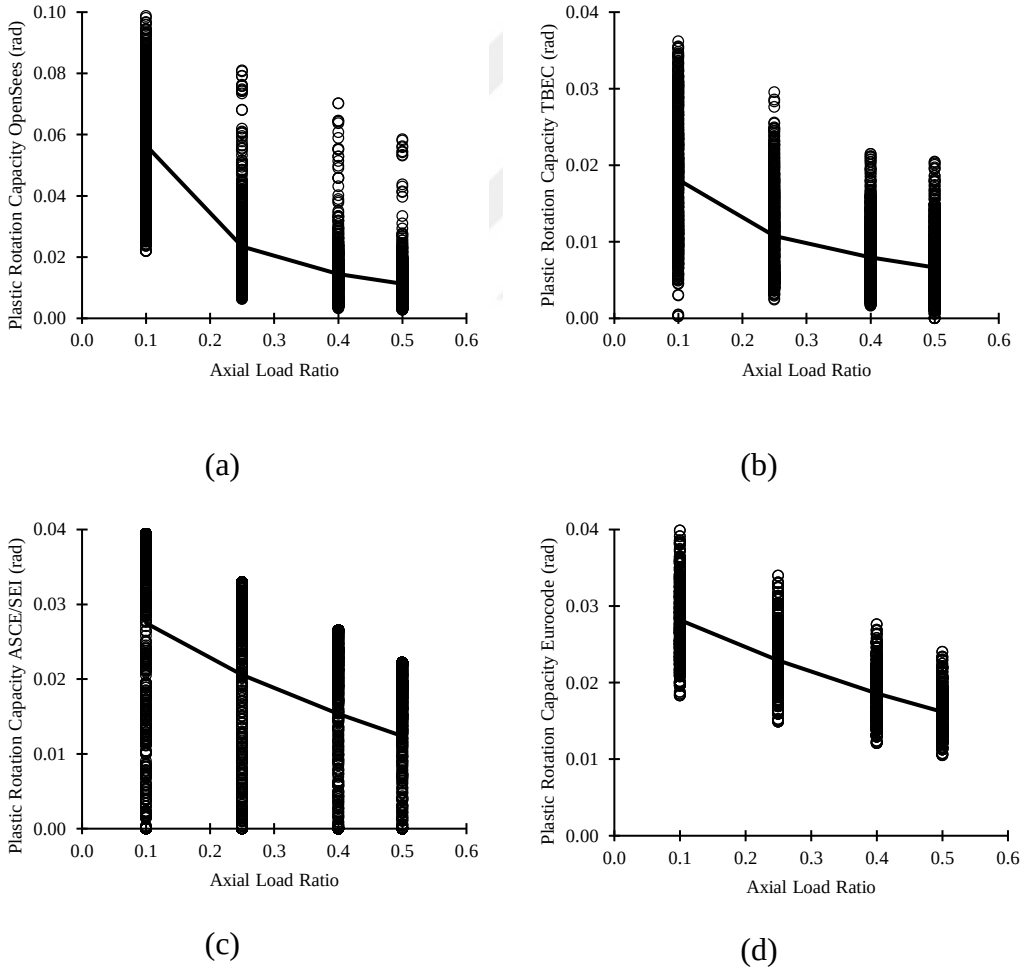

Figure 3.33 Effect of axial load ratio on plastic rotation capacities

3.9.5 Transverse Reinforcement Ratio

To observe the effect of transverse reinforcement ratio on the capacity curve, two columns were selected, both having identical properties except for the transverse reinforcement ratio. The properties of the columns are summarized in Table 3.12. The effect of transverse reinforcement ratio on the capacity curve is shown in Figure 3.34. The results show that the lateral load capacities of the columns increase as the transverse reinforcement ratio increases (Figure 3.35).

The impact of transverse reinforcement ratio on plastic rotation capacities is shown in Figure 3.36. The figure illustrates a significant increase in plastic rotation capacity with increasing transverse reinforcement ratio (Figure 3.36 (a)). This pattern is consistent across all three guidelines (Figure 3.36 (b), (c), and (d)).

Table 3.12 Properties of the selected columns

Cross-section (mm)	**L (m)**	**N/N_o**	**f_{ck} (MPa)**	**f_{yk} (MPa)**	**f_{ywk} (MPa)**	**ρ_l**	**ρ_s**
300x500	3	0.1	30	420	420	0.02	0.001
300x500	3	0.1	30	420	420	0.02	0.006
300x500	3	0.1	30	420	420	0.02	0.01

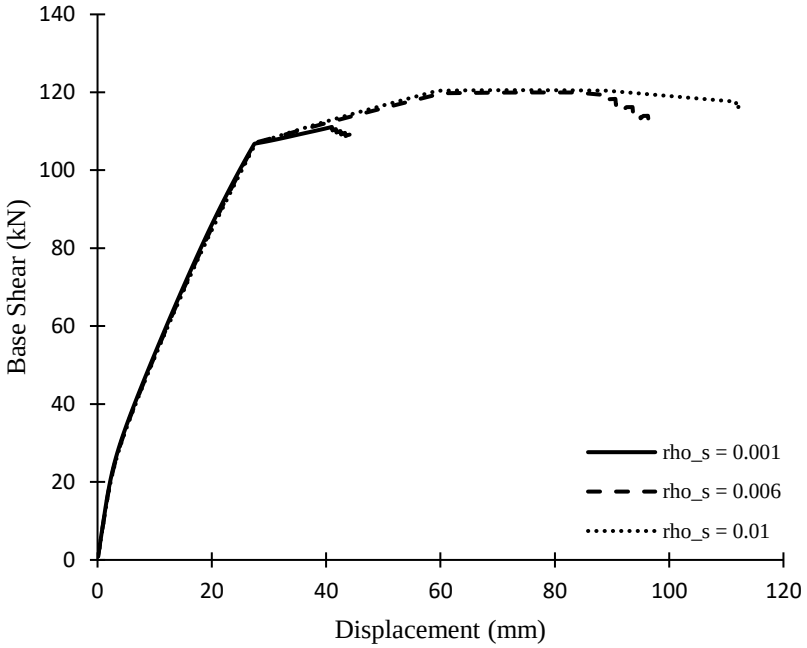

Figure 3.34 Effect of transverse reinforcement ratio on the capacity curve

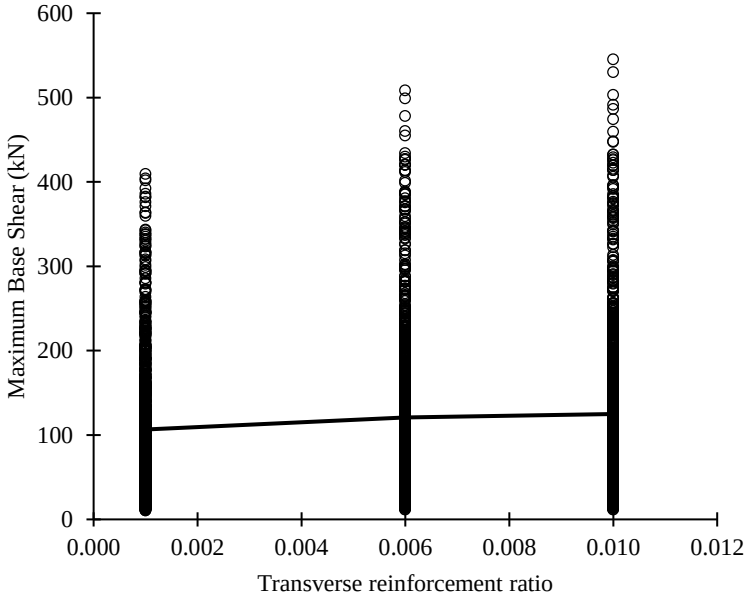

Figure 3.35 Effect transverse reinforcement ratio on maximum base shear

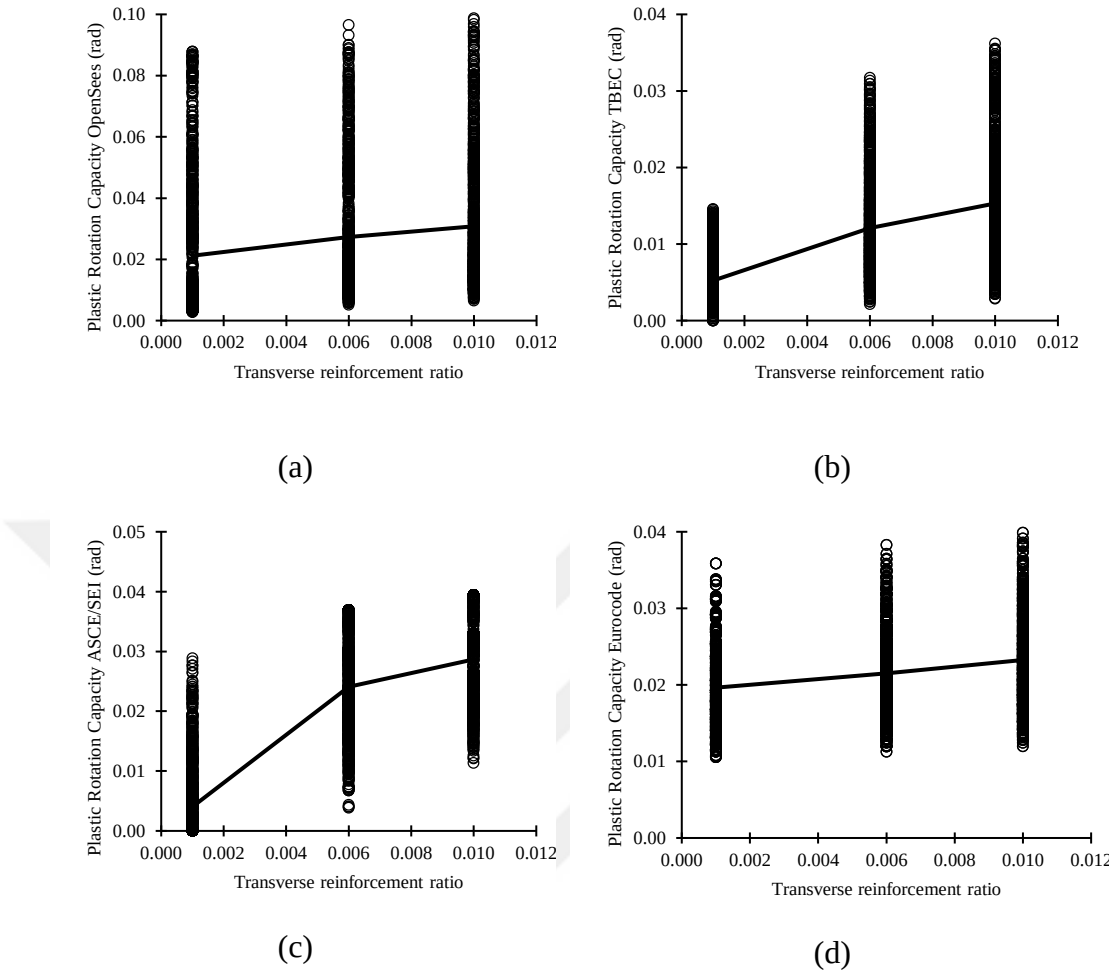

Figure 3.36 Effect of transverse reinforcement ratio on plastic rotation capacities

3.10 Proposed simplified rotation limits

A simple approach to determine the performance limits of RC columns is proposed. According to the new simplified approach, the columns are divided into three groups:

Table 3.13 Column classification

V_e/V_r	Satisfies the transverse reinforcement requirements of TBEC part 7.3.4	Does not satisfy the transverse reinforcement requirements of TBEC part 7.3.4
$V_e/V_r \leq 0.7$	A	B
$0.7 \leq V_e/V_r \leq 1.1$	B	B
$1.1 \leq V_e/V_r$	C	C

Where, V_e is the design shear force calculated under the impacts of vertical loads and earthquake loads. V_r can be calculated as follows:

$$V_{cr} = 0.65 f_{ctd} b_w d \left(1 + \gamma \frac{N_d}{A_g}\right) \quad \text{Eq. 3.6}$$

$$V_w = \frac{A_{sw}}{s} f_{ywd} d \quad \text{Eq. 3.7}$$

$$V_c = 0.8 V_{cr} \quad \text{Eq. 3.8}$$

$$V_r = V_c + V_w \quad \text{Eq. 3.9}$$

For compression case, $\gamma = 0.07$.

The transverse reinforcement requirements of TBEC part 7.3.4 are as follows:

- No transverse reinforcement with a diameter smaller than 8 mm shall be used in the confinement regions.
- The spacing between longitudinal stirrups and ties shall not be less than one-third of the smallest section dimension or greater than 150 mm. It shall be

greater than six times the diameter of the longitudinal reinforcement and not less than 50 mm.

- The horizontal distance between stirrup legs and/or ties shall not exceed 25 times the stirrup diameter.
- If $N_d > 0.20A_cf_{ck}$, the minimum total area of transverse reinforcement in the confinement regions shall be calculated in a manner that satisfies the least favorable condition stated in Equation 3.10 and Equation 3.11.

$$A_{sh} \geq 0.30sb_k\left[\left(\frac{A_c}{A_{ck}}\right)-1\right]\left(\frac{f_{ck}}{f_{ywk}}\right) \quad \text{Eq 3.10}$$

$$A_{sh} \geq 0.75sb_k\left(\frac{f_{ck}}{f_{ywk}}\right) \quad \text{Eq 3.11}$$

The following limits are proposed as rotation limits for each column classification:

For columns classified as A:

$$\theta_u = 4.5 - 5n\ (\%) \quad \text{Eq 3.12}$$

Where n is the axial load ratio.

For columns classified as B:

$$\theta_u = 645\rho_t - 1000\rho_t n + 0.725\ (\%) \quad \text{Eq 3.13}$$

For columns classified as C:

$$\theta_u = \theta_y \leq 0.75\% \quad \text{Eq 3.14}$$

For all three column groups,

$$\theta_y = \frac{M_y L}{3(EI)_{eff}} \quad \text{Eq 3.15}$$

$$\frac{EI_{eff}}{EI_g} = \begin{cases} 0.3, & n \leq 0.1 \\ n + 0.2, & 0.1 < n < 0.5 \\ 0.7, & n \geq 0.5 \end{cases} \quad \text{Eq 3.16}$$

The comparison of the proposed limits with experimental results and OpenSees results are given in Figure 3.37. It can be seen that for Immediate Occupancy there is a significant improvement compared to TBEC (2018) and Eurocode 8-3. For Collapse Prevention, for very low transverse reinforcement ratio (ρ_t = 0.001), it is observed that some of the OpenSees specimens' limits becomes too conservative. The excluded version of ρ_t = 0.001 can be seen in Figure 3.38.

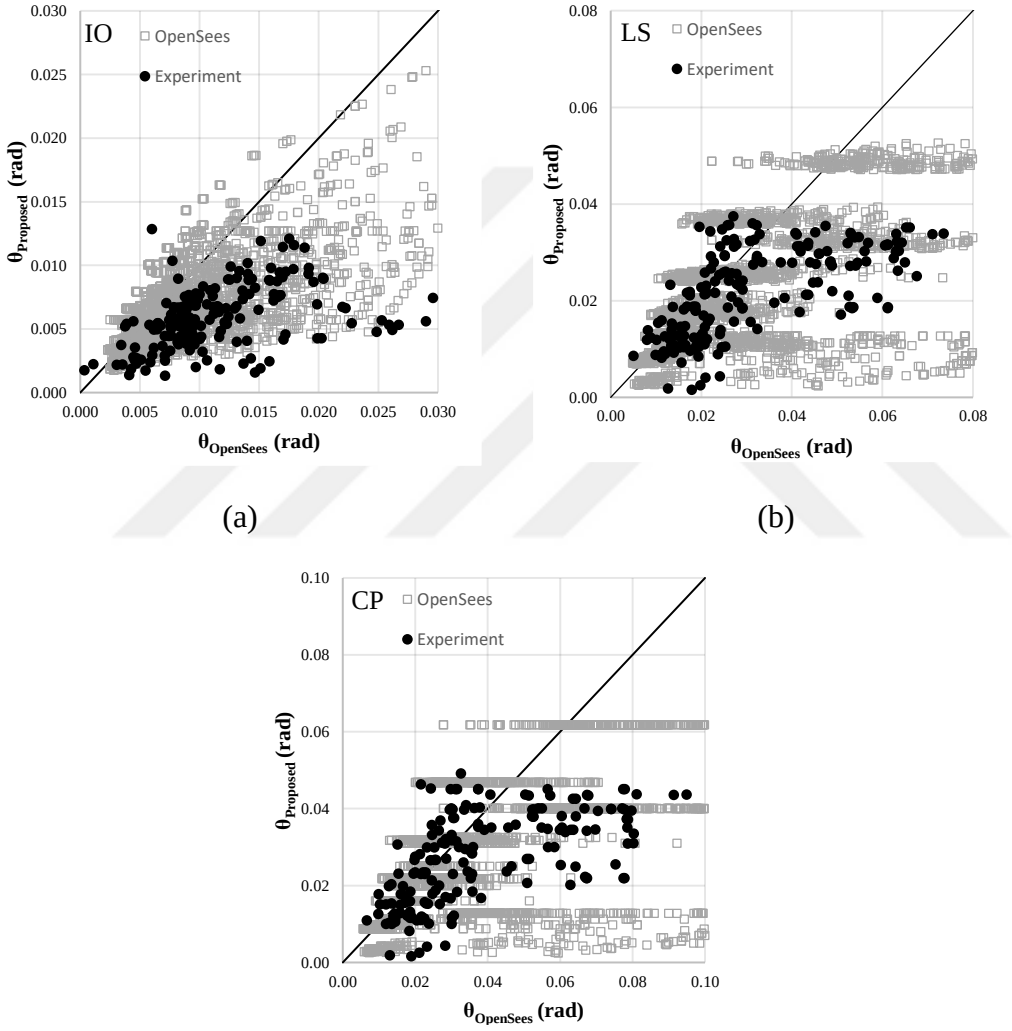

Figure 3.37 Comparison of experimental and OpenSees results with proposed limits for (a) Immediate Occupancy; (b) Life Safety; (c) Collapse Prevention.

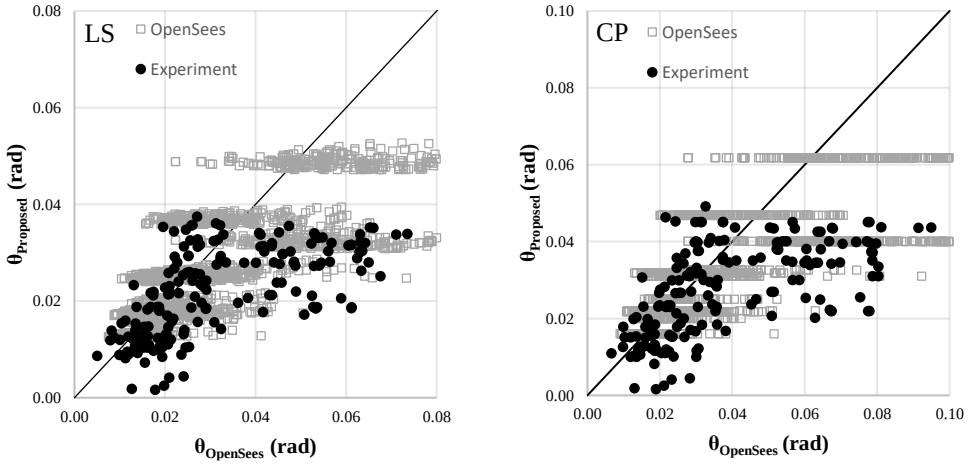

(a) (b)

Figure 3.38 Comparison of result excluding ρ_t = 0.001 with proposed limits for (a) Life Safety; (b) Collapse Prevention.

From Figure 3.38, it can be seen that the majority of the specimens (both for OpenSees and experimental) are on the safe side.

The experimentally obtained performance limits and OpenSees performance limits are normalized with respect to the proposed predictions. The average and standard deviation of each performance limit are given in Table 3.14.

Table 3.14 Average and standard deviation for $\frac{\theta_{Experiment\ \&\ Opensees}}{\theta_{Proposed}}$

	Experimental Results			**OpenSees Results**		
	IO	**LS**	**CP**	**IO**	**LS**	**CP**
$\boldsymbol{\mu}$	2.19	1.64	1.64	1.51	1.14	1.12
$\boldsymbol{\sigma}$	1.35	1.18	1.29	0.66	0.42	0.43

Figure 3.39 shows the comparison of analytical and experimental results with new proposed limits for Collapse Prevention, according to the column class.

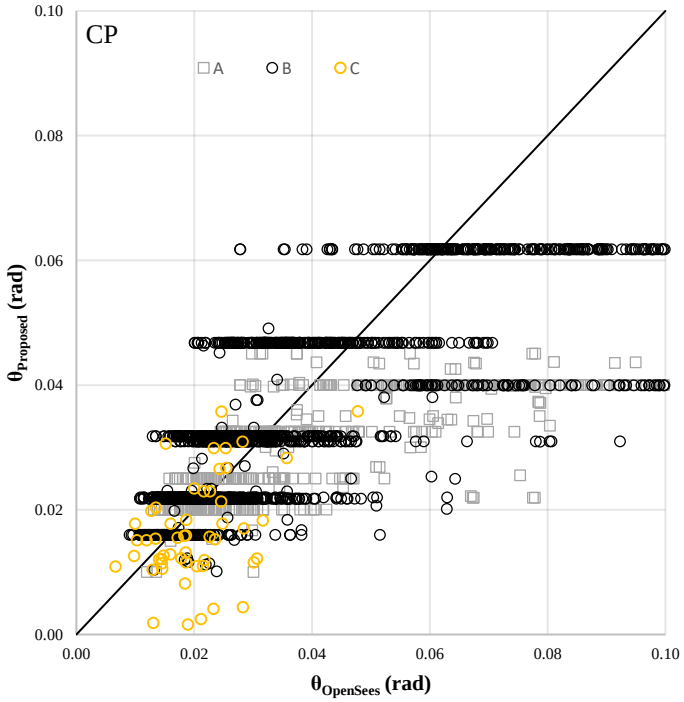

Figure 3.39 Collapse Prevention performance limits according to column class

CHAPTER 4

SUMMARY AND CONCLUSION

4.1 Summary

Performance limits of TBEC (2018), ASCE/SEI 41-17, and Eurocode 8-3 was evaluated at this study. Firstly, 186 experimental column specimens were extracted from Pacific Earthquake Engineering Research (PEER) Center's Structural Performance Database. The performance limits of the seismic guidelines are compared with the experimental database. Next, analytical study was performed to find a suitable model that accurately estimates seismic behavior of reinforced concrete columns, by using OpenSees software. For this purpose, 37 column specimens were chosen from the PEER database. By applying static pushover analysis in OpenSees, force-displacement curves were obtained and compared with the experimental findings. One portal frame experiment was also used for the verification of the OpenSees model. Once the results of analytical findings and experimental findings agree, 3072 unique columns were generated. After finding the yielding and ultimate displacements of these columns, their performance limits were obtained and compared with the limits of the seismic guidelines. Parametric study was performed to observe various parameters' effect on the vertical load-carrying capacity and plastic rotation capacity. Prediction safety for the seismic guidelines depending on transverse reinforcement and axial load ratio is examined.

4.2 Conclusion

The conclusions derived from this study can be summarized as follows:

- The axial load ratio and transverse reinforcement ratio are the primary factors that influence the plastic rotation capacity of reinforced concrete columns.

The plastic rotation capacity tends to increase as the axial load ratio decreases and the transverse reinforcement ratio increases. The equations for plastic rotation capacities on TBEC (2018), ASCE/SEI 41-17, and Eurocode 8-3 successfully captures this variation.

- The yielding strength of longitudinal reinforcement and the concrete compressive strength are the main parameters that affect the lateral load-carrying capacity of reinforced concrete columns.

- For Immediate Occupancy performance level (Damage Limitation in Eurocode 8-3 and Limited Damage in TBEC (2018)), ASCE/SEI 41-17 gives the best estimation. Among the three guidelines, ASCE/SEI 41-17 results are the safest with lowest dispersion level. For IO, TBEC (2018) and Eurocode 8-3 results are found to be unsafe.

- Predictive safety of Eurocode 8-3 for DL is affected by the axial load ratio. As the axial load ratio increases, predictive safety of Eurocode 8-3 decreases significantly. Among 98 experimental column specimens with axial load ratio smaller than 0.2 and among 768 OpenSees columns that have axial load ratio 0.1, 78% and 60% are on the safe side, respectively. Among 43 experimental column specimens with axial load ratio higher than 0.3 and among 1538 OpenSees columns that have axial load ratio 0.4 and 0.5, only 5% and 8% are on the safe side, respectively.

- Predictive safety of TBEC (2018) for LD is also affected by the axial load ratio. Among 98 experimental column specimens with axial load ratio smaller than 0.2 and among 768 OpenSees columns that have axial load ratio 0.1, 83% and 61% are on the safe side, respectively. Among 43 experimental column specimens with axial load ratio higher than 0.3 and among 1538

OpenSees columns that have axial load ratio 0.4 and 0.5, only 16% and 11% are on the safe side, respectively.

- For Life Safety and Collapse Prevention performance levels (Significant Damage and Near Collapse in Eurocode 8-3; and Controlled Damage and Collapse Prevention in TBEC (2018)), TBEC (2018) gives the most conservative results and ASCE/SEI 41-17 gives the least conservative results.

- For Life Safety and Collapse Prevention performance levels, as the transverse reinforcement increases, predictive safety of ASCE/SEI 41-17 decreases. On the other hand, predictive safety of Eurocode 8-3 increases with the increase on transverse reinforcement ratio.

- For well-confined columns with low axial load ratio, TBEC (2018) and Eurocode 8-3 becomes too conservative for Controlled Damage and Collapse Prevention performance levels.

REFERENCES

Aboutaha, R.S.; Engelhardt, M.D.; Jirsa, J.O.: and Kreger, M.E.; "Rehabilitation of Shear Critical Concrete Columns by Use of Rectangular Steel Jackets", American Concrete Institute, ACI Structural Journal, Vol. 96, No.1, January-February1999, pp.68-78.

Acun B, Sucuoglu H. Performance of Reinforced Concrete Columns Designed for Flexure under Severe Displacement Cycles. ACI Structural Journal 2010; 103: 364–371.

Ang Beng Ghee; Priestley, M.J.N.; and Park, R., "Ductility of Reinforced Bridge Piers Under Seismic Loading," Report 81-3, Department of Civil Engineering, University of Canterbury, Christchurch, New Zealand, February 1981, 109 pages.

Arakawa, Takashi; Arai, Yasuyuki; Egashira, Keiichi; and Fujita, Yutaka, "Effects of the Rate of Cyclic Loading on the Load-Carrying Capacity and Inelastic Behavior of Reinforced Concrete Columns," Transactions of the Japan Concrete Institute, Vol. 4, 198

ASCE, SEI 41-17 (2017) Seismic evaluation and retrofit of existing buildings. American Society of Civil Engineers, Reston

Atalay, M.B.; and Penzien, J. "The Seismic Behavior of Critical Regions of Reinforced Concrete Components as Influenced by Moment, Shear and Axial Force," Report No. EERC 75-19, University of California, Berkeley, December 1975, 226 pages.

Azizinamini, Atorod; Johal, Lakhpal S.; Hanson, Norman W.; Musser, Donald W.; and Corley, William G.; "Effects of Transverse Reinforcement on Seismic Performance of Columns - A Partial Parametric Investigation," Project No. CR-9617, Construction Technology

Berry M, Parrish M, Eberhard M. PEER Structural performance database user's manual. Berkeley, CA: Pacific Engineering Research Center, Univ. of California; 2004

Bett, Bart J.; Klingner, Richard E.; and Jirsa, James O., "Behavior of Strengthened and Repaired Reinforced Concrete Columns Under Cyclic Deformations" PMFSEL Report No. 85-3 Department of Civil Engineering, University of Texas at Austin, Austin, Texas

Elwood K.J, Moehle J.P, "Dynamic shear and axial-load failure of reinforced concrete columns" Journal of Structural Engineering. 2008;134(7):1189-1198.

Elwood, K., and Moehle, J. (2005). "Drift capacity of reinforced concrete columns with light transverse reinforcement." Earthquake Spectra, 21(1), 71–89.

Erduran, E., Yakut, A., Drift based damage functions for reinforced concrete columns, Comput. Struct. 82 (2004) 121–130.

Esaki, F. (1996). Reinforcing Effect of Steel Plate Hoops on Ductility of R/C Square Column. Eleventh World Conference on Earthquake Engineering. Acapulco, Mexico, Elsevier Science Ltd.

Eurocode 8: Design of structures for earthquake resistance. Part 3: assessment and retrofitting of building, (2010). EN 1998-3/AC:2010, Brussels, Belgium

Ghannoum WM, Matamoros AB. Nonlinear modeling parameters and acceptance criteria for concrete columns. ACI Spec Publ 2014;297:1–24

Gill, Wayne Douglas; Park, R.; and Priestley, M.J.N., "Ductility of Rectangular Reinforced Concrete Columns with Axial Load," Report 79-1, Department of Civil Engineering, University of Canterbury, Christchurch, New Zealand, February 1979, 136 pages.

Harries, K.A., Ricles, J., Pessiki, S. and Sause, R. (2006)"Seismic Retrofit of Lap Splices in Nonductile Square Columns using Carbon Fiber-Reinforced Jackets",ACI Structural Journal 103(6):874-884.

Ikeda, A. (1968). Report of the Training Institute for Engineering Teachers, Japan;Yokohama National Univeristy.

Imai, Hiroshi; and Yamamoto, Yoshie, "A Study on Causes of Earthquake Damage of Izumi High School Due to Miyagi-Ken-Oki Earthquake in 1978" Transactions of the Japan Concrete Institute, Vol. 8, 1986, pp. 405-418.

Iwasaki;T. K.;Kazuhiko; Hagiwara;Ryoji; Hasegawa;Kinji; Koyama;Tatsuhiko; Yoshida;Takeshi (1985). Experimental investigation on hysteretic behavior of reinforced concrete bridge pier columns 17th Joint Panel Meeting of the U.S.-Japan Cooperative Program in Wind and Seismic Effects; Gaithesburg; Maryland; Center for Building Technology

Kanda, Makoto; Shirai, Nobuaki; Adachi, Hiromi; and Sato, Toshio, "Analytical Study on Elasto-Plastic Hysteretic Behaviors of Reinforced Concrete Members," Transactions of the Japan Concrete Institute, Vol.10, 1988, pp. 257-264

Kokusho S., Fukuhara M., Reported by Hirosawa M., 1973, "A List of Past Experimental Results of Reinforced Concrete Columns." Tsukuba, Japan: Building Research Institute, Report No.2, 326.

Kokusho S., Reported by Hirosawa M., 1973, "A List of Past Experimental Results of Reinforced Concrete Columns." Tsukuba, Japan: Building Research Institute, Report No. 2, 326.

Kono, Susumu; and Watanabe, Fumio, " Damage Evaluation of Reinforced Concrete Columns Under Multiaxial Cyclic Loadings", The Second U.S.-Japan Workshop on Performance-Based Earthquake Engineering Methodology for Reinfoced Concrete Building Structures, Sap

Lam SSE, Wu B, Wong YL, Wang ZY, Liu ZQ, Li CS. Drift capacity of rectangular reinforced concrete columns with low lateral confinement and high-axial load. J Struct Eng – ASCE 2003; 129:733–42.

Lynn, A., Moehle, J.P., Mahin, S.A., Holmes, W.T., "Seismic Evaluation of Existing Reinforced Concrete Building Columns," Earthquake Spectra, Nov. 1996, 715-739

Matamoros, A.B.; "Study of Drift Limits for High-Strength Concrete Columns," Department of Civil Engineering, University of Illinois at Urbana-Champaign, Urbana, Illinois, Oct 1999.

Melek, M. and Wallace, J. W. (2004) "Cylic Behavior of Columns with Short Lap Splices", ACI Structural Journal 101(6):802-811.

Mo, Y.L.; and Wang, S.J., "Seismic Behavior of RC Columns with Various Tie Configurations", Journal of Structural Engineering, ASCE, Vol. 126 No.10, October, 2000, pp. 1122-1130

Nagasaka, Tomoya, "Effectiveness of Steel Fiber as Web Reinforcement in Reinforced Concrete Columns," Transactions of the Japan Concrete Institute, Vol. 4, 1982, pp. 493-500

Nakamura, T., and Yoshimura, M. 2002. Gravity load collapse of reinforced concrete columns with brittle failure modes. Journal of Asian Architecture and Building Engineering, 1(1): 21–27.

Nosho, Kirk; Stanton, John; and MacRae, Gregory; "Retrofit of Rectangular Reinforced Concrete Columns using Tonen Forca Tow Sheet Carbon Fiber Wrapping," Report No. SGEM 96-2, Department of Civil Engineering, University of Washington, Seattle, Washington,

Ohno, Tomonori; and Nishioka, Takashi, "An Experimental Study on Energy Absorption Capacity of Columns in Reinforced Concrete Structures,"

Proceedings of the JSCE, Structural Engineering/Earthquake Engineering, Vol. 1, No 2., October 1984, pp. 137-147.

Ohue, Minoru; Morimoto, Hisao, Fujii, Shigeru; and Morita, Shiro, "The Behavior of R.C. Short Columns Failing in Splitting Bond-Shear Under Dynamic Lateral Loading," Transactions of the Japan Concrete Institute, Vol. 7, 1985, pp. 293-300.

Ono, Arata; Shirai, Nobuaki; Adachi, Hiromi; and Sakamaki, Yoshio, "Elasto-Plastic Behavior of Reinforced Concrete Column with Fluctuating Axial Force," Transactions of the Japan Concrete Institute, Vol. 11, 1989, pp. 239-246.

Ousalem;H. K.;T.; Tasai A. (2003). Effect of Hysteretic Reversals on Lateral and Axial Capacities of Reinforced Concrete Columns. The Fifth U.S. - Japan Workshop on Performance-Based Earthquake Engineering Methodology for Reinforced Concrete Structures. Hakone;Japan;Pacific Earthquake Engineering Research Center (UC Berkeley): 211-221.

Ousalem;H. K.;T.; Tasai A.; Oshugi;Y. (2002). Experimental Study on Seismic Behavior of Reinforced Concrete Columns under Constant and Variable Axial Loadings. Annual Conference of Japan Concrete Institute; Japan.

Özcan, O., Binici, B. Plastic rotation capacity of RC columns under biaxial seismic demands. Bull Earthquake Eng 21, 1979–2012 (2023)

Özdemir MA, Kazaz İ, Özkaya SG (2017) Evaluation and comparison of ultimate deformation limits for RC columns. Eng Struct 153:569–581

Panagiotakos TB, Fardis MN (2001) Deformations of reinforced concrete members at yielding and ultimate. ACI Struct J 98(2):135–148

Pandey;G. R. M.;H. (2005). "Seismic Performance of Reinforced Concrete Piers with Bond-Controlled Reinforcements." ACI Structural Journal 102(2): 295-304

Park, R.; and Paulay, T., "Use of Interlocking Spirals for Transverse Reinforcement in Bridge Columns." Strength and Ductility of Concrete Substructures of Bridges, RRU (Road Research Unit) Bulletin 84, Vol. 1, 1990, pp. 77-92.

Priestley, M. J. N., Seible, F., Verma, R., and Xiao, Y. (1993a). "Seismic shear strength of reinforced concrete columns." Structural Systems Research Project Re- port No. SSRP 93/06, Univ. of California, San Diego, California.

Saatcioglu, Murat; and Grira, Mongi, "Confinement of Reinforced Concrete Columns with Welded Reinforcement Grids," American Concrete Institute, ACI Structural Journal, Vol. 96, No. 1, January-February 1999, pp. 29-39.

Saatcioglu, Murat; and Ozcebe, Guney, "Response of Reinforced Concrete Columns to Simulated Seismic Loading," American Concrete Institute, ACI Structural Journal, January - February, 1989, pp. 3-12

Sezen H.; Moehle, J.P.; "Seismic Behavior of Shear-Critical Reinforced Concrete Building Columns," Seventh U.S. National Conference on Earthquake Engineering, Boston, Massachusetts, July 21-25, 2002

Soesianawati, M.T.; Park, R; and Priestley, M.J.N., "Limited Ductility Design of Reinforced Concrete Columns," Report 86-10, Department of Civil Engineering, University of Canterbury, Christchurch, New Zealand, March 1986, 208 pages

Takemura, H.; Kawashima, K.; "Effect of loading hysteresis on ductility capacity of bridge piers," Journal of Structural Engineering, Vol. 43A, pp. 849-858, Japan

Tanaka, H.; and Park, R., "Effect of Lateral Confining Reinforcement on the Ductile Behavior of Reinforced Concrete Columns," Report 90-2, Department of Civil Engineering, University of Canterbury, June 1990, 458 pages.

TS500 (2000) Requirements for design and construction of reinforced concrete structures. Turkish Standards Institute, Ankara, Turkey

Turkish Building Earthquake Code, TBEC (2018) General Directorate for Foundations, Ankara, Turkey

Umehara, H.; and Jirsa, J.O., "Shear Strength and Deterioration of Short Reinforced Concrete Columns Under Cyclic Deformations," PMFSEL Report No. 82-3, Department of Civil Engineering, University of Texas at Austin, Austin Texas, July 1982, 256 pages

Vintzileou E, Stathatos A. Assessment of the seismic behavior of RC columns. Eng Struct 2007; 29:1296–311

Wang Z, Li L, Zhang Y, Zheng S. Reinforcement model considering slip effect. Eng Struct 2019;198. 109493

Watson, Soesianawati; and Park, R., "Design of Reinforced Concrete Frames of Limited Ductility," Report 89-4, Department of Civil Engineering, University of Canterbury, Christchurch, New Zealand, January 1989, 232 pages

Wehbe, N., Saiidi, M.S., and Sanders, D., "Confinement of Rectangular Bridge Columns for Moderate Seismic Areas," National Center for Earthquake Engineering Research (NCEER) Bulletin, Volume 12, Number 1, Spring 1998

Yakut A, Solmaz T. Performance based displacement limits for reinforced concrete columns under flexure. Paper presented at Fifteenth World Conference on Earthquake Engineering Lisbon, Portugal. 2012.

Yalcin;C. (1997). Seismic Evaluation and Retrofit of Existing Reinforced Concrete Bridge Columns. Department of Civil Engineering. Ottawa; Ontario (Canada); University of Ottawa. Doctor of Philosophy: 398.

Yarandi;M. S. (2007). Seismic Retrofit and Repair of Existing Reinforced Concrete Bridge Columns by Transverse Prestressing. Department of Civil

Engineering. Ottawa;Ontario (Canada);University of Ottawa. Doctor of Philosophy: 282.

Yoshimura;M. T.;Y. and Nakamura;T. (2003). Collapse Drift of Reinforced Concrete Columns. The Fifth U.S. - Japan Workshop on Performance-Based Earthquake Engineering Methodology for Reinforced Concrete Structures. Hakone;Japan;Pacific Earthquake Engineering Research Center (UC Berkeley): 239-253.

Yoshimura;M. Y.;N. (2000). Ultimate Limit State of RC Columns. The Second U.S.-Japan Workshop on Performance-Based Earthquake Engineering Methodology for Reinforced Concrete Structures. Sapporo;Hokkaido;Japan;Pacific Earthquake Engineering Research Center (UC Berkeley): 313-326.

Zahn, F.A.; Park, R; and Priestley, M.J.N., "Design of Reinforced Bridge Columns for Strength and Ductility," Report 86-7, Department of Civil Engineering, University of Canterbury, Christchurch, New Zealand, March 1986, 330 pages.

APPENDICES

Appendix A

Table A.1 Material and geometric properties of the experimental columns

Specimen No	Author	Specimen Name	L (mm)	b (mm)	h (mm)	P (kN)	f'c (MPa)	fyl (MPa)	fyw (MPa)	Clear Cover (mm)
1	Nagasaka	HPRC10-63	300	200	200	147	21.6	371	344	12
2	Umehara	CUS	455	230	410	534	34.9	441	414	25
3	Umehara	CUW	455	410	230	534	34.9	441	414	25
4	Bett	UNIT_1_1	455	305	305	288	29.9	462	414	25
5	Aboutaha	SC3	1219	914	457	0	21.9	434	400	38
6	Aboutaha	SC9	1219	457	914	0	16.0	434	400	38
7	Lynn	3CLH18	1473	457	457	503	26.9	331	400	38
8	Nagasaka	HPRC19-32	300	200	200	294	21.0	371	344	12
9	Ono	CA025C	300	200	200	265	25.8	361	426	19
10	Ono	CA060C	300	200	200	636	25.8	361	426	19
11	Lynn	2CLH18	1473	457	457	503	33.1	331	400	38
12	Lynn	2CMH18	1473	457	457	1512	25.5	331	400	38
13	Lynn	2SLH18	1473	457	457	503	33.1	331	400	38
14	Lynn	3SMD12	1473	457	457	1512	25.5	331	400	38
15	Sezen	Specimen_1	1473	457	457	667	21.1	434	476	41
16	Sezen	Specimen_2	1473	457	457	2669	21.1	434	476	41
17	Sezen	Specimen_4	1473	457	457	667	21.8	434	476	41
18	Lynn	3CMH18	1473	457	457	1512	27.6	331	400	38
19	Lynn	3CMD12	1473	457	457	1512	27.6	331	400	38
20	Lynn	3SLH18	1473	457	457	503	26.9	331	400	38
21	Gill et al.	No.1	1200	550	550	1815	23.1	375	297	40
22	Gill et al.	No.2	1200	550	550	2680	41.4	375	316	38
23	Gill et al.	No.3	1200	550	550	2719	21.4	375	297	40
24	Gill et al.	No.4	1200	550	550	4265	23.5	375	294	38
25	Soesianawati et al.	No.1	1600	400	400	744	46.5	446	364	13
26	Soesianawati et al.	No.2	1600	400	400	2112	44.0	446	360	13
27	Soesianawati et al.	No.3	1600	400	400	2112	44.0	446	364	13
28	Soesianawati et al.	No.4	1600	400	400	1920	40.0	446	255	13
29	Zahn	No.7	1600	400	400	1010	28.3	440	466	13
30	Zahn	No.8	1600	400	400	2502	40.1	440	466	13
31	Watson and Park	No.5	1600	400	400	3280	41.0	474	372	13
32	Watson and Park	No.6	1600	400	400	3200	40.0	474	388	13
33	Watson and Park	No.7	1600	400	400	4704	42.0	474	308	13
34	Watson and Park	No.8	1600	400	400	4368	39.0	474	372	13
35	Watson and Park	No.9	1600	400	400	4480	40.0	474	308	13
36	Tanaka and Park	No1	1600	400	400	819	25.6	474	333	40
37	Tanaka and Park	No2	1600	400	400	819	25.6	474	333	40

Table A.1 (cont'd) Material and geometric properties of the experimental columns

Specimen No	Author	Specimen Name	L (mm)	b (mm)	h (mm)	P (kN)	f'c (MPa)	fyl (MPa)	fyw (MPa)	Clear Cover (mm)
38	Tanaka and Park	No3	1600	400	400	819	25.6	474	333	40
39	Tanaka and Park	No4	1600	400	400	819	25.6	474	333	40
40	Tanaka and Park	No5	1650	550	550	968	32.0	511	325	40
41	Tanaka and Park	No6	1650	550	550	968	32.0	511	325	40
42	Tanaka and Park	No7	1650	550	550	2913	32.0	511	325	40
43	Tanaka and Park	No8	1650	550	550	2913	32.1	511	325	40
44	Kanda et al.	85STC-1	750	250	250	184	27.9	374	506	12
45	Kanda et al.	85STC-2	750	250	250	184	27.9	374	506	35
46	Kanda et al.	85STC-3	750	250	250	184	27.9	374	506	35
47	Kanda et al.	85PDC-2	750	250	250	184	27.9	374	506	35
48	Kanda et al.	85PDC-3	750	250	250	184	27.9	374	506	35
49	Atalay and Penzein	No.1S1	1676	305	305	267	29.1	367	363	32
50	Atalay and Penzein	No.2S1	1676	305	305	267	30.7	367	363	32
51	Atalay and Penzein	No.3S1	1676	305	305	267	29.2	367	363	32
52	Atalay and Penzein	No.4S1	1676	305	305	267	27.6	429	363	32
53	Atalay and Penzein	No.5S1	1676	305	305	534	29.4	429	392	32
54	Atalay and Penzein	No.6S1	1676	305	305	534	31.8	429	392	32
55	Atalay and Penzein	No.9	1676	305	305	801	33.3	363	392	32
56	Atalay and Penzein	No.10	1676	305	305	801	32.4	363	392	32
57	Atalay and Penzein	No.11	1676	305	305	801	31.0	363	373	32
58	Atalay and Penzein	No.12	1676	305	305	801	31.8	363	373	32
59	Azizinamini et al.	NC-2	1372	457	457	1690	39.3	439	454	38
60	Azizinamini et al.	NC-4	1372	457	457	2580	39.8	439	616	41
61	Wehbe et al.	A1	2335	380	610	615	27.2	448	428	28
62	Wehbe et al.	A2	2335	380	610	1505	27.2	448	428	28
63	Wehbe et al.	B1	2335	380	610	601	28.1	448	428	25
64	Wehbe et al.	B2	2335	380	610	1514	28.1	448	428	25
65	Nosho et al	No.1	2134	279	279	1076	40.6	407	351	25
66	Saatcioglu and Giria	BG-1	1645	350	350	1782	34.0	455	570	29
67	Saatcioglu and Giria	BG-2	1645	350	350	1782	34.0	455	570	29
68	Saatcioglu and Giria	BG-3	1645	350	350	831	34.0	455	570	29
69	Saatcioglu and Giria	BG-4	1645	350	350	1923	34.0	455	570	29
70	Saatcioglu and Giria	BG-5	1645	350	350	1923	34.0	455	570	29
71	Saatcioglu and Giria	BG-6	1645	350	350	1900	34.0	478	570	29
72	Saatcioglu and Giria	BG-7	1645	350	350	1923	34.0	455	580	29
73	Saatcioglu and Giria	BG-8	1645	350	350	961	34.0	455	580	29
74	Saatcioglu and Giria	BG-9	1645	350	350	1923	34.0	428	580	29
75	Saatcioglu and Giria	BG-10	1645	350	350	1923	34.0	428	570	29
76	Matamoros et al.	C10-05N	610	203	203	142	69.6	586	407	40
77	Matamoros et al.	C10-05S	610	203	203	142	69.6	586	407	40
78	Matamoros et al.	C10-10N	610	203	203	285	67.8	572	514	26
79	Matamoros et al.	C10-10S	610	203	203	285	67.8	573	515	24
80	Matamoros et al.	C10-20N	610	203	203	569	65.5	572	514	22

Table A.1 (cont'd) Material and geometric properties of the experimental columns

Specimen No	Author	Specimen Name	L (mm)	b (mm)	h (mm)	P (kN)	f'c (MPa)	fyl (MPa)	fyw (MPa)	Clear Cover (mm)
81	Matamoros et al.	C10-20S	610	203	203	569	65.5	573	515	14
82	Matamoros et al.	C5-00N	610	203	203	0	37.9	572	514	24
83	Matamoros et al.	C5-00S	610	203	203	0	37.9	573	515	28
84	Matamoros et al.	C5-20N	610	203	203	285	48.3	586	407	38
85	Matamoros et al.	C5-20S	610	203	203	285	48.3	587	408	39
86	Matamoros et al.	C5-40N	610	203	203	569	38.0	572	514	21
87	Matamoros et al.	C5-40S	610	203	203	569	38.0	573	515	21
88	Mo and Wang	C1-1	1400	400	400	450	24.9	497	459	34
89	Mo and Wang	C1-2	1400	400	400	675	26.7	497	459	34
90	Mo and Wang	C1-3	1400	400	400	900	26.1	497	459	34
91	Mo and Wang	C2-1	1400	400	400	450	25.3	497	459	34
92	Mo and Wang	C2-2	1400	400	400	675	27.1	497	459	34
93	Mo and Wang	C2-3	1400	400	400	900	26.8	497	459	34
94	Mo and Wang	C3-1	1400	400	400	450	26.4	497	459	34
95	Mo and Wang	C3-2	1400	400	400	675	27.5	497	459	34
96	Mo and Wang	C3-3	1400	400	400	900	26.9	497	459	34
97	Kono et al.	D1N30	625	250	250	705	37.6	461	485	21
98	Kono et al.	D1N60	625	250	250	1410	37.6	461	485	21
99	Kono et al.	L1D60	1200	600	600	8000	39.2	388	524	44
100	Kono et al.	L1N60	1200	600	600	8000	39.2	388	524	36
101	Kono et al.	L1N6B	1200	560	560	6000	32.2	388	524	16
102	Imai	UNIT_1	825	400	500	392	27.1	318	336	37
103	Ohue	2D16RS	400	200	200	183	32.0	369	316	11
104	Ohue	4D13RS	400	200	200	183	29.9	370	316	12
105	Park and Paulay	No9	1784	400	600	646	26.9	432	305	24
106	Arakawa	No.102	375	250	250	429	20.6	393	323	28
107	Ohno and Nishioka	L1	1600	400	400	127	24.8	362	325	31
108	Ohno and Nishioka	L2	1600	400	400	127	24.8	362	325	31
109	Ohno and Nishioka	L3	1600	400	400	127	24.8	362	325	31
110	Kanda et al.	85PDC-1	750	250	250	184	24.8	374	352	35
111	Saatcioglu and Ozcebe	U3	1000	350	350	600	34.8	430	470	23
112	Saatcioglu and Ozcebe	U4	1000	350	350	600	32.0	438	470	23
113	Saatcioglu and Ozcebe	U6	1000	350	350	600	37.3	437	425	26
114	Saatcioglu and Ozcebe	U7	1000	350	350	600	39.0	437	425	26
115	Takemura and Kawashima	Test1	1245	400	400	157	35.9	363	368	27
116	Takemura and Kawashima	Test2	1245	400	400	157	35.7	363	368	27
117	Takemura and Kawashima	Test3	1245	400	400	157	34.3	363	368	27
118	Takemura and Kawashima	Test4	1245	400	400	157	33.2	363	368	27
119	Takemura and Kawashima	Test5	1245	400	400	157	36.8	363	368	27
120	Takemura and Kawashima	Test6	1245	400	400	157	35.9	363	368	27
121	Ang et al.	No.3	1600	400	400	1435	23.6	427	320	24
122	Ang et al.	No.4	1600	400	400	840	25.0	427	280	23
123	Iwasaki	I18	1000	500	500	0	33.1	323	258	35

Table A.1 (cont'd) Material and geometric properties of the experimental columns

Specimen No	Author	Specimen Name	L (mm)	b (mm)	h (mm)	P (kN)	f'c (MPa)	fyl (MPa)	fyw (MPa)	Clear Cover (mm)
124	Iwasaki	I21	1000	500	500	0	31.7	323	258	35
125	Verma	UnitR3A	1219	610	406	508	34.5	469	324	22
126	Verma	UnitR5A	1219	610	406	508	32.4	469	324	22
127	Pandey	Specimen_B1	800	300	300	90	32.5	380	396	26
128	Yoshimura	No.1	600	300	300	553	30.7	402	392	31
129	Yoshimura	No.3	600	300	300	553	30.7	402	392	31
130	Yoshimura	No.4	600	300	300	829	30.7	402	392	31
131	Ousalem	C1	450	300	300	364	13.5	340	587	29
132	Ousalem	C4	450	300	300	364	13.5	340	587	27
133	Ousalem	C8	450	300	300	486	18.0	340	384	27
134	Ousalem	C12	450	300	300	324	18.0	340	384	27
135	Ousalem	D1	300	300	300	540	27.7	447	398	27
136	Ousalem	D11	450	300	300	540	28.1	447	398	27
137	Ousalem	D12	450	300	300	540	28.1	447	398	27
138	Ousalem	D14	450	300	300	540	26.1	447	398	27
139	Ousalem	D16	300	300	300	540	26.1	447	398	27
140	Nakamura et al.	N-18M	450	300	300	429	26.5	380	380	31
141	Nakamura et al.	N-27C	450	300	300	644	26.5	380	380	31
142	Nakamura et al.	N-27M	450	300	300	644	26.5	380	380	31
143	Yoshimura	S-1	900	400	400	803	25.1	547	355	29
144	Pandey	A1	650	300	300	90	28.8	380	396	26
145	Iwasaki	I_03	2400	800	400	0	30.7	323	258	50
146	Iwasaki	I_04	2400	800	400	0	28.4	323	258	50
147	Iwasaki	I_10	2500	500	500	0	31.2	323	258	35
148	Iwasaki	I_14	2500	500	500	0	32.0	323	258	35
149	Iwasaki	I_16	2500	500	500	0	31.8	323	258	35
150	Iwasaki	I_17	1750	500	500	0	31.8	323	258	35
151	Iwasaki	I_20	1750	500	500	0	33.3	323	258	35
152	Iwasaki	I_25	1160	500	500	0	33.0	323	258	35
153	Ikeda	IK_43	500	200	200	78	19.6	434	559	14
154	Ikeda	IK_44	500	200	200	78	19.6	434	559	14
155	Ikeda	IK_45	500	200	200	157	19.6	434	559	14
156	Ikeda	IK_46	500	200	200	157	19.6	434	559	14
157	Ikeda	IK_62	500	200	200	78	19.6	345	476	16
158	Ikeda	IK_63	500	200	200	157	19.6	345	476	16
159	Ikeda	IK_64	500	200	200	157	19.6	345	476	16
160	Kokusho	KO_372	500	200	200	157	19.9	524	352	17
161	Kokusho	KO_373	500	200	200	157	20.4	524	352	15
162	Kokusho & Fukuhara	KO_452	500	200	200	392	21.9	359	316	14
163	Kokusho & Fukuhara	KO_454	500	200	200	392	21.9	359	316	12
164	Yalcin	BR-S1	1485	550	550	1800	45.0	445	425	50
165	Elwood	Specimen1	736	229	229	128	24.5	479	718	20
166	Elwood	Specimen2	736	229	229	303	23.9	479	718	20

Table A.1 (cont'd) Material and geometric properties of the experimental columns

Specimen No	Author	Specimen Name	L (mm)	b (mm)	h (mm)	P (kN)	f'c (MPa)	fyl (MPa)	fyw (MPa)	Clear Cover (mm)
167	Verma	UnitR1A	1219	406	610	507	37.9	324	359	22
168	Saatcioglu	U2	1000	350	350	600	30.2	453	470	23
169	Esaki	H-2-1_3	400	200	200	319	23.0	362	364	12
170	Esaki	H-2-1_5	400	200	200	192	23.0	362	364	12
171	Esaki	HT-2-1_3	400	200	200	280	20.2	362	364	12
172	Esaki	HT-2-1_5	400	200	200	168	20.2	362	364	12
173	Yarandi	RRC	1500	350	700	1294	35.0	400	400	45
174	Yarandi	SRC	1500	350	700	1508	42.0	400	400	45
175	Pandey	A4	650	300	300	90	33.1	380	396	26
176	Pandey	C1	1050	300	300	90	36.4	396	427	26
177	Yoshimura	FS0	900	300	300	632	27.0	387	355	26
178	Yoshimura	FS1	900	300	300	632	27.0	387	355	26
179	Saatcioglu and Ozcebe	U1	1000	350	350	0	43.6	430	470	23
180	Harries	L0	2400	457	457	1290	24.6	460	438	29
181	Melek	S10MI	1829	457	457	534	36.2	510	481	38
182	Melek	S20MI	1829	457	457	1068	36.2	510	481	38
183	Melek	S30MI	1829	457	457	1601	36.2	510	481	38
184	Melek	S20HI	1676	457	457	1068	35.3	510	481	38
185	Melek	S20HIN	1676	457	457	1068	35.3	510	481	38
186	Melek	S30XI	1524	457	457	1601	35.3	510	481	38

Table A.2 Reinforcement detailing

Specimen No	Longitudinal reinforcement diameter (mm)	Top longitudinal reinforcement number	Middle longitudinal reinforcement row number	Bottom longitudinal reinforcement number	Transverse reinforcement diameter (mm)	Transverse reinforcement spacing (mm)	Number of transverse bars in width direction	Number of transverse bars in height direction
1	13	2	0	2	5	35	2	2
2	19	2	3	2	6	89	2	4
3	19	2	3	2	6	89	4	2
4	19	3	1	3	6	210	3.41	3.41
5	25	8	0	8	9	406	2	5
6	25	2	6	2	9	406	5	2
7	32	3	1	3	10	457	2	2
8	13	2	0	2	5	20	2	2
9	9	4	2	4	6	70	4	4
10	9	4	2	4	6	70	4	4
11	25	3	1	3	9	457	2	2
12	25	3	1	3	9	457	2	2
13	25	3	1	3	10	457	2	2
14	32	3	1	3	10	305	2	2
15	29	3	1	3	9	305	3.41	3.41
16	29	3	1	3	9	305	3.41	3.41
17	29	3	1	3	9	305	3.41	3.41
18	32	3	1	3	9	457	2	2
19	32	3	1	3	9	305	3.41	3.41
20	32	3	1	3	10	457	2	2
21	24	4	2	4	10	80	4	4
22	24	4	2	4	12	75	4	4
23	24	4	2	4	10	75	4	4
24	24	4	2	4	12	62	4	4
25	16	4	2	4	7	85	4	4
26	16	4	2	4	8	78	4	4
27	16	4	2	4	7	91	4	4
28	16	4	2	4	6	94	4	4
29	16	4	2	4	10	117	4	4
30	16	4	2	4	10	92	4	4
31	16	4	2	4	8	81	4	4
32	16	4	2	4	6	96	4	4
33	16	4	2	4	12	96	4	4
34	16	4	2	4	8	77	4	4
35	16	4	2	4	12	52	4	4
36	20	3	1	3	12	80	3	3
37	20	3	1	3	12	80	3	3
38	20	3	1	3	12	80	3	3
39	20	3	1	3	12	80	3	3
40	20	4	2	4	12	110	4	4
41	20	4	2	4	12	110	4	4
42	20	4	2	4	12	90	4	4
43	20	4	2	4	12	90	4	4
44	13	3	1	3	5	50	2	2
45	13	3	1	3	5	50	2	2
46	13	3	1	3	5	50	2	2
47	13	3	1	3	5	50	2	2
48	13	3	1	3	5	50	2	2
49	22	2	0	2	9	76	2	2
50	22	2	0	2	9	127	2	2

Table A.2 (cont'd) Reinforcement detailing

Specimen No	Longitudinal reinforcement diameter (mm)	Top longitudinal reinforcement number	Middle longitudinal reinforcement row number	Bottom longitudinal reinforcement number	Transverse reinforcement diameter (mm)	Transverse reinforcement spacing (mm)	Number of transverse bars in width direction	Number of transverse bars in height direction
51	22	2	0	2	9	76	2	2
52	22	2	0	2	9	127	2	2
53	22	2	0	2	9	76	2	2
54	22	2	0	2	9	127	2	2
55	22	2	0	2	9	76	2	2
56	22	2	0	2	9	127	2	2
57	22	2	0	2	9	76	2	2
58	22	2	0	2	9	127	2	2
59	25	3	1	3	13	102	3.41	3.41
60	25	3	1	3	9	102	3.41	3.41
61	19	4	5	4	6	110	4	4
62	19	4	5	4	6	110	4	4
63	19	4	5	4	6	83	4	4
64	19	4	5	4	6	83	4	4
65	16	2	0	2	6	229	2	2
66	19	3	1	3	10	152	3	3
67	19	3	1	3	10	76	3	3
68	19	3	1	3	10	76	3	3
69	19	4	2	4	9	152	4	4
70	19	4	2	4	10	76	4	4
71	30	2	0	2	10	76	4	4
72	19	4	2	4	7	76	4	4
73	19	4	2	4	7	76	4	4
74	16	6	4	6	7	76	4	4
75	16	6	4	6	10	76	4	4
76	16	2	0	2	9	76	2	2
77	16	2	0	2	9	76	2	2
78	16	2	0	2	9	76	2	2
79	16	2	0	2	9	77	2	2
80	16	2	0	2	9	76	2	2
81	16	2	0	2	9	77	2	2
82	16	2	0	2	9	76	2	2
83	16	2	0	2	9	77	2	2
84	16	2	0	2	9	76	2	2
85	16	2	0	2	9	77	2	2
86	16	2	0	2	9	76	2	2
87	16	2	0	2	9	77	2	2
88	19	4	2	4	6	50	4	4
89	19	4	2	4	6	50	4	4
90	19	4	2	4	6	50	4	4
91	19	4	2	4	6	52	4	4
92	19	4	2	4	6	52	4	4
93	19	4	2	4	6	52	4	4
94	19	4	2	4	6	54	4	4
95	19	4	2	4	6	54	4	4
96	19	4	2	4	6	54	4	4
97	13	4	2	4	4	40	4	4
98	13	4	2	4	4	40	4	4
99	25	4	2	4	13	100	4	4
100	25	4	2	4	13	100	4	4

Table A.2 (cont'd) Reinforcement detailing

Specimen No	Longitudinal reinforcement diameter (mm)	Top longitudinal reinforcement number	Middle longitudinal reinforcement row number	Bottom longitudinal reinforcement number	Transverse reinforcement diameter (mm)	Transverse reinforcement spacing (mm)	Number of transverse bars in width direction	Number of transverse bars in height direction
101	25	4	2	4	13	100	4	4
102	22	5	2	5	9	100	2	2
103	16	2	0	2	5	50	2	2
104	13	4	0	4	5	50	2	2
105	24	3	2	3	12	80	3	3
106	9	3	0	3	5	32	3	3
107	19	4	0	4	9	100	2	2
108	19	4	0	4	9	100	2	2
109	19	4	0	4	9	100	2	2
110	13	3	1	3	5	50	2	2
111	25	3	1	3	10	75	2	2
112	25	3	1	3	10	50	2	2
113	25	3	1	3	6	65	6	6
114	25	3	1	3	6	65	6	6
115	13	6	4	6	6	70	2	2
116	13	6	4	6	6	70	2	2
117	13	6	4	6	6	70	2	2
118	13	6	4	6	6	70	2	2
119	13	6	4	6	6	70	2	2
120	13	6	4	6	6	70	2	2
121	16	4	2	4	12	100	4	4
122	16	4	2	4	10	90	4	4
123	13	11	9	11	9	254	4	4
124	13	11	9	11	9	254	4	4
125	19	5	6	5	6	127	2	2
126	19	5	6	5	6	127	2	2
127	16	6	0	6	6	250	2	2
128	16	4	2	4	6	100	2	2
129	16	4	2	4	6	200	2	2
130	16	4	2	4	6	100	2	2
131	13	4	2	4	5	160	2	2
132	13	4	2	4	6	75	2	2
133	13	4	2	4	6	75	2	2
134	13	4	2	4	6	75	2	2
135	13	4	2	4	6	50	2	2
136	13	5	3	5	6	150	2	2
137	13	5	3	5	6	150	2	2
138	13	5	3	5	6	50	2	2
139	13	4	2	4	6	50	2	2
140	16	4	2	4	6	100	2	2
141	16	4	2	4	6	100	2	2
142	16	4	2	4	6	100	2	2
143	22	5	3	5	9	180	2	2
144	16	4	2	4	6	150	2	2
145	19	2	6	2	9	199	4	4
146	19	4	6	4	9	199	4	4
147	13	11	9	11	9	254	4	4
148	13	11	9	11	9	254	4	4
149	13	11	9	11	9	254	4	4
150	13	11	9	11	9	254	4	4

Table A.2 (cont'd) Reinforcement detailing

Specimen No	Longitudinal reinforcement diameter (mm)	Top longitudinal reinforcement number	Middle longitudinal reinforcement row number	Bottom longitudinal reinforcement number	Transverse reinforcement diameter (mm)	Transverse reinforcement spacing (mm)	Number of transverse bars in width direction	Number of transverse bars in height direction
151	13	11	9	11	9	254	4	4
152	13	11	9	11	9	50	4	4
153	13	3	0	3	6	100	2	2
154	13	3	0	3	6	100	2	2
155	13	3	0	3	6	100	2	2
156	13	3	1	3	6	100	2	2
157	10	5	0	5	6	100	2	2
158	10	5	0	5	6	100	2	2
159	10	5	0	5	6	100	2	2
160	13	2	0	2	7	100	2	2
161	16	2	0	2	7	100	2	2
162	19	2	0	2	7	100	2	2
163	22	2	0	2	7	100	2	2
164	25	4	2	4	11	300	2	2
165	13	3	1	3	5	152	3.41	3.41
166	13	3	1	3	5	152	3.41	3.41
167	19	5	6	5	6	127	2	2
168	25	3	1	3	10	150	2	2
169	13	3	1	3	6	40	2	2
170	13	3	1	3	6	50	2	2
171	13	3	1	3	6	60	3	3
172	13	3	1	3	6	75	3	3
173	20	4	2	4	6	300	2	2
174	20	4	2	4	11	300	2	2
175	16	4	2	4	6	70	2	2
176	16	4	2	4	6	150	2	2
177	19	4	2	4	9	75	2	2
178	19	4	2	4	9	75	2	2
179	25	3	1	3	10	150	2	2
180	22	3	1	3	10	356	2	2
181	25	3	1	3	10	457	2	2
182	25	3	1	3	10	457	2	2
183	25	3	1	3	10	457	2	2
184	25	3	1	3	10	457	2	2
185	25	3	1	3	10	457	2	2
186	25	3	1	3	10	457	2	2

Table A.3 Performance limits for experiment and TBEC (2018)

	Experiment (rad)			TBEC (2018) (rad)		
Specimen No	**IO**	**LS**	**CP**	**IO**	**LS**	**CP**
1	0.0137	0.0196	0.0216	0.0072	0.0162	0.0192
2	0.0147	0.0179	0.0190	0.0070	0.0103	0.0114
3	0.0140	0.0210	0.0233	0.0099	0.0136	0.0148
4	0.0159	0.0198	0.0211	0.0082	0.0122	0.0135
5	0.0117	0.0241	0.0283	0.0080	0.0218	0.0264
6	0.0117	0.0127	0.0130	0.0060	0.0096	0.0108
7	0.0131	0.0141	0.0145	0.0077	0.0141	0.0163
8	0.0097	0.0175	0.0200	0.0083	0.0155	0.0179
9	0.0107	0.0271	0.0326	0.0071	0.0152	0.0179
10	0.0055	0.0113	0.0132	0.0104	0.0141	0.0154
11	0.0093	0.0253	0.0307	0.0067	0.0166	0.0199
12	0.0094	0.0121	0.0130	0.0084	0.0112	0.0121
13	0.0093	0.0157	0.0178	0.0067	0.0167	0.0200
14	0.0124	0.0194	0.0218	0.0091	0.0119	0.0128
15	0.0142	0.0273	0.0316	0.0107	0.0161	0.0179
16	0.0071	0.0156	0.0185	0.0240	0.0252	0.0256
17	0.0162	0.0309	0.0358	0.0106	0.0166	0.0186
18	0.0122	0.0140	0.0146	0.0088	0.0119	0.0129
19	0.0134	0.0203	0.0226	0.0089	0.0132	0.0146
20	0.0115	0.0134	0.0140	0.0077	0.0141	0.0163
21	0.0089	0.0278	0.0341	0.0074	0.0149	0.0174
22	0.0089	0.0221	0.0265	0.0068	0.0149	0.0176
23	0.0061	0.0175	0.0213	0.0085	0.0145	0.0165
24	0.0051	0.0133	0.0160	0.0101	0.0157	0.0176
25	0.0097	0.0437	0.0550	0.0083	0.0221	0.0267
26	0.0086	0.0292	0.0360	0.0102	0.0188	0.0217
27	0.0082	0.0261	0.0321	0.0102	0.0169	0.0192
28	0.0090	0.0215	0.0257	0.0101	0.0152	0.0168
29	0.0111	0.0488	0.0614	0.0097	0.0240	0.0287
30	0.0096	0.0589	0.0753	0.0112	0.0211	0.0244
31	0.0076	0.0219	0.0266	0.0138	0.0185	0.0200
32	0.0058	0.0152	0.0184	0.0138	0.0168	0.0177
33	0.0038	0.0099	0.0120	0.0211	0.0245	0.0257
34	0.0039	0.0111	0.0135	0.0207	0.0234	0.0243
35	0.0045	0.0237	0.0301	0.0183	0.0251	0.0274

Table A.3 (cont'd) Performance limits for experiment and TBEC (2018)

	Experiment (rad)			TBEC (2018) (rad)		
Specimen No	**IO**	**LS**	**CP**	**IO**	**LS**	**CP**
36	0.0129	0.0375	0.0457	0.0121	0.0311	0.0375
37	0.0122	0.0485	0.0605	0.0121	0.0311	0.0374
38	0.0107	0.0335	0.0411	0.0121	0.0306	0.0368
39	0.0116	0.0441	0.0549	0.0121	0.0309	0.0372
40	0.0123	0.0436	0.0540	0.0085	0.0226	0.0273
41	0.0109	0.0606	0.0772	0.0085	0.0221	0.0267
42	0.0088	0.0447	0.0567	0.0104	0.0186	0.0213
43	0.0076	0.0458	0.0585	0.0104	0.0185	0.0213
44	0.0088	0.0417	0.0527	0.0071	0.0217	0.0265
45	0.0075	0.0411	0.0524	0.0080	0.0211	0.0255
46	0.0088	0.0417	0.0527	0.0080	0.0209	0.0252
47	0.0080	0.0242	0.0296	0.0080	0.0209	0.0252
48	0.0085	0.0273	0.0335	0.0080	0.0214	0.0259
49	0.0126	0.0256	0.0300	0.0110	0.0332	0.0407
50	0.0134	0.0317	0.0379	0.0109	0.0311	0.0379
51	0.0141	0.0308	0.0364	0.0110	0.0332	0.0406
52	0.0180	0.0273	0.0304	0.0131	0.0321	0.0384
53	0.0169	0.0323	0.0374	0.0144	0.0295	0.0345
54	0.0170	0.0323	0.0374	0.0140	0.0255	0.0293
55	0.0162	0.0254	0.0285	0.0130	0.0239	0.0275
56	0.0167	0.0267	0.0301	0.0132	0.0208	0.0233
57	0.0136	0.0240	0.0275	0.0135	0.0236	0.0270
58	0.0168	0.0278	0.0314	0.0133	0.0206	0.0231
59	0.0116	0.0453	0.0566	0.0094	0.0202	0.0238
60	0.0101	0.0279	0.0338	0.0105	0.0169	0.0190
61	0.0151	0.0490	0.0603	0.0084	0.0170	0.0199
62	0.0141	0.0417	0.0509	0.0094	0.0151	0.0170
63	0.0175	0.0634	0.0787	0.0083	0.0183	0.0216
64	0.0173	0.0525	0.0643	0.0093	0.0156	0.0178
65	0.0170	0.0207	0.0219	0.0179	0.0206	0.0214
66	0.0091	0.0281	0.0345	0.0165	0.0220	0.0238
67	0.0088	0.0362	0.0453	0.0162	0.0264	0.0298
68	0.0140	0.0625	0.0786	0.0124	0.0313	0.0376
69	0.0100	0.0291	0.0354	0.0172	0.0232	0.0251
70	0.0125	0.0536	0.0673	0.0167	0.0270	0.0304

Table A.3 (cont'd) Performance limits for experiment and TBEC (2018)

	Experiment (rad)			TBEC (2018) (rad)		
Specimen No	**IO**	**LS**	**CP**	**IO**	**LS**	**CP**
71	0.0103	0.0528	0.0669	0.0206	0.0339	0.0383
72	0.0109	0.0533	0.0675	0.0167	0.0236	0.0259
73	0.0188	0.0650	0.0804	0.0129	0.0258	0.0301
74	0.0113	0.0612	0.0778	0.0148	0.0215	0.0238
75	0.0124	0.0612	0.0775	0.0149	0.0246	0.0278
76	0.0262	0.0548	0.0644	0.0132	0.0400	0.0489
77	0.0249	0.0539	0.0636	0.0132	0.0406	0.0497
78	0.0220	0.0611	0.0741	0.0123	0.0266	0.0313
79	0.0223	0.0612	0.0742	0.0122	0.0268	0.0317
80	0.0253	0.0541	0.0637	0.0139	0.0200	0.0220
81	0.0228	0.0529	0.0630	0.0130	0.0202	0.0225
82	0.0290	0.0653	0.0774	0.0124	0.0311	0.0374
83	0.0305	0.0660	0.0779	0.0128	0.0327	0.0394
84	0.0259	0.0460	0.0527	0.0162	0.0272	0.0309
85	0.0267	0.0461	0.0525	0.0164	0.0271	0.0307
86	0.0203	0.0437	0.0515	0.0190	0.0237	0.0252
87	0.0199	0.0431	0.0509	0.0191	0.0237	0.0252
88	0.0160	0.0568	0.0705	0.0106	0.0240	0.0285
89	0.0158	0.0630	0.0788	0.0109	0.0242	0.0286
90	0.0159	0.0545	0.0674	0.0115	0.0221	0.0256
91	0.0179	0.0643	0.0797	0.0106	0.0242	0.0287
92	0.0167	0.0631	0.0785	0.0109	0.0232	0.0273
93	0.0144	0.0486	0.0600	0.0114	0.0217	0.0251
94	0.0192	0.0632	0.0779	0.0105	0.0240	0.0285
95	0.0192	0.0636	0.0784	0.0108	0.0235	0.0277
96	0.0165	0.0565	0.0698	0.0114	0.0218	0.0253
97	0.0082	0.0284	0.0352	0.0097	0.0157	0.0177
98	0.0062	0.0194	0.0238	0.0168	0.0194	0.0203
99	0.0071	0.0242	0.0298	0.0101	0.0141	0.0155
100	0.0047	0.0213	0.0268	0.0097	0.0137	0.0151
101	0.0046	0.0184	0.0230	0.0095	0.0145	0.0162
102	0.0076	0.0230	0.0282	0.0055	0.0110	0.0129
103	0.0171	0.0401	0.0478	0.0075	0.0161	0.0190
104	0.0172	0.0228	0.0246	0.0073	0.0148	0.0174
105	0.0090	0.0523	0.0668	0.0076	0.0187	0.0224

Table A.3 (cont'd) Performance limits for experiment and TBEC (2018)

	Experiment (rad)			TBEC (2018) (rad)		
Specimen No	**IO**	**LS**	**CP**	**IO**	**LS**	**CP**
106	0.0151	0.0220	0.0243	0.0076	0.0153	0.0178
107	0.0089	0.0452	0.0573	0.0074	0.0217	0.0264
108	0.0085	0.0530	0.0678	0.0074	0.0217	0.0264
109	0.0092	0.0408	0.0514	0.0074	0.0217	0.0264
110	0.0076	0.0222	0.0270	0.0082	0.0179	0.0212
111	0.0312	0.0561	0.0644	0.0095	0.0165	0.0188
112	0.0196	0.0852	0.1071	0.0100	0.0179	0.0205
113	0.0204	0.0824	0.1030	0.0095	0.0201	0.0236
114	0.0204	0.0814	0.1017	0.0094	0.0198	0.0233
115	0.0094	0.0329	0.0408	0.0059	0.0190	0.0234
116	0.0131	0.0411	0.0504	0.0059	0.0191	0.0234
117	0.0100	0.0531	0.0675	0.0059	0.0192	0.0236
118	0.0102	0.0711	0.0914	0.0060	0.0193	0.0237
119	0.0089	0.0631	0.0811	0.0059	0.0190	0.0233
120	0.0094	0.0736	0.0949	0.0059	0.0190	0.0234
121	0.0065	0.0266	0.0333	0.0116	0.0253	0.0298
122	0.0085	0.0315	0.0391	0.0097	0.0259	0.0312
123	0.0071	0.0188	0.0227	0.0048	0.0146	0.0178
124	0.0103	0.0188	0.0216	0.0048	0.0139	0.0169
125	0.0077	0.0130	0.0148	0.0082	0.0116	0.0127
126	0.0060	0.0089	0.0098	0.0083	0.0116	0.0127
127	0.0076	0.0158	0.0186	0.0069	0.0282	0.0353
128	0.0096	0.0164	0.0187	0.0079	0.0112	0.0123
129	0.0069	0.0137	0.0160	0.0079	0.0103	0.0111
130	0.0092	0.0163	0.0186	0.0086	0.0110	0.0118
131	0.0004	0.0051	0.0066	0.0072	0.0096	0.0104
132	0.0043	0.0135	0.0166	0.0072	0.0121	0.0138
133	0.0036	0.0105	0.0128	0.0069	0.0104	0.0115
134	0.0046	0.0162	0.0200	0.0065	0.0109	0.0124
135	0.0071	0.0132	0.0152	0.0076	0.0116	0.0130
136	0.0011	0.0080	0.0103	0.0077	0.0101	0.0109
137	0.0047	0.0101	0.0119	0.0077	0.0101	0.0109
138	0.0143	0.0211	0.0233	0.0079	0.0118	0.0131
139	0.0041	0.0200	0.0253	0.0077	0.0117	0.0130
140	0.0045	0.0113	0.0135	0.0073	0.0109	0.0121

Table A.3 (cont'd) Performance limits for experiment and TBEC (2018)

	Experiment (rad)			TBEC (2018) (rad)		
Specimen No	**IO**	**LS**	**CP**	**IO**	**LS**	**CP**
141	0.0031	0.0082	0.0099	0.0077	0.0106	0.0115
142	0.0059	0.0135	0.0160	0.0077	0.0106	0.0115
143	0.0088	0.0208	0.0248	0.0118	0.0145	0.0154
144	0.0118	0.0243	0.0284	0.0067	0.0115	0.0131
145	0.0199	0.0474	0.0566	0.0083	0.0272	0.0335
146	0.0131	0.0313	0.0374	0.0086	0.0270	0.0332
147	0.0166	0.0322	0.0375	0.0067	0.0194	0.0237
148	0.0099	0.0259	0.0312	0.0067	0.0194	0.0236
149	0.0098	0.0261	0.0316	0.0067	0.0194	0.0236
150	0.0121	0.0259	0.0305	0.0056	0.0181	0.0222
151	0.0094	0.0292	0.0358	0.0056	0.0179	0.0220
152	0.0091	0.0246	0.0298	0.0049	0.0146	0.0179
153	0.0072	0.0211	0.0258	0.0094	0.0183	0.0212
154	0.0080	0.0169	0.0198	0.0094	0.0183	0.0212
155	0.0086	0.0168	0.0196	0.0102	0.0163	0.0183
156	0.0086	0.0137	0.0154	0.0104	0.0145	0.0159
157	0.0065	0.0231	0.0286	0.0069	0.0179	0.0216
158	0.0065	0.0183	0.0222	0.0075	0.0127	0.0144
159	0.0062	0.0187	0.0229	0.0075	0.0127	0.0144
160	0.0068	0.0208	0.0254	0.0125	0.0179	0.0197
161	0.0112	0.0210	0.0243	0.0140	0.0200	0.0220
162	0.0077	0.0148	0.0172	0.0104	0.0131	0.0140
163	0.0074	0.0120	0.0135	0.0097	0.0134	0.0146
164	0.0084	0.0198	0.0235	0.0079	0.0132	0.0150
165	0.0147	0.0508	0.0629	0.0103	0.0191	0.0220
166	0.0150	0.0324	0.0382	0.0118	0.0165	0.0181
167	0.0082	0.0158	0.0183	0.0050	0.0100	0.0116
168	0.0137	0.0384	0.0466	0.0104	0.0144	0.0157
169	0.0091	0.0208	0.0247	0.0086	0.0132	0.0148
170	0.0086	0.0252	0.0308	0.0078	0.0126	0.0143
171	0.0092	0.0249	0.0301	0.0088	0.0150	0.0171
172	0.0091	0.0252	0.0305	0.0080	0.0145	0.0167
173	0.0035	0.0117	0.0145	0.0060	0.0089	0.0099
174	0.0083	0.0205	0.0246	0.0060	0.0089	0.0099
175	0.0095	0.0292	0.0357	0.0065	0.0147	0.0174

Table A.3 (cont'd) Performance limits for experiment and TBEC (2018)

	Experiment (rad)			TBEC (2018) (rad)		
Specimen No	**IO**	**LS**	**CP**	**IO**	**LS**	**CP**
176	0.0096	0.0154	0.0174	0.0078	0.0181	0.0215
177	0.0097	0.0478	0.0605	0.0101	0.0152	0.0169
178	0.0112	0.0420	0.0522	0.0101	0.0152	0.0169
179	0.0296	0.0676	0.0803	0.0080	0.0196	0.0234
180	0.0082	0.0190	0.0226	0.0132	0.0173	0.0186
181	0.0096	0.0165	0.0188	0.0109	0.0192	0.0220
182	0.0090	0.0165	0.0190	0.0116	0.0168	0.0185
183	0.0090	0.0184	0.0215	0.0125	0.0162	0.0175
184	0.0090	0.0162	0.0186	0.0112	0.0161	0.0177
185	0.0078	0.0246	0.0301	0.0112	0.0161	0.0177
186	0.0088	0.0175	0.0205	0.0115	0.0147	0.0158

Table A.4 Performance limits for ASCE/SEI 41-17 and Eurocode 8-3

	ASCE/SEI 41-17 (rad)			Eurocode 8-3 (rad)		
Specimen No	**IO**	**LS**	**CP**	**DL**	**SD**	**NC**
1	0.0062	0.0350	0.0481	0.0080	0.0165	0.0219
2	0.0036	0.0228	0.0313	0.0080	0.0129	0.0172
3	0.0054	0.0249	0.0332	0.0109	0.0154	0.0205
4	0.0040	0.0226	0.0306	0.0091	0.0161	0.0215
5	0.0044	0.0112	0.0140	0.0088	0.0229	0.0305
6	0.0051	0.0322	0.0443	0.0068	0.0150	0.0200
7	0.0068	0.0187	0.0235	0.0083	0.0203	0.0270
8	0.0056	0.0335	0.0461	0.0093	0.0144	0.0193
9	0.0060	0.0343	0.0470	0.0079	0.0159	0.0212
10	0.0027	0.0108	0.0145	0.0121	0.0103	0.0137
11	0.0055	0.0152	0.0190	0.0073	0.0233	0.0310
12	0.0050	0.0079	0.0091	0.0093	0.0170	0.0227
13	0.0054	0.0151	0.0190	0.0073	0.0233	0.0310
14	0.0060	0.0121	0.0145	0.0099	0.0160	0.0213
15	0.0093	0.0313	0.0407	0.0117	0.0186	0.0249
16	0.0044	0.0080	0.0094	0.0267	0.0108	0.0144
17	0.0091	0.0308	0.0402	0.0116	0.0189	0.0252
18	0.0054	0.0083	0.0095	0.0097	0.0166	0.0221
19	0.0059	0.0172	0.0217	0.0097	0.0169	0.0225
20	0.0068	0.0187	0.0235	0.0083	0.0203	0.0270
21	0.0068	0.0306	0.0413	0.0083	0.0181	0.0242
22	0.0081	0.0317	0.0428	0.0077	0.0215	0.0287
23	0.0050	0.0255	0.0345	0.0096	0.0152	0.0202
24	0.0050	0.0144	0.0192	0.0116	0.0143	0.0191
25	0.0121	0.0334	0.0436	0.0081	0.0293	0.0390
26	0.0098	0.0237	0.0305	0.0115	0.0235	0.0314
27	0.0088	0.0187	0.0236	0.0114	0.0227	0.0302
28	0.0072	0.0127	0.0151	0.0114	0.0215	0.0287
29	0.0119	0.0371	0.0490	0.0107	0.0256	0.0341
30	0.0092	0.0275	0.0362	0.0127	0.0225	0.0300
31	0.0068	0.0169	0.0216	0.0156	0.0183	0.0244
32	0.0053	0.0104	0.0124	0.0157	0.0172	0.0229
33	0.0068	0.0106	0.0127	0.0241	0.0152	0.0203
34	0.0058	0.0068	0.0074	0.0237	0.0144	0.0192
35	0.0082	0.0141	0.0175	0.0208	0.0184	0.0245

Table A.4 (cont'd) Performance limits for ASCE/SEI 41-17 and Eurocode 8-3

	ASCE/SEI 41-17 (rad)			Eurocode 8-3 (rad)		
Specimen No	**IO**	**LS**	**CP**	**DL**	**SD**	**NC**
36	0.0122	0.0410	0.0548	0.0132	0.0265	0.0353
37	0.0122	0.0410	0.0548	0.0132	0.0265	0.0353
38	0.0124	0.0413	0.0551	0.0132	0.0265	0.0353
39	0.0123	0.0412	0.0549	0.0132	0.0265	0.0353
40	0.0106	0.0399	0.0537	0.0095	0.0263	0.0351
41	0.0109	0.0402	0.0540	0.0095	0.0263	0.0351
42	0.0088	0.0303	0.0404	0.0117	0.0215	0.0287
43	0.0088	0.0304	0.0404	0.0117	0.0216	0.0288
44	0.0102	0.0385	0.0516	0.0079	0.0231	0.0308
45	0.0103	0.0404	0.0543	0.0086	0.0230	0.0307
46	0.0104	0.0406	0.0545	0.0086	0.0230	0.0307
47	0.0104	0.0406	0.0544	0.0086	0.0230	0.0307
48	0.0102	0.0403	0.0541	0.0086	0.0230	0.0307
49	0.0155	0.0453	0.0594	0.0109	0.0292	0.0389
50	0.0145	0.0398	0.0518	0.0107	0.0287	0.0383
51	0.0150	0.0447	0.0588	0.0109	0.0292	0.0389
52	0.0162	0.0425	0.0548	0.0129	0.0278	0.0370
53	0.0142	0.0391	0.0510	0.0143	0.0261	0.0348
54	0.0133	0.0330	0.0426	0.0138	0.0261	0.0348
55	0.0122	0.0330	0.0431	0.0129	0.0247	0.0329
56	0.0112	0.0265	0.0341	0.0130	0.0236	0.0315
57	0.0123	0.0327	0.0425	0.0133	0.0238	0.0317
58	0.0112	0.0260	0.0333	0.0131	0.0234	0.0312
59	0.0110	0.0377	0.0503	0.0104	0.0241	0.0322
60	0.0083	0.0288	0.0382	0.0117	0.0204	0.0272
61	0.0149	0.0406	0.0521	0.0093	0.0228	0.0304
62	0.0106	0.0271	0.0344	0.0105	0.0192	0.0257
63	0.0156	0.0432	0.0557	0.0092	0.0238	0.0318
64	0.0118	0.0309	0.0395	0.0104	0.0201	0.0268
65	0.0114	0.0122	0.0125	0.0178	0.0250	0.0333
66	0.0098	0.0250	0.0320	0.0180	0.0188	0.0250
67	0.0111	0.0334	0.0438	0.0177	0.0216	0.0288
68	0.0153	0.0440	0.0575	0.0134	0.0284	0.0379
69	0.0102	0.0276	0.0356	0.0188	0.0169	0.0225
70	0.0126	0.0372	0.0485	0.0182	0.0210	0.0280

Table A.4 (cont'd) Performance limits for ASCE/SEI 41-17 and Eurocode 8-3

	ASCE/SEI 41-17 (rad)			Eurocode 8-3 (rad)		
Specimen No	**IO**	**LS**	**CP**	**DL**	**SD**	**NC**
71	0.0121	0.0368	0.0482	0.0222	0.0246	0.0328
72	0.0103	0.0275	0.0352	0.0182	0.0177	0.0236
73	0.0153	0.0392	0.0503	0.0141	0.0234	0.0312
74	0.0105	0.0276	0.0354	0.0163	0.0171	0.0227
75	0.0126	0.0372	0.0485	0.0164	0.0203	0.0270
76	0.0113	0.0401	0.0542	0.0140	0.0295	0.0394
77	0.0111	0.0399	0.0540	0.0140	0.0295	0.0394
78	0.0125	0.0421	0.0562	0.0133	0.0279	0.0373
79	0.0123	0.0417	0.0557	0.0132	0.0279	0.0373
80	0.0105	0.0339	0.0452	0.0151	0.0244	0.0325
81	0.0101	0.0324	0.0432	0.0143	0.0244	0.0326
82	0.0118	0.0447	0.0603	0.0133	0.0286	0.0382
83	0.0118	0.0448	0.0605	0.0137	0.0285	0.0380
84	0.0113	0.0405	0.0545	0.0172	0.0246	0.0328
85	0.0113	0.0405	0.0546	0.0174	0.0245	0.0327
86	0.0083	0.0322	0.0434	0.0207	0.0186	0.0247
87	0.0083	0.0321	0.0433	0.0208	0.0185	0.0247
88	0.0147	0.0467	0.0615	0.0117	0.0264	0.0353
89	0.0133	0.0426	0.0562	0.0120	0.0250	0.0333
90	0.0127	0.0399	0.0523	0.0127	0.0234	0.0311
91	0.0145	0.0464	0.0610	0.0116	0.0262	0.0349
92	0.0138	0.0429	0.0563	0.0120	0.0248	0.0331
93	0.0127	0.0396	0.0519	0.0126	0.0233	0.0310
94	0.0146	0.0462	0.0608	0.0115	0.0261	0.0348
95	0.0136	0.0424	0.0557	0.0119	0.0247	0.0329
96	0.0125	0.0390	0.0512	0.0126	0.0231	0.0307
97	0.0071	0.0263	0.0347	0.0110	0.0178	0.0237
98	0.0036	0.0098	0.0123	0.0193	0.0124	0.0165
99	0.0041	0.0157	0.0209	0.0118	0.0144	0.0192
100	0.0041	0.0156	0.0207	0.0114	0.0144	0.0192
101	0.0047	0.0148	0.0192	0.0111	0.0142	0.0190
102	0.0059	0.0319	0.0433	0.0061	0.0167	0.0223
103	0.0067	0.0297	0.0399	0.0083	0.0194	0.0259
104	0.0067	0.0303	0.0407	0.0081	0.0189	0.0253
105	0.0130	0.0452	0.0603	0.0085	0.0250	0.0333

Table A.4 (cont'd) Performance limits for ASCE/SEI 41-17 and Eurocode 8-3

	ASCE/SEI 41-17 (rad)			Eurocode 8-3 (rad)		
Specimen No	**IO**	**LS**	**CP**	**DL**	**SD**	**NC**
106	0.0052	0.0317	0.0436	0.0086	0.0157	0.0209
107	0.0109	0.0353	0.0468	0.0080	0.0266	0.0355
108	0.0104	0.0346	0.0462	0.0080	0.0266	0.0355
109	0.0104	0.0347	0.0463	0.0080	0.0266	0.0355
110	0.0100	0.0376	0.0502	0.0089	0.0218	0.0291
111	0.0112	0.0391	0.0519	0.0105	0.0206	0.0275
112	0.0133	0.0441	0.0583	0.0110	0.0210	0.0280
113	0.0134	0.0432	0.0568	0.0104	0.0246	0.0327
114	0.0133	0.0431	0.0568	0.0103	0.0247	0.0330
115	0.0078	0.0240	0.0320	0.0065	0.0256	0.0342
116	0.0077	0.0240	0.0320	0.0065	0.0256	0.0341
117	0.0079	0.0247	0.0329	0.0066	0.0254	0.0338
118	0.0080	0.0253	0.0337	0.0066	0.0252	0.0336
119	0.0078	0.0239	0.0317	0.0065	0.0258	0.0344
120	0.0080	0.0245	0.0325	0.0065	0.0256	0.0342
121	0.0097	0.0336	0.0449	0.0128	0.0221	0.0295
122	0.0111	0.0358	0.0476	0.0107	0.0250	0.0334
123	0.0054	0.0195	0.0261	0.0053	0.0207	0.0276
124	0.0054	0.0203	0.0272	0.0053	0.0205	0.0274
125	0.0104	0.0182	0.0213	0.0091	0.0210	0.0280
126	0.0128	0.0213	0.0246	0.0092	0.0206	0.0275
127	0.0050	0.0159	0.0203	0.0076	0.0238	0.0318
128	0.0039	0.0183	0.0241	0.0088	0.0154	0.0206
129	0.0037	0.0108	0.0136	0.0088	0.0153	0.0203
130	0.0033	0.0133	0.0172	0.0096	0.0137	0.0182
131	0.0018	0.0157	0.0213	0.0080	0.0114	0.0152
132	0.0041	0.0308	0.0423	0.0080	0.0123	0.0164
133	0.0028	0.0226	0.0308	0.0077	0.0125	0.0167
134	0.0041	0.0279	0.0381	0.0072	0.0142	0.0189
135	0.0034	0.0259	0.0357	0.0085	0.0133	0.0178
136	0.0023	0.0135	0.0180	0.0087	0.0138	0.0184
137	0.0023	0.0135	0.0181	0.0087	0.0138	0.0184
138	0.0043	0.0272	0.0371	0.0089	0.0139	0.0186
139	0.0031	0.0259	0.0358	0.0087	0.0130	0.0173
140	0.0032	0.0214	0.0288	0.0081	0.0139	0.0185

Table A.4 (cont'd) Performance limits for ASCE/SEI 41-17 and Eurocode 8-3

	ASCE/SEI 41-17 (rad)			Eurocode 8-3 (rad)		
Specimen No	**IO**	**LS**	**CP**	**DL**	**SD**	**NC**
141	0.0022	0.0158	0.0213	0.0086	0.0125	0.0166
142	0.0024	0.0161	0.0215	0.0086	0.0125	0.0166
143	0.0049	0.0200	0.0260	0.0132	0.0147	0.0196
144	0.0056	0.0233	0.0306	0.0074	0.0190	0.0253
145	0.0108	0.0213	0.0270	0.0081	0.0314	0.0418
146	0.0124	0.0243	0.0304	0.0084	0.0299	0.0399
147	0.0112	0.0248	0.0317	0.0073	0.0282	0.0376
148	0.0110	0.0243	0.0311	0.0072	0.0284	0.0378
149	0.0113	0.0248	0.0316	0.0072	0.0283	0.0378
150	0.0085	0.0226	0.0294	0.0061	0.0250	0.0333
151	0.0084	0.0217	0.0283	0.0061	0.0252	0.0337
152	0.0093	0.0387	0.0526	0.0054	0.0255	0.0340
153	0.0103	0.0421	0.0562	0.0103	0.0199	0.0265
154	0.0100	0.0418	0.0558	0.0103	0.0199	0.0265
155	0.0081	0.0344	0.0458	0.0112	0.0176	0.0235
156	0.0080	0.0342	0.0455	0.0115	0.0157	0.0210
157	0.0091	0.0394	0.0530	0.0076	0.0198	0.0264
158	0.0074	0.0318	0.0426	0.0083	0.0175	0.0234
159	0.0074	0.0318	0.0426	0.0083	0.0175	0.0234
160	0.0073	0.0307	0.0409	0.0137	0.0175	0.0234
161	0.0076	0.0314	0.0415	0.0152	0.0178	0.0237
162	0.0045	0.0169	0.0219	0.0114	0.0143	0.0190
163	0.0044	0.0167	0.0216	0.0106	0.0153	0.0203
164	0.0060	0.0149	0.0190	0.0088	0.0215	0.0286
165	0.0114	0.0400	0.0527	0.0113	0.0219	0.0292
166	0.0083	0.0284	0.0372	0.0130	0.0184	0.0245
167	0.0049	0.0167	0.0218	0.0056	0.0188	0.0250
168	0.0094	0.0316	0.0413	0.0115	0.0187	0.0250
169	0.0057	0.0294	0.0396	0.0096	0.0133	0.0178
170	0.0070	0.0334	0.0449	0.0086	0.0154	0.0205
171	0.0059	0.0311	0.0419	0.0097	0.0142	0.0189
172	0.0072	0.0351	0.0472	0.0088	0.0159	0.0212
173	0.0037	0.0089	0.0109	0.0069	0.0194	0.0259
174	0.0056	0.0199	0.0264	0.0068	0.0203	0.0271
175	0.0071	0.0305	0.0410	0.0072	0.0200	0.0267

Table A.4 (cont'd) Performance limits for ASCE/SEI 41-17 and Eurocode 8-3

	ASCE/SEI 41-17 (rad)			Eurocode 8-3 (rad)		
Specimen No	**IO**	**LS**	**CP**	**DL**	**SD**	**NC**
176	0.0091	0.0235	0.0301	0.0085	0.0238	0.0318
177	0.0096	0.0327	0.0431	0.0111	0.0164	0.0219
178	0.0095	0.0326	0.0430	0.0111	0.0164	0.0219
179	0.0101	0.0331	0.0434	0.0088	0.0245	0.0327
180	0.0090	0.0155	0.0180	0.0144	0.0218	0.0291
181	0.0069	0.0176	0.0218	0.0118	0.0257	0.0342
182	0.0070	0.0142	0.0171	0.0127	0.0236	0.0315
183	0.0070	0.0109	0.0125	0.0137	0.0217	0.0289
184	0.0068	0.0140	0.0169	0.0123	0.0227	0.0302
185	0.0067	0.0140	0.0169	0.0123	0.0227	0.0302
186	0.0058	0.0097	0.0113	0.0127	0.0201	0.0268

Appendix B

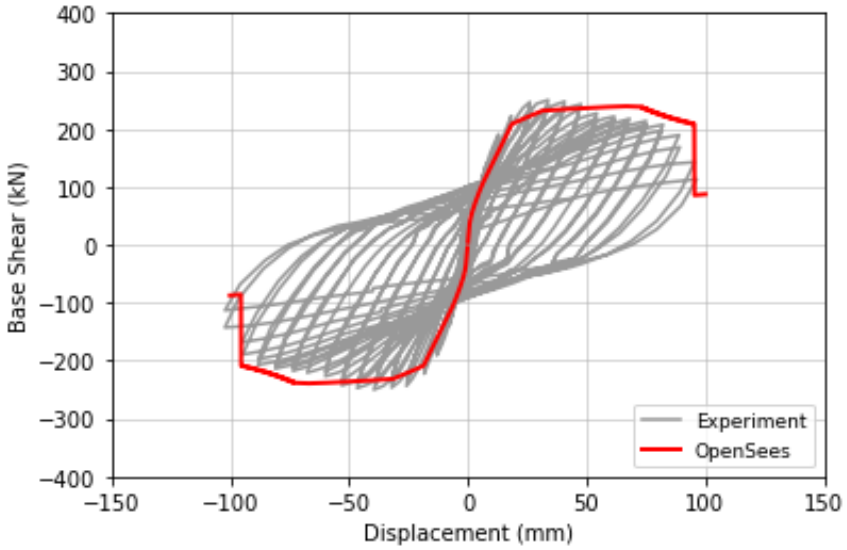

Figure B.1 Mo and Wang 2000, C1-1

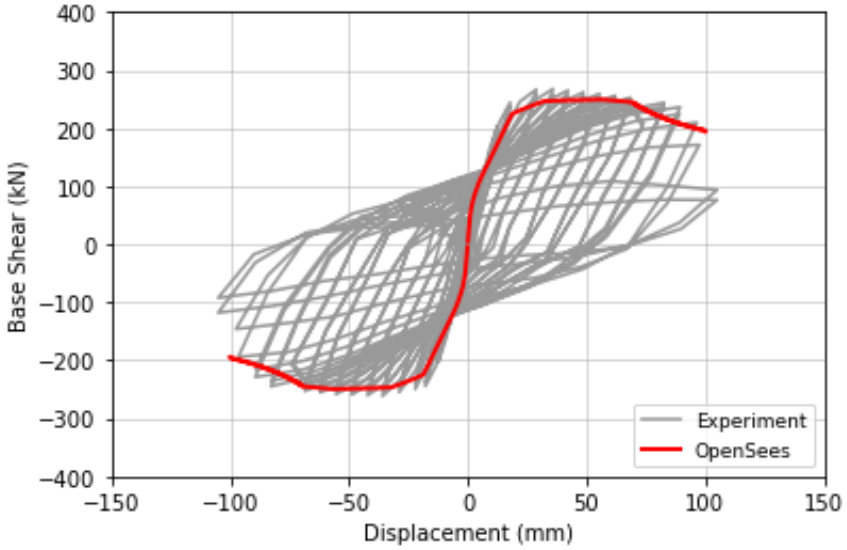

Figure B.2 Mo and Wang 2000, C1-2

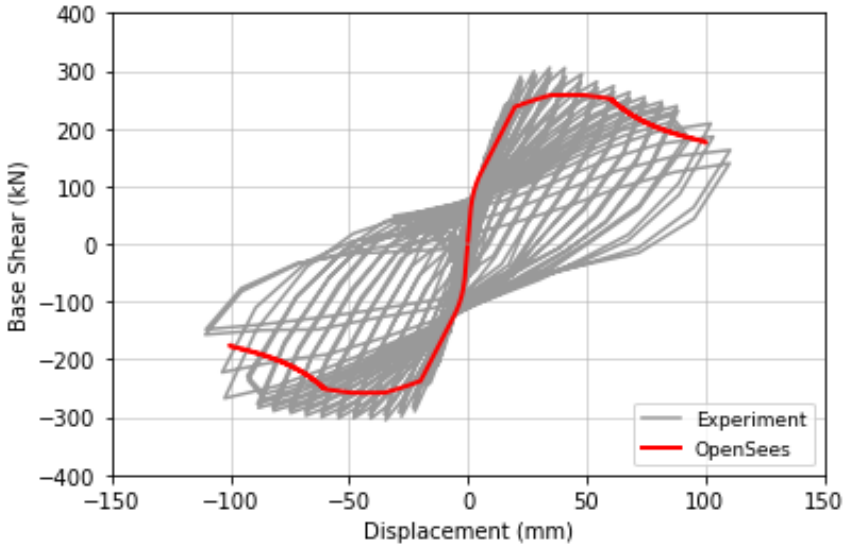

Figure B.3 Mo and Wang 2000, C1-3

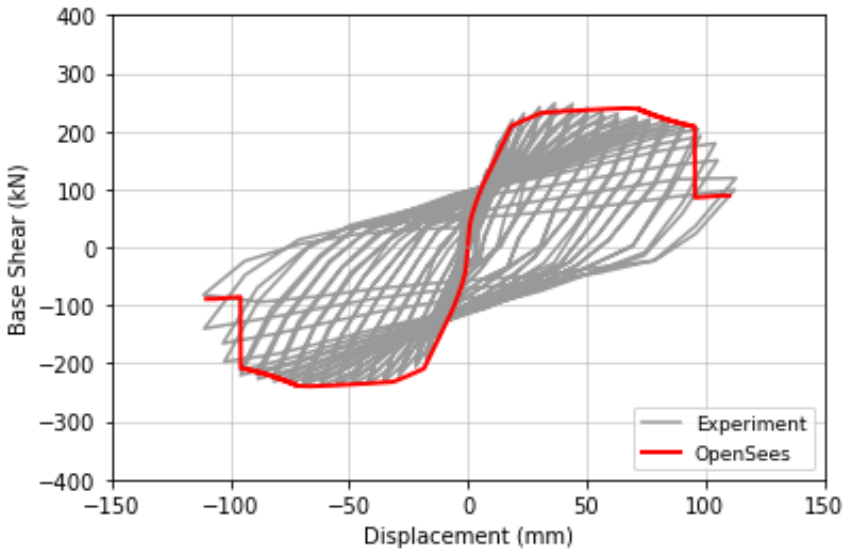

Figure B.4 Mo and Wang 2000, C2-1

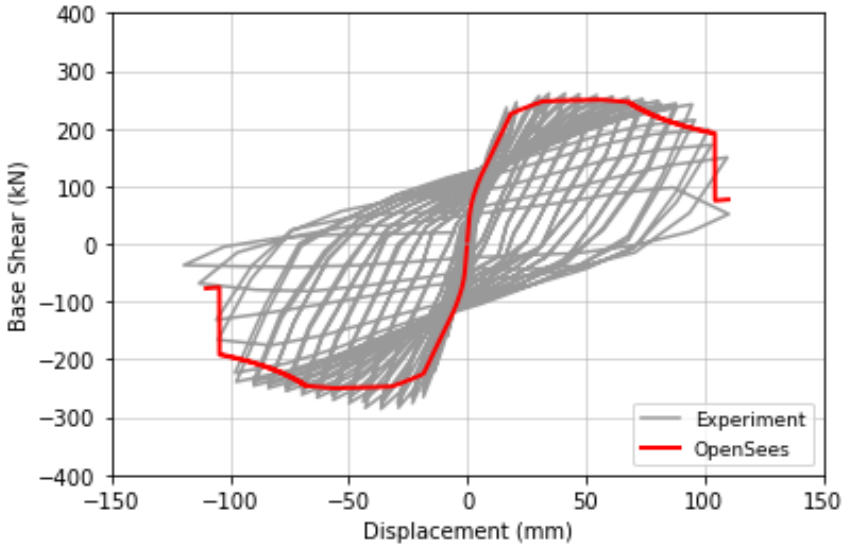

Figure B.5 Mo and Wang 2000, C2-2

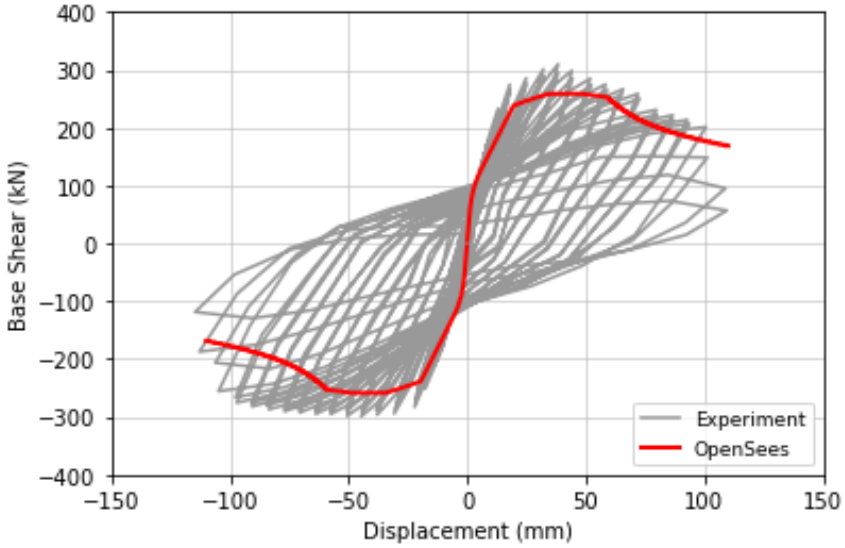

Figure B.6 Mo and Wang 2000, C2-3

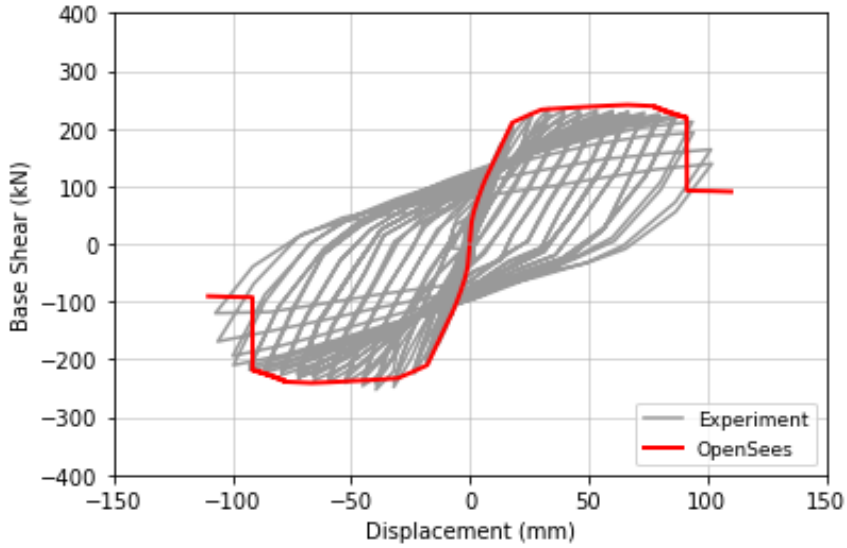

Figure B.7 Mo and Wang 2000, C3-1

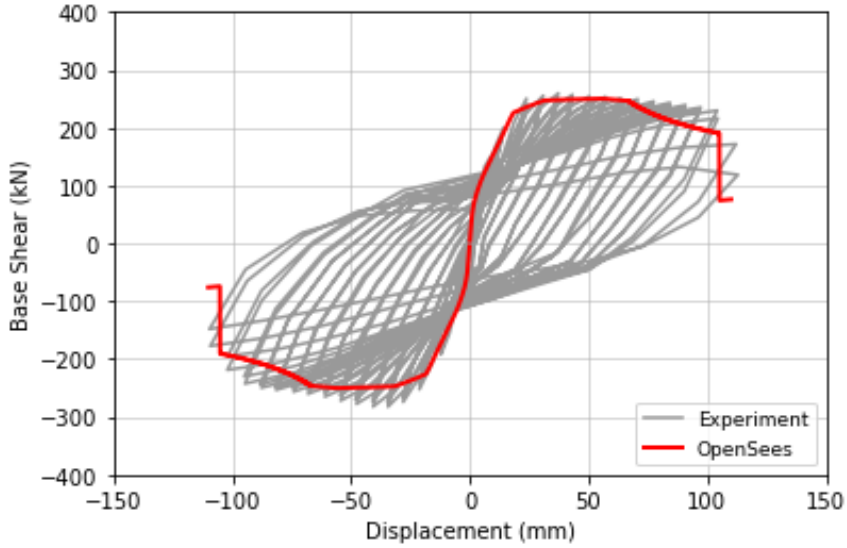

Figure B. 8 Mo and Wang 2000, C3-2

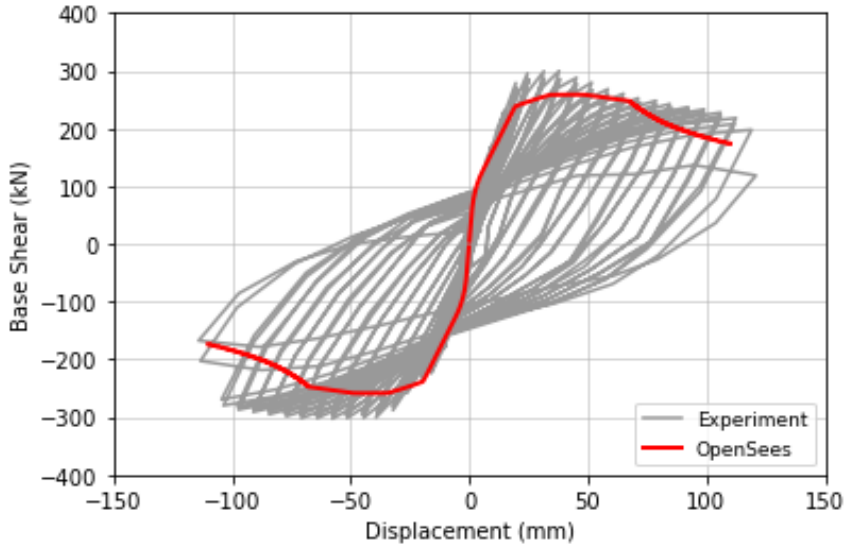

Figure B.9 Mo and Wang 2000, C3-3

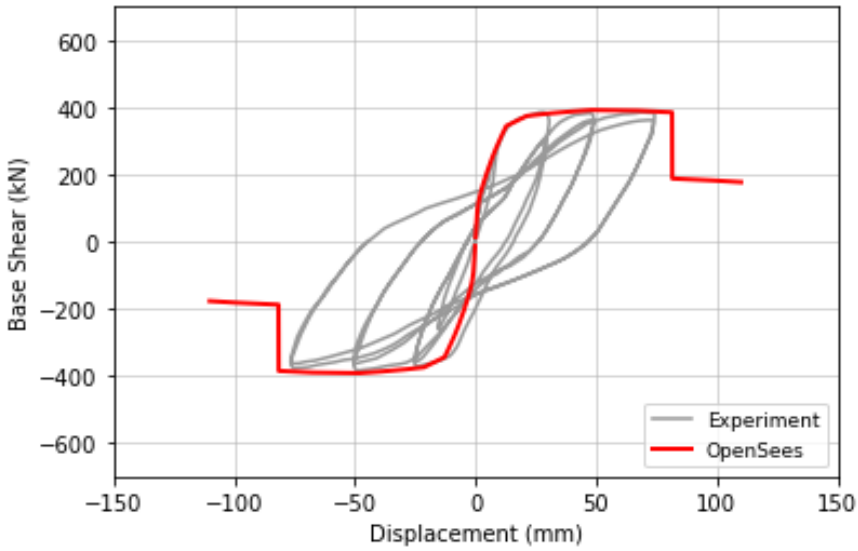

Figure B.10 Tanaka and Park 1990, No.5

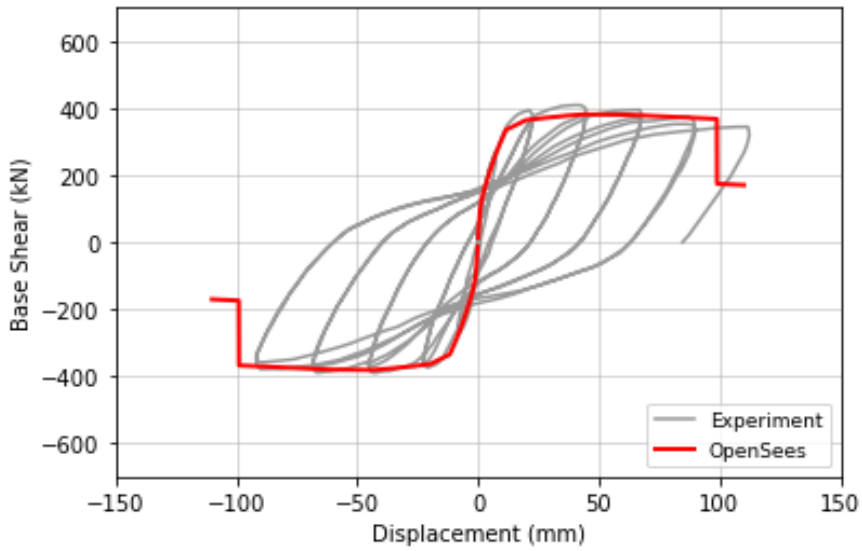

Figure B.11 Tanaka and Park 1990, No.6

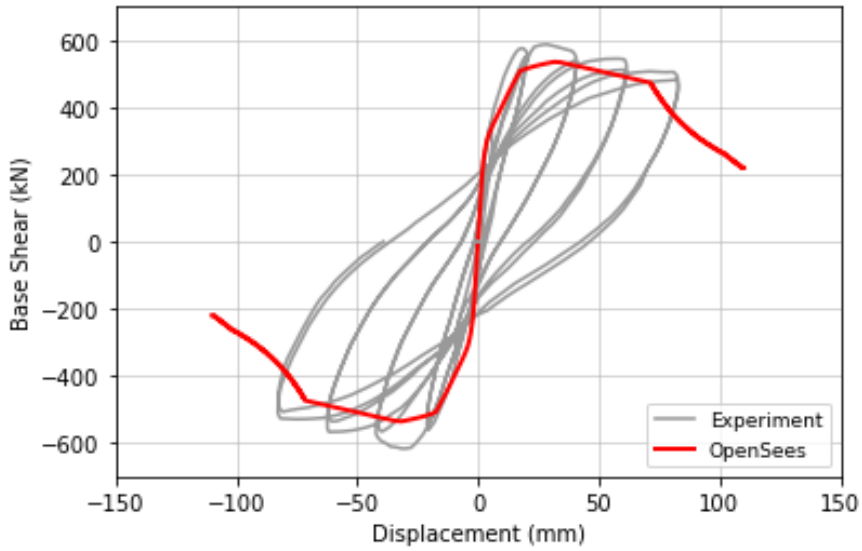

Figure B.12 Tanaka and Park 1990, No.7

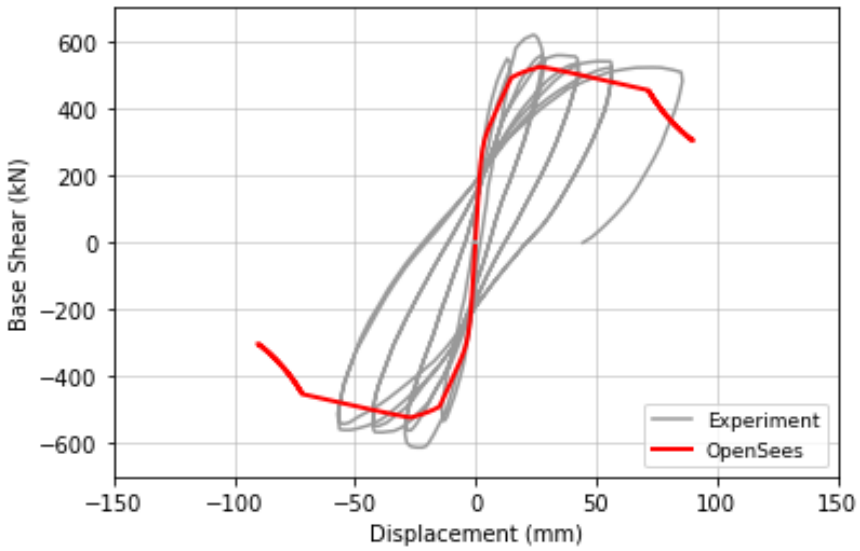

Figure B.13 Tanaka and Park 1990, No.8

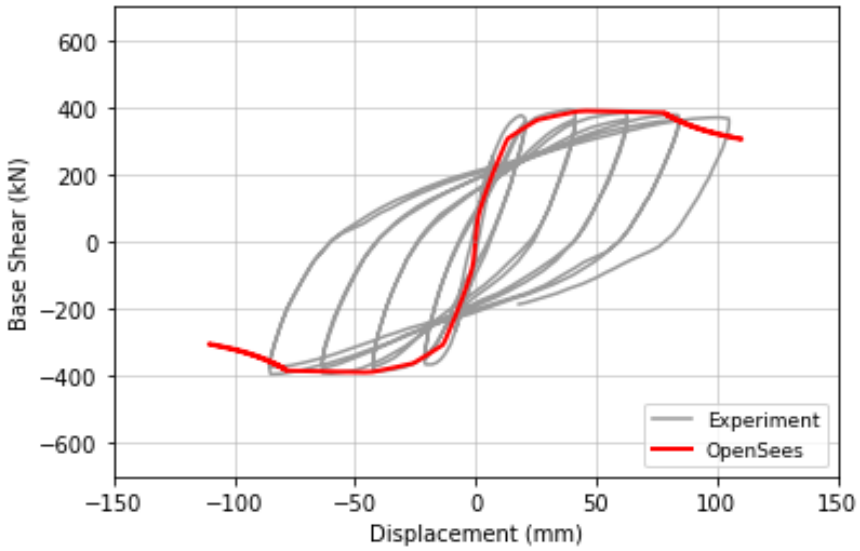

Figure B.14 Park and Paulay 1990, No.9

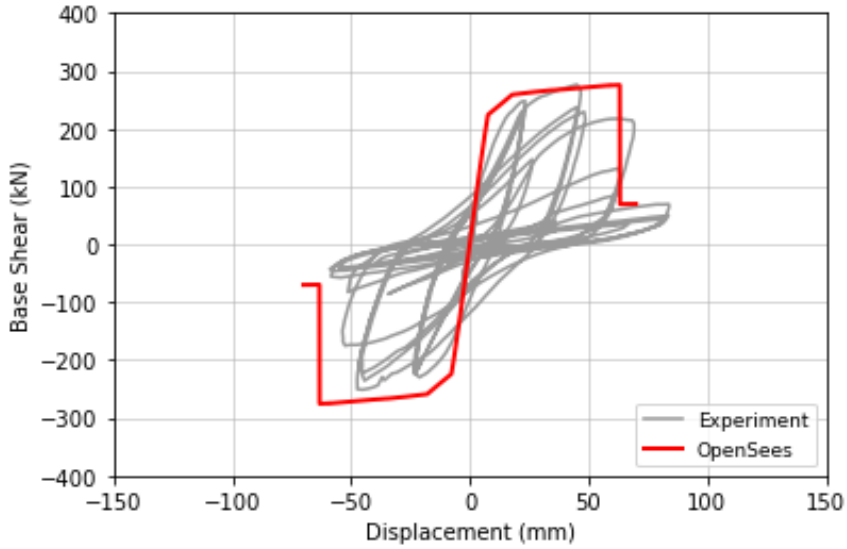

Figure B.15 Saatcioglu and Ozcebe 1989, U1

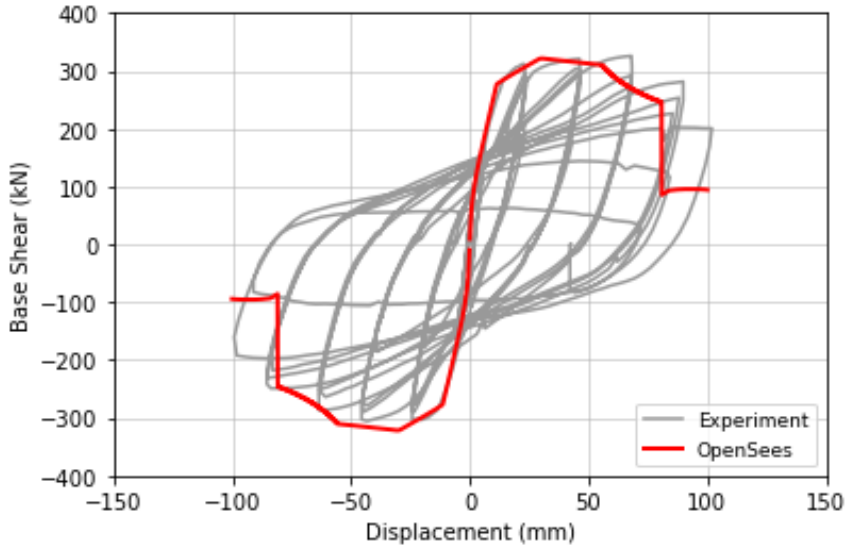

Figure B.16 Saatcioglu and Ozcebe 1989, U4

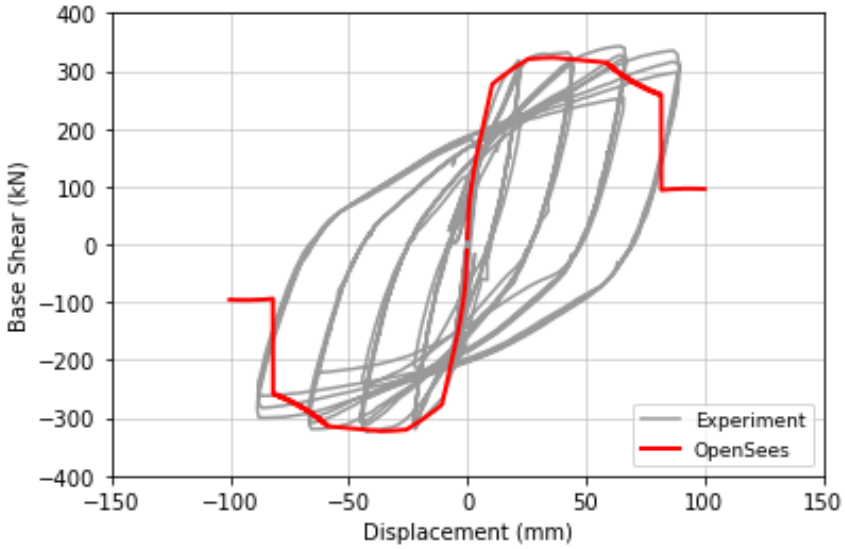

Figure B.17 Saatcioglu and Ozcebe 1989, U6

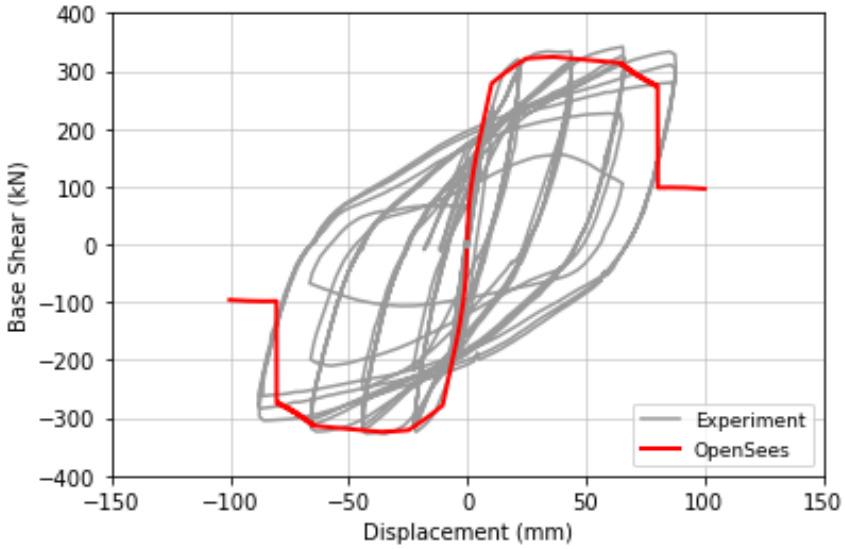

Figure B.18 Saatcioglu and Ozcebe 1989, U7

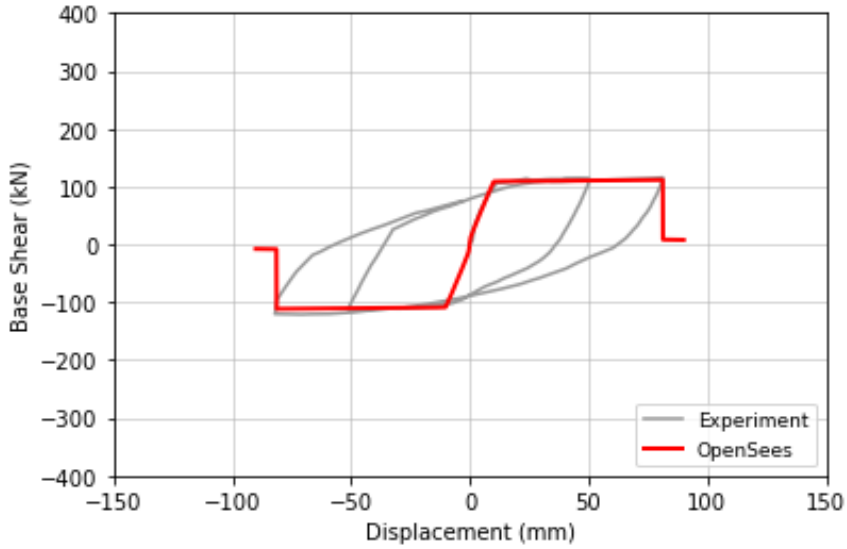

Figure B.19 Ohno and Nishioka 1984, L1

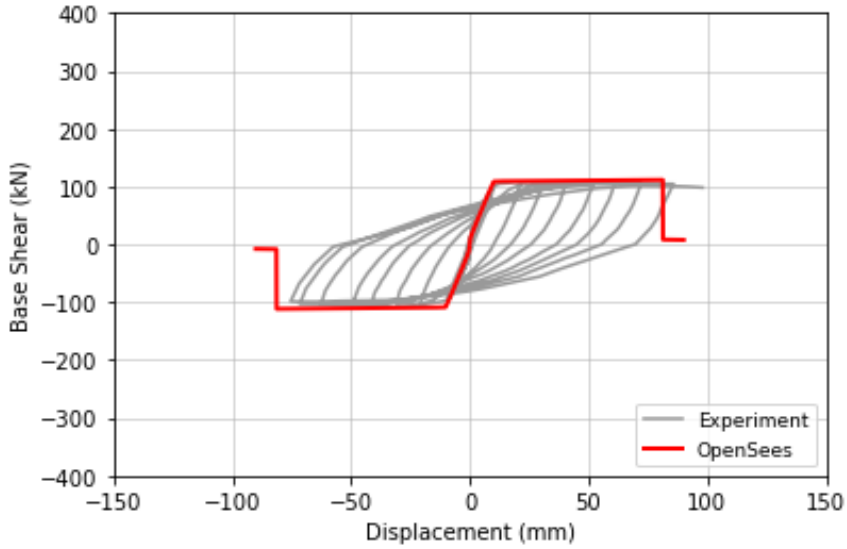

Figure B.20 Ohno and Nishioka 1984, L2

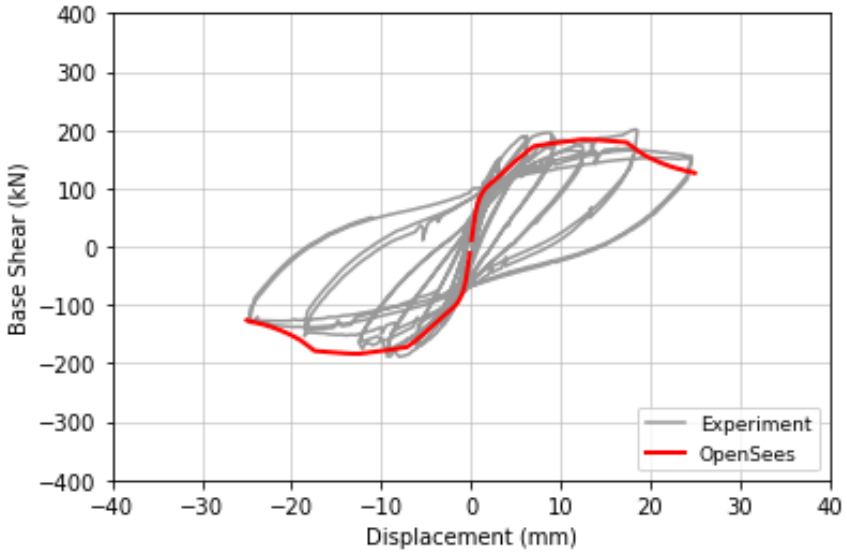

Figure B.21 Kono et al. 2002, D1N30

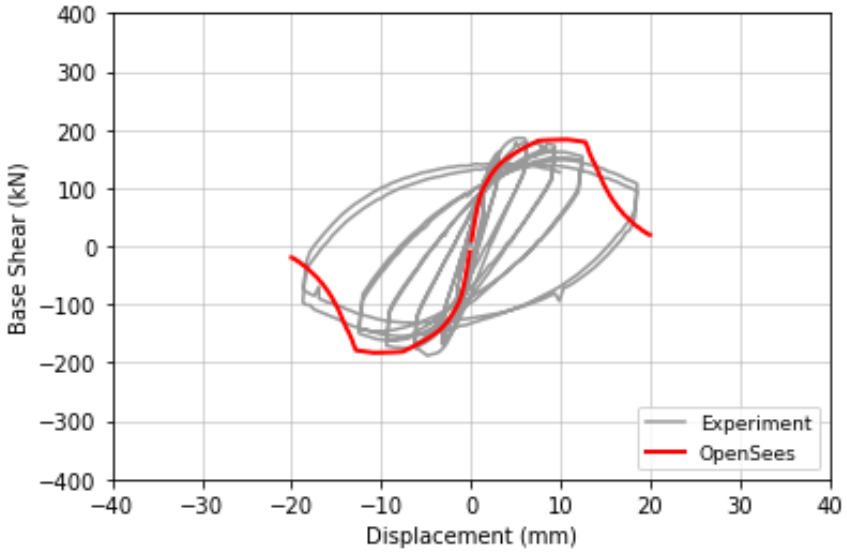

Figure B.22 Kono et al. 2002, D1N60

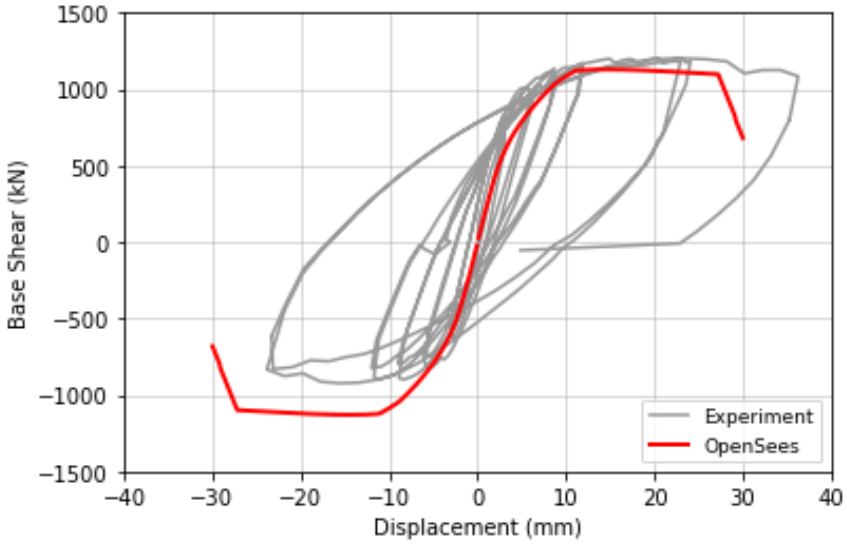

Figure B.23 Kono et al. 2002, L1N6B

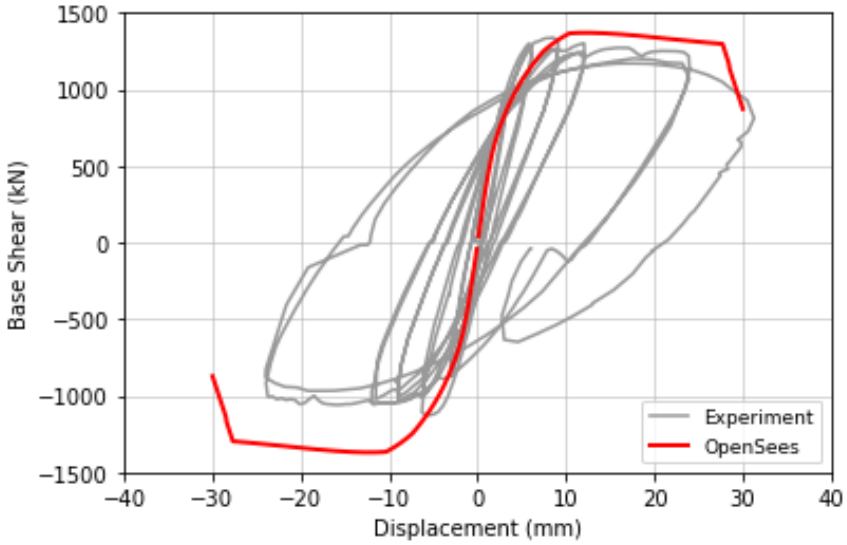

Figure B.24 Kono et al. 2002, L1N60

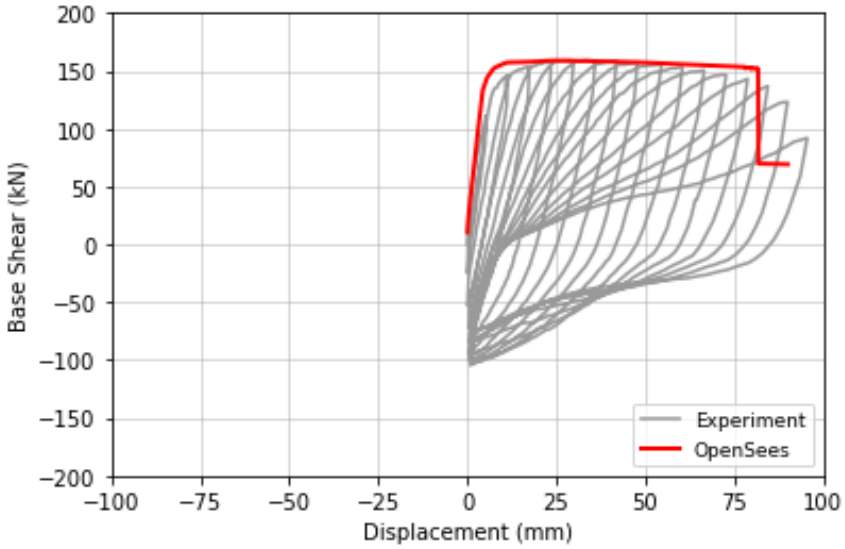

Figure B.25 Takemura and Kawashima 1997, Test 5

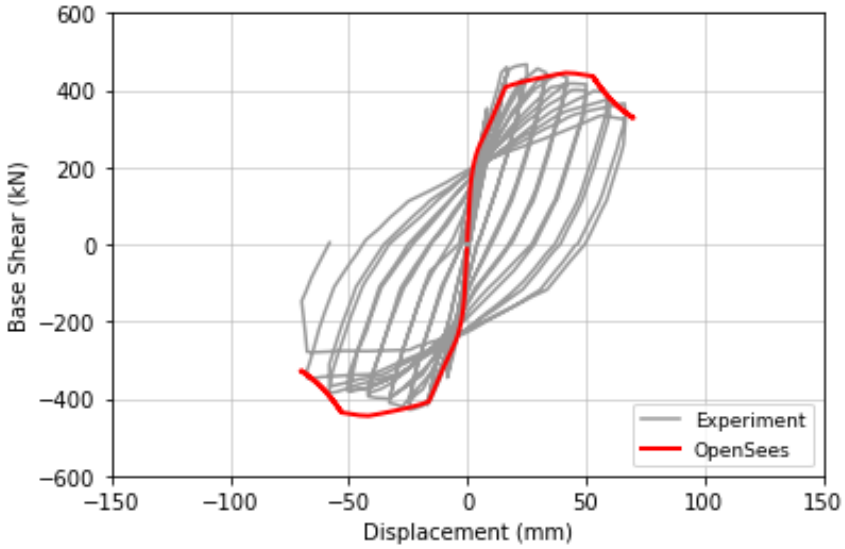

Figure B.26 Azizinamini et al. 1988, NC-2

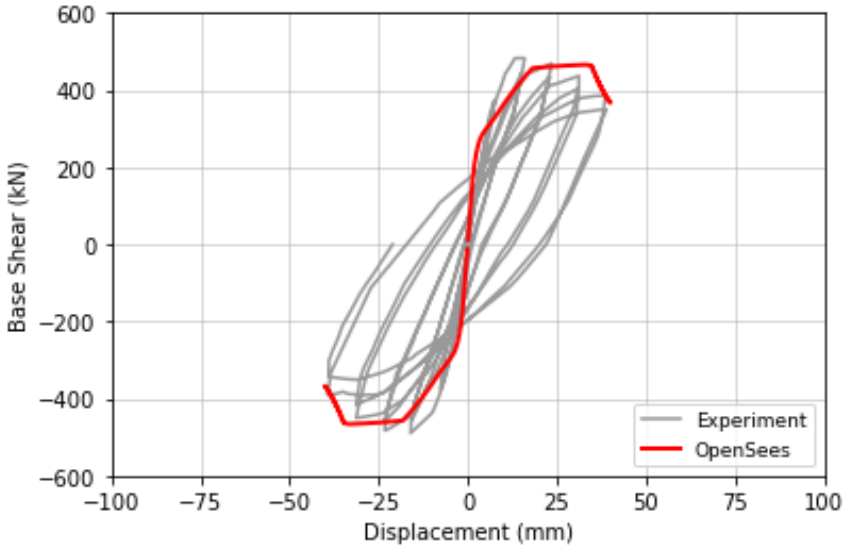

Figure B.27 Azizinamini et al. 1988, NC-4

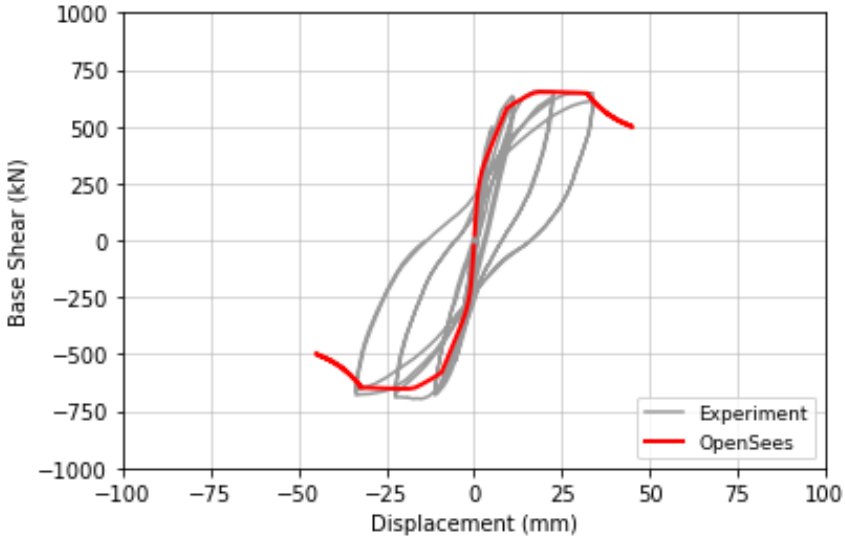

Figure B.28 Gill et al. 1979, No.1

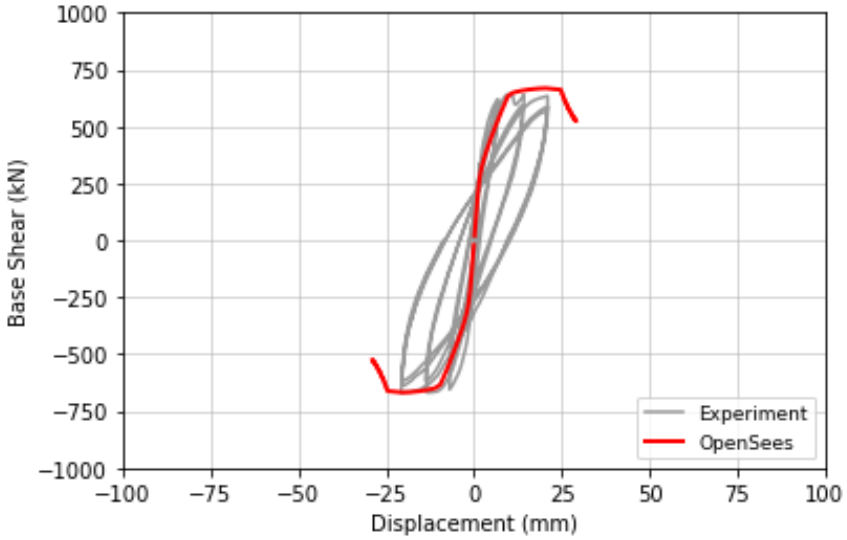

Figure B.29 Gill et al. 1979, No.3

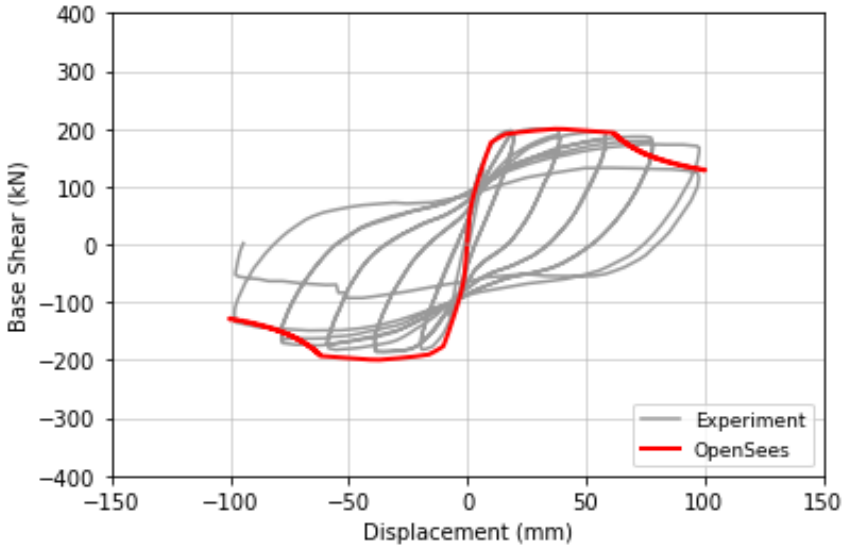

Figure B.30 Soesianawati et al. 1986, No.1

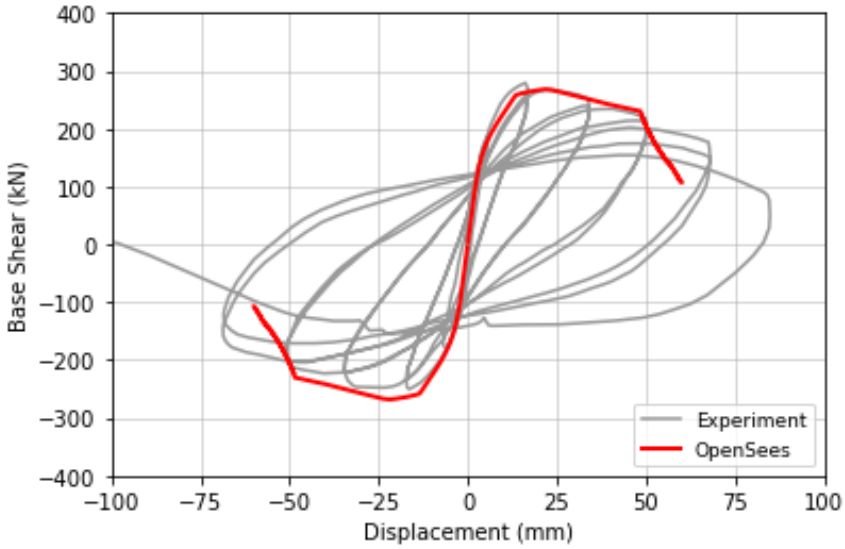

Figure B.31 Soesianawati et al. 1986, No.2

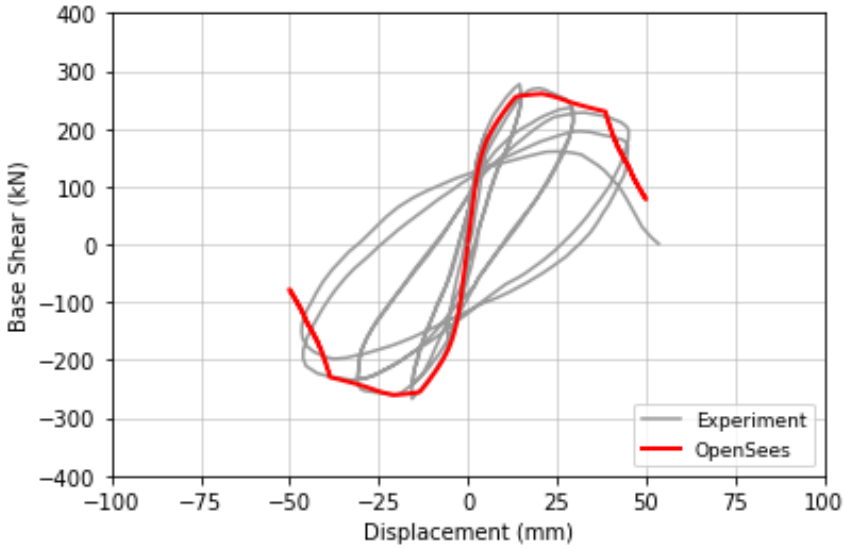

Figure B.32 Soesianawati et al. 1986, No.3

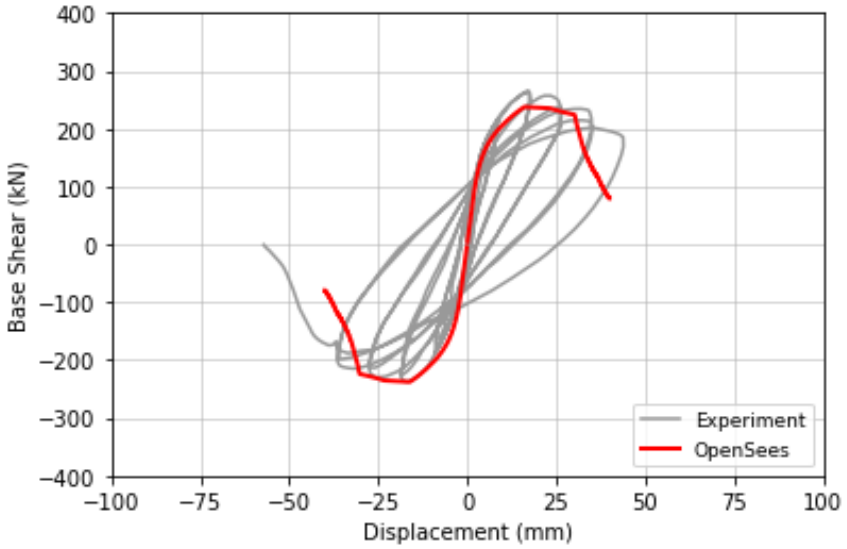

Figure B.33 Soesianawati et al. 1986, No.4

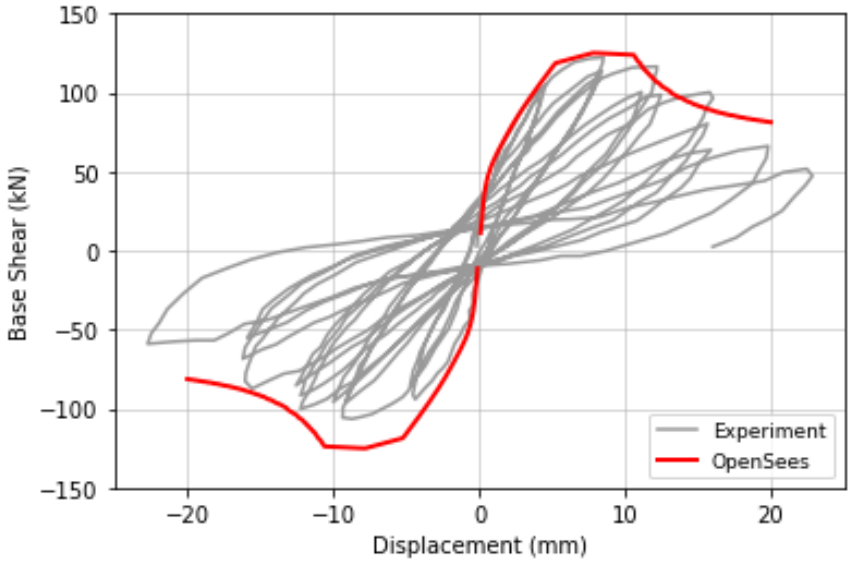

Figure B. 34 Esaki 1996, H-2-1_3

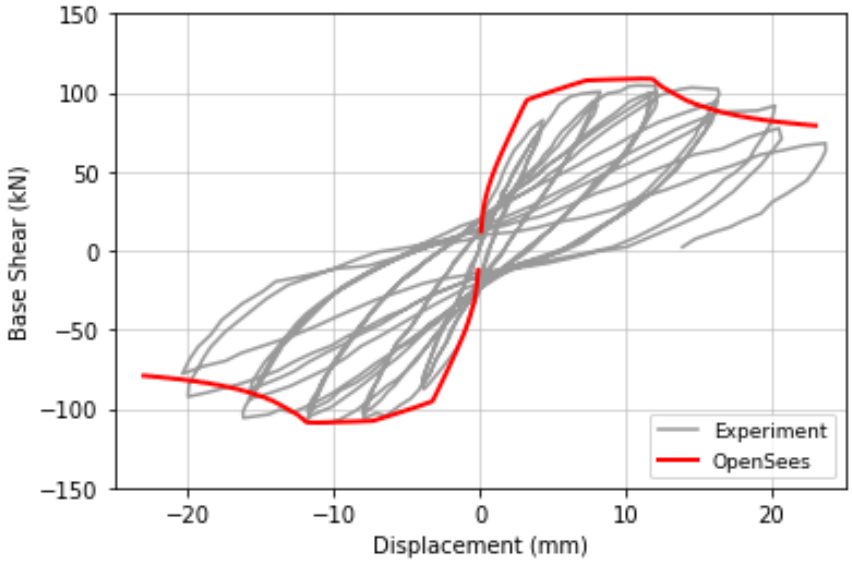

Figure B. 35 Esaki 1996, H-2-1_5

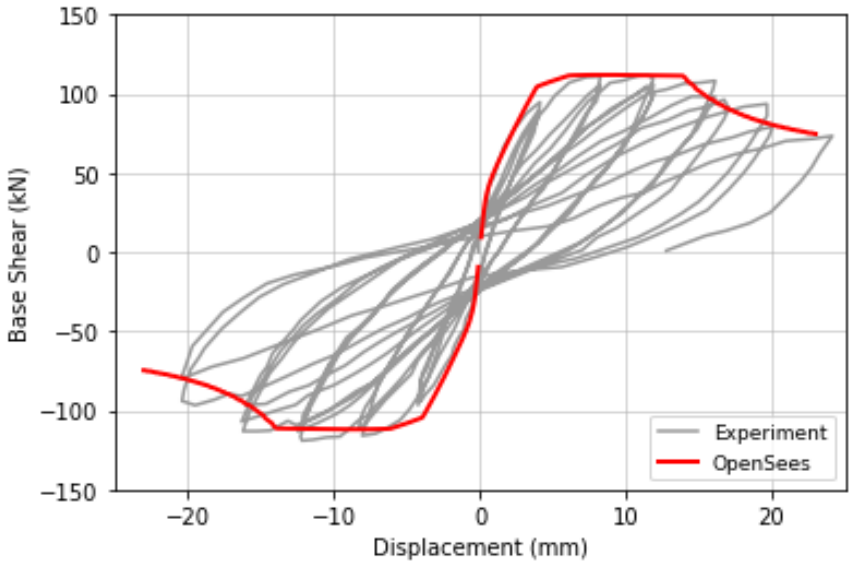

Figure B. 36 Esaki 1996, HT-2-1_3

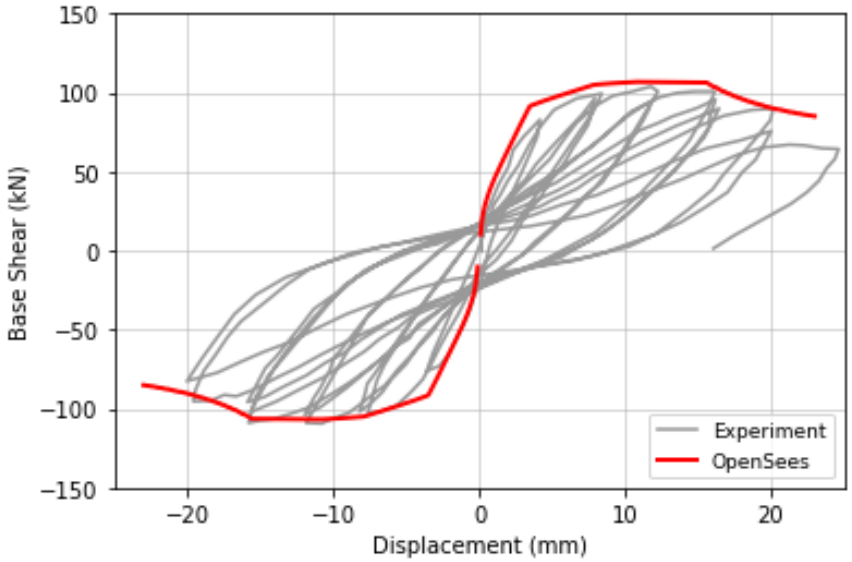

Figure B. 37 Esaki 1996, HT-2-1_5